2023-01

Hydrologic responses to climate and land use/cover changes in world heritage site of Ngorongoro conservation area and surrounding catchments, northern Tanzania

Mwabumba, Mohamed

NM-AIST

https://doi.org/10.58694/20.500.12479/2187

HYDROLOGIC RESPONSES TO CLIMATE AND LAND USE/COVER CHANGES IN WORLD HERITAGE SITE OF NGORONGORO CONSERVATION AREA AND SURROUNDING CATCHMENTS, NORTHERN TANZANIA

Mohamed Fadhili Mwabumba

A Dissertation submitted in Partial Fulfilment of the Requirements for the Degree of Doctor of Philosophy in Hydrology and Water Resources Engineering of the Nelson Mandela African Institution of Science and Technology

Arusha, Tanzania

January, 2023

ABSTRACT

In Tanzania, various studies have analyzed the impact of climate and land use/cover changes on water resources. However, information on the interactions between climate and land use/cover change, temporal and spatial variability of hydrological components and water quality at the local scale is insufficient. The objective of this study was to evaluate the hydrological response to climate and land use/cover changes in Ngorongoro Conservation Area (NCA) and surroundings. The study performed climate change analysis using outputs from a multi-model ensemble of Regional Climate Models (RCMs) and statistically downscaled Global Climate Models (GCMs). The CA–Markov model applied to project Land use/cover for the future 2025 and 2035. This study further used the Soil Water Assessment Tool (SWAT) modelling approaches to analyse the hydrological responses and HYDRUS 1D to determine the change in Groundwater quality due to climate and land use/cover changes. The analysis of climate change between historical period (1982-2011) and future period (2021-2050) indicated an increase in the mean annual rainfall and temperature, seasonal rainfall except June to September (JJAS) season which showed a decreasing trend. Spatially, rainfall and temperatures would increase over the entire area. The projected Land use/cover change for the period 2025 to 2035 compared to the baseline 2016, showed a reduction in bushland, forest, water, and woodland, but an intensification in cultivated land, grassland, bare land, and the built-up area. The surface runoff, evapotranspiration, lateral flow, and water yield would significantly increase in the future, while groundwater would decrease under combined climate and land use/cover change. It is predicted that two anions (Cl^- and PO_4^{-3}) and two cations (Na^+ and K^+) would exceed the permissible limits for the drinking water set by the World Health organisation (WHO) and Tanzania Bureau of Standards (TBS), from 2036 to 2050. Changes in groundwater quality due to major cations and anions is significantly correlated to evapotranspiration and temperature with Pearson correlation (*r*) between 0.35 and 0.85. Furthermore, correlate to the changes in all land use/ cover types with Pearson correlation (*r*) between 0.56 and 0.96. The results obtained provide further insight into future water resources management planning and adaptation strategies.

DECLARATION

I, Mohamed Fadhili Mwabumba, do declare to the Senate of the Nelson Mandela African Institution of Science and Technology that this dissertation is my own original work and that it has neither been submitted nor concurrently submitted for the degree award in any other institution.

Mohamed Fadhili Mwabumba — Date: 10/02/2023

The above declaration is confirmed by

Dr. Mwemezi J. Rwiza — Date: 15.03.2023

Dr. Madaka Tumbo — Date: 13/2/2023

Prof. Dr. Brijesh K. Yadav — Date: 24/2/2023

Dr. B. K. Yadav
विभागाध्यक्ष / Head
जल विज्ञान विभाग / Department of Hydrology
भारतीय प्रौद्योगिकी संस्थान रुड़की
Indian Institute of Technology Roorkee
रुड़की / Roorkee-247 667 (U.K.)

COPYRIGHT

CERTIFICATION

The undersigned certify that have read and hereby recommend for acceptance by the Nelson Mandela African Institution of Science and Technology a dissertation titled "*Hydrologic Response to Climate and Land use/cover Changes in the World Heritage Site of Ngorongoro Conservation Area and Surrounding Catchments, Northern Tanzania*", in Partial Fulfilment of the Requirements for the Degree of Doctor of Philosophy in Hydrology and Water Resources Engineering of the Nelson Mandela African Institution of Science and Technology.

15.03.2023

Dr. Mwemezi J. Rwiza — Date

13.2.2023

Dr. Madaka Tumbo — Date

24/2/2023

Prof. Brijesh K. Yadav — Date

Dr. B. K. Yadav
विभागाध्यक्ष / Head
जल विज्ञान विभाग / Department of Hydrology
भारतीय प्रौद्योगिकी संस्थान रुड़की
Indian Institute of Technology Roorkee
रुड़की / Roorkee-247 667 (U.K.)

ACKNOWLEDGMENTS

It is a great pleasure to acknowledge those who contributed to the success of this research. My heartfelt thanks and utmost gratitude is expressed to my supervisors, Prof. Dr. Brijesh Kumar Yadav, Dr. Mwemezi J. Rwiza and Dr. Madaka Tumbo, who kept my confidence and spirit high throughout the research process. Their professional yet friendly ways of communication have helped me complete my research work.

My profound gratitude goes to the Water Infrastructure and Sustainable Energy Futures (WISE-Futures) Center for their support during this study. I thank my employee, the Tanzania Meteorological Authority (TMA), for providing study leave and quality climate datasets to facilitate this study. Special appreciation to the Indian Institute of Technology Roorkee (IITR) for the support provided to my research work and my stay in India during the exchange program, which aimed to strengthen the Africa Center of Excellence (ACEs) through the World Bank and the Department of Science and Technology India.

Gratitude also goes to the former project supervisor, the late Prof. Alfred N. N. Muzuka, who passed on during this work for the foundations laid for this study. Also, to Dr. Isaac Larbi of the University of Environment and Sustainable Development, Ghana, Dr. Jahngeer Jahangeer of IITR and Dr. Sahila Beegum of University of Nebraska-Lincoln for their support in hydrological modelling. I would also like to express my sincere thanks to all staff of the department of Hydrology IITR, the National Institute of Hydrology (NIH) and my fellow PhD scholars at the Department of hydrology IITR for the support they provided in my research work at IITR.

Special thanks to Prof. M. L. Kansal and Prof. Arun Kumar of IITR for their support during my stay in India. I also want to express my gratitude to my colleagues at the Nelson Mandela African Institution of Science and Technology (NM-AIST), especially to Mr. Gustavior Okwir, Mr. Onesmo Zakaria Sigalla, Ms. Latifa Nyembo, Ms. Risala Murithi, Ms. Rosette Nyiraziza and Ms. Goldwin Lukas for their support during my studies. Also, to the WISE-Future's staff members under Dr. Hans Komakech and Dr. Yusufu Abed Jande for their support during my study.

Finally, I want to express my gratitude to my lovely wife, Dr. Sekela Twisa, for her continuing support and perseverance during this period in my life. Recognition is needed for her encouragement, support and belief in me, which has helped me keep pushing hard and continuing with my studies until the end. Also, to my two lovely children, Nadia Mwabumba and Alpha Mwabumba, I want to thank them for their love and patience during my long absence.

DEDICATION

I dedicate this dissertation with gratitude and love to my dear wife, Dr. Sekela Twisa, and my children, Nadia and Alpha, for their patience and understanding during my studies. Also, to my parents, my father, the late Mr. Fadhili Issa Mwabumba, and my beloved mother, Mrs. Saida Mwabumba, for the foundation they have laid in my life.

TABLE OF CONTENTS

LIST OF TABLES

LIST OF FIGURES

LIST OF ABBREVIATIONS AND SYMBOLS

Q_{gw}	Amount Of Return Flow or Base Flow
E_a	Evapotranspiration Amount
P_{day}	Precipitation Amount on a Day
Q_{sur}	Surface Runoff
SW_0	Initial Soil Water Content
SW_t	Final Soil Water Content
W_{seep}	Amount of Water Entering the Vadose Zone from the Soil Profile
ACE	African Center of Excellence
ANN	Artificial Neural Network
ARS	Agricultural Research Service
BL	Bare Land
BLT	Built-up Land
BUL	Bushland
CanESM	Canadian Earth System Model
CHIRPS	Climate Hazards Group Infrared Precipitation with Station
CL	Cultivated Land
CMIP6 -	Coupled Model Intercomparison Project Phase 6
CORDEX	Coordinated Regional Climate Downscaling Experiment
CREAMS	Chemicals, Runoff, and Erosion from Agricultural Management Systems
DEM	Digital Elevation Model
DO	Dissolved Oxygen
EC	Electrical
EPIC	Environmental Impact Policy Climate
EROS	Earth Resources Observation and Science
ET	Evapotranspiration
FAO	Food and Agriculture Organization
FR	Forest
GCM	Global Climate Model
GIS	Geographical Information System
GL	Grassland
GLEAMS	Groundwater Loading Effects on Agricultural Management Systems
GPS	Global Positioning System

h	Soil Water Pressure Head
HDPE	High-Density Polyethylene
HRUs	Hydrologic Response Units
HWSD	Harmonize World Soil Database
HYDRUS 1D	A Public Domain Windows-Based Modeling Environment for Analysis of Water Flow and Solute Transport in Variably Saturated Porous Media
ICP-MS	Inductively coupled Plasma Mass Spectrometry
IDB	Internal Drainage Basin
IDW	Inverse Distance Weighted
IITR	Indian Institute of Technology Roorkee
IPCC	Intergovernmental Panel on Climate Change
ISODATA	Iterative, Self-Organizing Data Analysis
KNMI	Koninklijk Nederlands Meteorologisch Instituut
L^2T^{-1}	Dispersion Coefficient
LARS-WG	Long Ashton Research Station Weather Generator
LT^{-1}	Unsaturated Hydraulic Conductivity
MERRA-2	The Modern-Era Retrospective Analysis for Research and Applications, Version 2
mg/L	milligram per Liter
ML^{-3}	Solution Concentration
MLC	Likelihood Classification
MM^{-1}	Sorbed Concentration
MOLA	Multi-Objective Land Allocation
MPI-CSC	Max Planck Institute- Computational Methods in Systems and Control Theory Germany
NASA POWER	National Aeronautics and Space Administration of Worldwide Energy Resource
NCA	Ngorongoro Conservation Area
NCEP	National Centre for Environmental Prediction
NIH	National Institute of Hydrology
NM-AIST	Nelson Mandela African Institution of Science and Technology
NSE	Nash–Sutcliffe efficiency
PBIAS	Percent Bias
PLS	Partial Least Squares

PLSR	Partial Least Squares Regression
QUAL2E	The Enhanced Stream Water Quality Models
r	Pearson correlation
RCM	Regional Climate Model
RCMs	Regional Climate Models
RCP	Representative Concentration pathways
RCs	Regression Coefficients
RH	Relative Humidity
RMSE	Root Mean Squire Error
RMSE	Ratio of Root Mean Square Error
ROC	Relative Operating Characteristic
ROTO	Routing Outputs to Outlet
RS	Remote Sensing
RSR	Ratio of Root Mean Square Error to the Standard Deviation
SDSM	Statistical Downscaling System Model
SMHI	Swedish Meteorological and Hydrological Institute, Rossby Centre
SRTM	Shuttle Radar Topography Mission Digital Elevation Mode
SUMATRA	Land Transport Regulatory Authority
SWAT	Soil Water Assessment Tool
SWRRB	Simulator for Water Resources in Rural Basins
t	Time
TBS	Tanzania Bureau of Standards
TMA	Tanzania Meteorological Authority
UCSB	University of California Santa Barbara
UNFCCC	United Nations Framework Convention on Climate Change
USDA	United States Department of Agriculture
USGS	U.S Geological Survey
VIP	Variable Importance of Projection
VIP	variable importance of the projection
WET	Wetland
WG	Weather Generator
WHO	World Health Organization
WISE-Future	Water Infrastructure and Sustainable Energy-Future
WL	Woodland

WT	Water
z	Vertical Coordinate
θ	Volumetric Water Content (Dimensionless)

CHAPTER ONE

INTRODUCTION

1.1 Background of the Problem

Water resources are the fundamental requirement for the communities' livelihood and socio-economic development worldwide (Vörösmarty *et al.*, 2010; Wada *et al.*, 2010). However, water resources deprivation caused by factors like climate change, land use/cover changes, and unsustainable or improper management of water resources has resulted in freshwater unavailability in different parts of the world (Joshi *et al.*, 2020; Kumar, 2017; Singh *et al.*, 2021). The provision of water resources is closely related to the hydrological processes, which are mainly affected by the climate and land use/cover changes (Al-Bakri *et al.*, 2013; Chang & Franczyk, 2008). Climate and Land use/cover change influence water resources exploitation and depletion of its quantity and quality, particularly in arid and semiarid zones (Abou-Zaki *et al.*, 2018; Macdonald *et al.*, 2012; Yadav & Hassanizadeh, 2011). Impacts of climate and land use/cover change on water resource depletion are likely to continue to increase in sub-Saharan Africa, particularly in arid and semi-arid regions, which are considered vulnerable (Onyutha *et al.*, 2021; Vörösmarty *et al.*, 2010). In Tanzania, water resource reductions have been reported in different parts of the country, including protected areas (Deus *et al.*, 2013; Mkiramweni *et al.*, 2016; Nyembo *et al.*, 2022). In these areas, climate and land use/cover changes have been a concern in recent years as their impacts on water resources are significant for the environment and ecosystem (Deus *et al.*, 2013; Mkiramweni *et al.*, 2016).

Assessing the impacts of land use/cover and climate change on water resources is challenge for hydrological research as boundary conditions change from site to site (Ty *et al.*, 2012). However, predicting the simultaneous and interactive impacts of climate and land use/cover changes on the quantity and quality of water resources is a task that requires models from multiple disciplines (Näschen *et al.*, 2019). Hydrological models play a vital role in understanding watershed behaviours and responses (Bárdossy & Singh, 2008). In addition, these models provide valuable frameworks for investigating the changes in various hydrological pathways that are caused by climate and human activities (Andaryani *et al.*, 2021; Fowler *et al.*, 2007; Näschen *et al.*, 2019). The hydrological responses to land use/cover and climate changes are often investigated through scenario simulations using the Soil Water Assessment Tool (SWAT) model (Näschen *et al.*, 2019). However, for water quality, a public domain Windows-based modeling environment for analysis of water flow and solute transport

in variably saturated porous media (HYDRUS 1D) has been extensively used to investigate solute mass and concentration in the subsurface and groundwater (Šimůnek *et al.*, 2008b).

In Tanzania, different studies analyzed the impact of climate and Land use/cover change on water resources (Näschen *et al.*, 2019; Notter *et al.*, 2013; Twisa *et al.*, 2020). The results of the studies differ due to several factors including the type of Land use/cover, the hydrologic nature of the area, the study period and chosen model used to simulate climate change. Few studies have analysed the impacts of changing climate on hydrologic processes using the downscaled data from Regional Climate Models (RCM) as input in the hydrological models (Hyandye *et al.*, 2018; Näschen *et al.*, 2019). The RCMs at their finer resolution simulates the detailed local climate conditions and provide future prediction, however, RCMs perform different from one location to another (Larbi *et al.*, 2021). Other Studies also applied the land cover classifications and modelling techniques to assess the hydrologic responses on impact of land use/cover change in various parts Tanzania (Hyandye *et al.*, 2018; Näschen *et al.*, 2019; Twisa *et al.*, 2020). These studies have shown the individual impact of either climate change, or land use/cover change on hydrology. However, the combined effect of climate and Land use/cover change on the hydrologic processes and water resources quality are not adequately analyzed, especially in the conserved areas.

The Ngorongoro conservation area (NCA) is internationally recognized for its scenic beauty, spectacular wildlife, and natural ecosystem. It is also exceptional for its inventive joint land-use policy, which integrates wildlife conservation and human activities in the world (Deocampo, 2004; Masao *et al.*, 2015). The NCA is one of the main tourist destinations and the most visited conserved area in Tanzania and East Africa (Melita & Mendlinger, 2013). During the dry season, wildlife, Maasai communities, and migratory species from Serengeti National Park are highly dependent on available water resources in the NCA (Estes *et al.*, 2006). However, water availability for human and wildlife consumption in the NCA and the surrounding areas have been decreasing since the 2000s due to reduced rainfall and prolonged drought conditions (Estes *et al.*, 2006; Leweri *et al.*, 2021; Mkiramweni *et al.*, 2016). The reduction of water resource in the NCA and the surroundings has significantly impacted local communities, wildlife tourism, and the country's economy. However, there is inadequate information about climate and land use/cover change effects on water resources in the NCA and surrounding catchments. Therefore, studies on the climate and land use/cover change impacts to water resources around the NCA are highly encouraged (Mkiramweni *et al.*, 2016). This study was carried out to describe the response of hydrological processes in the NCA and

surrounding catchments to climate change and land use/cover change. Furthermore, due to the increased groundwater utilization in the study area, this study also analyzed the impact of climate change and land use cove change on groundwater quality.

This study assessed precipitation and temperature projections and their impact on water resources in the NCA and surrounding catchments. In this assessment, the study used an ensemble mean of four bias-corrected regional climate models and simulations from the Statistical Downscaling System Model (SDSM) (Wilby *et al.*, 2002) and the Long Ashton Research Station Weather Generator (LARS-WG) (Semenov & Stratonovitch, 2010). Furthermore, the study analyzed the land use/cover change of Ngorongoro Conservation Area (NCA) and its surroundings using Remote Sensing and Geographical Information System (GIS) integrated with Cellular Automata-Markov model. The output from climate and land use/cover models was applied in the SWAT model to perform scenario based analysis to determine the hydrologic response of climate and land use/ cover change. Additionally, the study applied to the HYDRUD 1D model to determine the movement of major cations and anions to the ground water due to climate and land use/cover changes. The information generated from this study is important for sustainable water resources management plan and for reducing and /or mitigating the threats posed by water scarcity and stress on the ecosystem and human welfare. Moreover, the study established the baseline information of groundwater quality which is necessary to guide the management of water resources and ecological monitoring for the NCA and surroundings.

1.2 Statement of the Problem

In Tanzania, changes in water resources have been reported from various parts of the country, including protected areas. In these areas, water resources play a critical role in conservation practices, human well-being and providing habitats for wildlife, including migratory species, during the dry season. Several studies (Estes *et al.*, 2006; Mkiramweni *et al.*, 2016; Nyembo *et al.*, 2022) reported a decline in water resources due to prolonged drought conditions and increased human activity in the NCA and surrounding areas. This condition results in reduced hydrological services, which has a significant impact on local communities, wildlife tourism and the economy. Various studies have analyzed the impact of climate and land use/cover changes on water resources in different areas of Tanzania (Hyandye *et al.*, 2018; Näschen *et al.*, 2019; Notter *et al.*, 2013; Twisa *et al.*, 2020). These studies have analyzed the effects of climate and land use/cover changes using hydrological models ranging from very simple water

balance models to complex models, which can simulate a variety of water resource components. These studies have improved our understanding of the impact of climate and land use/cover change on hydrology and water resources. However, determining how climate and land use/cover changes might affect hydrological conditions at the local scale is still a challenge. The challenge arises from the uncertain magnitude of climate and land use/cover changes at the local scale, particularly in areas with scarce data. In these areas, the performance of the hydrological models varied between catchments as well as between sub-catchments within a large catchment. The variations in hydrological modeling explained the heterogeneous effects of catchment properties, variations in local climate conditions and prevailing hydrological regimes. This condition creates a knowledge gap in understanding the interaction between climate change and changes in land use/land cover on temporal and spatial variations of hydrological variables (e.g., surface and groundwater recharge and runoff, evapotranspiration, and so on), as well as groundwater quality at the local scale. Studies addressing both climate change, land use/cover change and watershed hydrological processes are among the priorities for water management issues and for reducing a gap between current knowledge and policy needs. Therefore, this study aimed to carry out a scenario analysis approach to evaluate the hydrological response of water resources to climate change and land use change; to ensure the sustainability of water resources in wildlife hotspot areas. The outcome of this study will provide the essential information to guide the development of a water resource management plan for sustainable water resources available for ecosystem human well-being, as well as for adaptation and mitigation measures.

1.3 Rationale of the Study

The study area covers tourist centers with a unique ecosystem which integrates humans and wildlife. It includes the Ngorongoro conservation area (NCA), the most visited conserved area in Tanzania and East Africa (Melita & Mendlinger, 2013). The high number of tourists visiting the area generates millions of dollars and supports many jobs. The area is also essential for migratory species from Serengeti national park during the dry season (Estes *et al.,* 2006). However, water availability for human consumption and wildlife has remarkably decreased since the 2000s due to climate change and land use/cover changes (Mkiramweni *et al.,* 2016). This condition may lead to reduced hydrological services, significantly impacting local communities, wildlife tourism, and the economy. In this regard, appropriate studies are necessary to analyze and characterize how hydrological systems respond to the changes to

enable policymakers to develop better adaptation strategies. These studies will provide a framework to ensure the sustainability of water resources in the wildlife hotspot areas. Furthermore, will provide vital information that will guide the development of a water resource management plan. This information will enable policymakers to develop better adaptation strategies for sustainable water resources available for the human welfare ecosystem and climate change impact adaptation and mitigation measures.

1.4 Research Objectives

1.4.1 Main Objective

The main objective of this study is to evaluate the response of hydrological components to climate and land use/cover changes for future water resources management and sustainable development. This work is supported by four specific objectives, which include:

1.4.2 Specific Objectives

(i) To evaluate temporal and spatial changes of climate in the study area for the future period, 2021-2050 compared to baseline 1982-2011.

(ii) To examine the land use/cover change between 1995 and 2016 and model the future scenarios for 2025 and 2036 in the study area.

(iii) To model the response of hydrological processes (runoffs and stream flows) to future (2021-2050) climate change compared to baseline (1982-2011), and land use/cover change of 2025 and 2035 compared to baseline 2016 in the study area.

(iv) To characterize the hydrochemical composition of water resources in the study area and analyze their movement to groundwater as influenced by climate and land use/cover changes in the study area.

1.5 Research Questions

(i) How would climate changes in space and time for the future 2021-2050in the study area?

(ii) How did land use/cover change between 1995 and 2016, and what would be the future change?

(iii) How do hydrological processes in the study area respond to climate and land use/cover change?

(iv) What is the hydrochemical composition of water sources in the study area in the natural state, and how does climate change influence their movement to the groundwater?

1.6 Significance of the Study

The present study is for the watersheds surrounding the Ngorongoro Conservation Area (NCA) in Northern Tanzania. The NCA is one of the major tourist and biodiversity hotspots on the African continent and an essential ecosystem for migrating wildlife species from the Serengeti national park during the dry season (Estes *et al.*, 2006; Mkiramweni *et al.*, 2016). The area is at high risk of climate change impacts due to the increased frequency of drought conditions and limited water resources for the local community and wildlife (Mkiramweni *et al.*, 2016). Given the area's high sensitivity to climate extremes and land use/cover changes, an in-depth study at the local scale is urgently needed to develop long-term adaptation strategies. As a result, this research aimed to conduct a scenario-based analysis of hydrological responses to climate and land use/cover change for water resources management plan. Effective water management under changing conditions, in particular, necessitates reliable data on flows and models that can be used to simulate flow regimes under various land use and climate scenarios.

1.7 Delineation of the Study

This research focuses on the Tanzania mainland in the conservation areas of Northern Tanzania, mainly the Ngorongoro Conservation Area (NCA) and the surrounding regions. The study performed climate downscaling and land use/ cover modelling to determine the hydrological response to future climate and land use/cover change in NCA and surrounding catchments. The SWAT modelling approach was applied to determine the quantitative impacts. In contrast, the HYDRUS 1D model was applied to determine water quality's hydrochemical movement from surface to groundwater. The National Institute of Hydrology (NIH) Laboratory at the Indian Institute of Technology Roorkee (IITR), India, analyzed the sample for key cations (Na^+, K^+, Mg^{2+}, Ca^{2+}) and anions (Cl^-, SO_4^{2-}, NO_3^-, PO_4^{3-}). The water samples were analyzed using an ion chromatograph instrument (930 Compact IC Flex model). The concentration of major cations and anions

The major limitation of this study was data scarcity in the study area for climate change analysis and hydrological modeling. The most critical but also most limiting was discharge data, which was available in a time series from 1975 to 1989 at downstream gauging stations of Mtowambu and Hynu. Only eight years (1982-1989) of the existing discharge data were suitable for SWAT model setup (model warm-up (1982-1984), calibration (1985 -1987) and validation (1988-1989), which could minimize the confidence of SWAT model in simulating changes in the hydrological components. Furthermore, the observed climate data was unavailable in the study area. Therefore, the study used satellite-based climate data with time series from 1982 to 2020 for historical climate information. The satellite-based data have some constraints in capturing daily rainfall events, which limits this study from assessing the possible climate extremes in the study area. The use of satellite-based climate data and downscaling of GCMs and RCMs scenarios may lead to uncertainties in the output results, likewise, the unavailability of good time series of discharge data for model calibrations and validations. Therefore, the interpretation of the results should consider these limitations. However, the results from this study provide a valuable framework for water resource management plans, better conservation practices around the NCA, and adaptation strategies.

CHAPTER TWO

LITERATURE REVIEW

2.1 Overview

This Chapter provides a summary of the reviewed literature which enabled this study. This study performed the climate downscaling and climate change analysis, land use /cover analysis and prediction, and modelled the hydrological responses to climate and land use/cover changes. Furthermore, the study analyzed the statistical relationship between climate and land use/cover components with hydrochemical transport to the groundwater. Therefore the reviewed literature focused on that subject as follows.

2.2 Climate Change and Climate Downscaling

Climate change is a change in the average weather patterns during an extended period of time (from decades to millions of years) (Haunschild *et al.*, 2016). The United Nations Framework Convention on Climate Change (UNFCCC) refers to climate change only to the anthropogenic changes over comparable periods. However, the intergovernmental panel on climate change (IPCC) regards climate change as both natural variability and human-induced change, even though most of the observed increase in global average temperature since the mid-twentieth century is likely related to the anthropogenic activity (Scott *et al.*, 2016).

The IPCC reported the increase in the greenhouse gases such as carbon dioxide (CO_2), methane (CH_4) nitrous oxide (N_2O) due to anthropogenic activities (Aggarwal, 2007; Parry *et al.*, 2007). This report has indicated that global temperature has risen by 0.74°C from 1906-to 2005 at the rate of 0.13°C /10year for the past half-century due to the increase of greenhouses in the atmosphere. A further rise in temperature of about 1.1- 6.4°C has also been predicted during the next century (Pachauri *et al.*, 2014). Long term changes (1906-2005) in rainfall have also been reported in different parts of the globe, with more extended drought over a large area from 1970 (Pachauri *et al.*, 2014).

This study consider a climate change for a period of 30 years including 1982-2011 baseline period to compare with 2021-2050 future climate under Representative Concentration Pathways (RCPs) 4.5 and 8.5). The analysis of climate change mostly relies on the Global circulation Models (GCM) and Regional Climate Model (RCM); however, these models are reported as less capable of capturing local scale change (Gebrechorkos *et al.*, 2019; Gulacha

& Mulungu, 2017; Luhunga *et al.*, 2018; Wilby *et al.*, 2002). These models cannot resolve small-scale features like clouds and topography, reducing their capability to capture local climate; however, the downscaling approach was established (Gebrechorkos *et al.*, 2019; Huang *et al.*, 2011; Li *et al.*, 2019).

Downscaling approach is of two major types, dynamic downscaling and statistical downscaling. Dynamical downscaling is based on using a Regional Climate Model (RCMs), which is similar to a GCM in its principles but with much higher resolution. The RCMs take the large-scale atmospheric information supplied by GCM output at the lateral boundaries. It incorporate more complex topography in order to generate realistic climate information at a spatial resolution of approximately 20 - 50 kilometres (Gebrechorkos *et al.*, 2019; Wilby & Dawson, 2013). Dynamic downscaling depends heavily on the choice of RCMs and physics parameterization. Additionally, errors can occur when RCMs consider GCM's biases as internal variability or true boundary forcing (Zorita & Von-Storch, 1999).

In contrast to dynamical downscaling, statistical downscaling techniques involve establishing empirical relationships between large-scale atmospheric predictors and local climate variables. Once the relationships are determined and validated, the GSM-predicted future atmospheric variables predict future local climate variables (Wilby *et al.*, 2002). The statistical downscaling model's challenge is the need for long-term data for at least 30 years to build a reliable statistical relationship between predictors and predictands (Li *et al.*, 2019; Wilby *et al.*, 2002). Statistical downscaling is cheap in the computation process and can provide the local scale information needed for impact analysis studies.

However, this approach is based on the key assumption that current large-scale circulation and local climate relationships are still valid under a variety of possible forcing conditions in future climatic zones (Zorita &Von-Storch, 1999). In the dynamical downscaling, the internal variability in a Regional Climate Model can become large if the local processes that contribute to the climate are changing. This weakness in Dynamical Downscaling has led to the continued employment of statistical downscaling or bias correction in order to use dynamic downscaled information for application studies (Sieck & Jacob, 2016).

The statistical downscaling has been applied by different scholars in East Africa at the regional or local scale using the GCM output (Gebrechorkos *et al.*, 2019; Gulacha & Mulungu, 2017). However, few have performed the statistical downscaling in Tanzania for hydrological impact

assessment (Ayugi *et al.*, 2021; Shagega *et al.*, 2019; Tibangayuka *et al.*, 2022; Wambura, 2014). However, most of these studies were carried out at the regional level, which are less relevant for planning and managing water resource infrastructures at the catchment scale (Pachauri & Meyer, 2014). Furthermore, each catchment possesses different information regarding climate change impacts; therefore, hydro-climatic studies at the watershed level are necessary (Mbungu & Kashaigili, 2017).

Rainfall and temperature are two main climatological elements that affect the hydrological processes. It has been found that the prediction of these elements is complex in tropical areas like Tanzania (Gulacha & Mulungu, 2017; Wambura *et al.*, 2014). Small scale convective processes mainly control the rainfall in Tanzania; hence modelling the future changes needs a downscaling approach at a local scale (Luhunga *et al.*, 2018).

The Statistical Downscaling System Model (SDSM) is one of the most applied climate downscaling models for regional and local climate impact studies. The SDSM is an open-access software developed using a stochastic weather generator and transferred statistical function method. The SDSM is designed to statistically downscale simulated climate information from either coarse-resolution GCM output or large atmospheric variables to high-resolution forms needed for local impact studies using predictors and predictands (Gebrechorkos *et al.*, 2019; Hashmi *et al.*, 2011). The SDSM uses multivariate linear regression to simulate future climate scenarios by combining stochastic weather generator and transfer function models (Wilby *et al.*, 2002). The stochastic data was included in the SDSM to improve the model's performance in reproducing the observed daily series by inflating the model output variance (Wilby *et al.*, 2002).

Apart from SDSM, other statistical downscaling models exist, for instance, LARS-WG, which is a stochastic weather generator designed to simulate the daily climate data at a station scale for climate change impact studies (Chen *et al.*, 2013; Chisanga *et al.*, 2020; Hassan *et al.*, 2014; Semenov & Barrow, 2002). The LARS-WG is a numerical model which synthesizes daily time series of various climate variables, such as precipitation, temperature and solar radiation, with certain statistical properties (Racsko *et al.*, 1991; Richardson, 1981; Richardson & Wright, 1984), which resembles the daily series at the station level.

There are various advantages to developing stochastic weather generators and using synthetic weather data instead of observed weather data. For instance, the production of long-enough weather data time series to be used in risk assessments in hydrological or agricultural

applications (Semenov *et al.*, 1998). The usefulness of the SDSM and LARS-WG is linked to their ability to capture inter-annual climate variability (Gebrechorkos *et al.*, 2019; Hashmi *et al.*, 2011; Hassan *et al.*, 2014). Furthermore, in the absence of ground-based data, high-resolution satellite-based products and reanalysis products may be used to generate high resolution station-based rainfall and temperature weather series (Gebrechorkos *et al.*, 2019; Saraf & Regulwar, 2016).

Despite the significant progress in climate change impact assessment studies, a comprehensive basin-scale study attributable to national level water availability is necessary for Tanzania. Also, little is known about climate change impacts on hydrology and water resources in Tanzania, particularly at the watershed level. Moreover, there are limited studies carried out using statistical downscaling to assess the impacts of climate change at a local scale (Gebrechorkos *et al.*, 2019; Gulacha & Mulungu, 2017).

Downscaling is a key step in understanding future climate impacts at a watershed level, as the underlying processes that determine impact require an understanding of the local climate and its drivers, such as topography (Gebrechorkos *et al.*, 2019). The watershed modeler may use downscaled GCM products to calculate the best water resources. There are many different downscaling methods and techniques available, so it is important to understand which one is best for specific study and location (Zorita & Von-Storch, 1999) as hydrological possesses are site-specific.

This study applied the SDSM and LARS-WG to simulate the rainfall and temperature scenarios for future 2021-2050 from GCM to point (station scale). The study used fourteen gridded daily rainfall point data from the Climate Hazards Group Infrared Precipitation with Station (CHIRPS) with 0.05°spatial resolution (Funk *et al.*, 2015). In addition, the study used maximum and minimum Modern-Era Retrospective analysis for Research and Applications, version 2 (MERRA-2) temperature data with 0.5°spatial resolution. The MERRA-2 was obtained from the National Aeronautics and Space Administration of Worldwide Energy Resource (NASA POWER) project (Westberg *et al.*, 2013). The data were extracted the period of 30 years (1982-2011) which was considered as a baseline climate condition.

Statistical downscaling could be appropriate for this study as it is located in heterogeneous areas where point scale information is required. However, this study opted to assess rainfall and temperature projections and its impact on the water Resources using a Hybrid of dynamically and statistically downscaled data (Adeyeri *et al.*, 2020; Larbi *et al.*, 2021). The

study used an ensemble mean of four bias-corrected four CORDEX RCMS and output from SDSM and LARS-WG simulations for climate change analysis and hydrological model input.

2.3 Land use/cover Change

Land use/cover change is a topic that has inspired a diversity of research efforts and resulted in various approaches to identify past change and forecasting future development. The phrases Land use and Land cover are not practically similar; this study draws attention to their distinct qualities to distinguish them. Scientists have different definitions of land use and land cover; for example Ellis and Pontius (2006) refer to land cover as the physical and biological cover over the surface of the land, including water, vegetation, bare soil, and/or artificial structures. However, other scientists argued that land use encompasses both the technique in which the land's biophysical features are altered and the intent underlying that manipulation, the purpose for which the land is utilized (Millette *et al.*, 1995).

Furthermore, Turner *et al.* (2007) distinguish between land cover and land use by terming what can be seen, such as grass or a building, as a land cover while how land types are actually used, such as grassland for cattle grazing or water bodies for irrigation as land use. However, this study will often use the word land use/cover throughout to refer to both the land cover and the actual land usage. Land use/cover change is recognized as a complex process resulting from the mutual relationship between natural environmental and human activities at various geographical and temporal dimensions (Rindfuss *et al.*, 2004; Valbuena *et al.*, 2008).

Globally variations in land use/cover are the key anthropogenic drivers of ecological change on all time-based and spatial scales (Lambin *et al.*, 2003; Näschen *et al.*, 2019; Turner *et al.*, 2007). These changes are complex and caused by many factors, including physical and human factors (Huang *et al.*, 2008). Furthermore, they encompass ecological fears, including; biodiversity loss, climate change, and natural resource pollution such as soils, water and air (Slingenberg *et al.*, 2009; Twisa *et al.*, 2020). Land use/cover change has developed unique concerns in natural resource control and sustainable development on a local and global scale (Foley *et al.*, 2005; Fu *et al.*, 2015; Yirsaw *et al.*, 2017). Furthermore, monitoring and mitigating the adverse effects of land use/cover while supporting fundamental resource production has become a key priority for policymakers and researchers worldwide (Ansari & Golabi, 2019).

Impacts of Land use/cover change on ecological changes are commonly studied in several areas using multi-temporal image methods (Basommi *et al.*, 2016). The studies revealed that human actions and natural disturbances are the fundamental drivers of Land use/cover changes (Lamichhane, 2008; Mishra *et al.*, 2014; Singh *et al.*, 2018). Also, findings acknowledged agricultural development and population growth as the major drivers of land use/cover changes (Chomitz & Thomas, 2003; Defries & Rosenzweig, 2010; Kindu *et al.*, 2015; Mannan *et al.*, 2018; Pullanikkatil *et al.*, 2016; Serneels *et al.*, 2001; Solomon *et al.*, 2019). Stress on changed land uses are rising worldwide, and examining the consequences of Land use/cover change patterns on natural resources is necessary for future generations (Munthali *et al.*, 2020).

Tanzania, like many other countries, experienced land use/cover changes over the past decades, while very few studies have been conducted to predict future land use/cover change in the country (Näschen *et al.*, 2019; Twisa & Buchroithner, 2019). Studies that assess Land use/cover change patterns to monitor changes with a focus on the conservation of ecosystem services are urgently needed. These will benefit the country to monitor natural resources and strategies toward sustainable development to ensure ecosystem service wellbeing in future (Lu *et al.*, 2022). Therefore, one of the objectives of this study is to analyze the land use/cover patterns of the Ngorongoro Conservation Area (NCA) and monitor the land use /cover over the area.

The NCA is the habitat of the world's predator animals (lions, leopards, cheetahs, and spotted hyenas) and major herds, such as wildebeest, gazelles, and zebras which attracts the tourism activities (Estes & Small, 1981; Kabigumila, 1993). However, the NCA's attraction and economic potential due to organized safari tourism come with its challenges, including increasing human activities (Charnley, 2005; Nyahongo *et al.*, 2009). Several human activities result in increased environmental degradation (Nyahongo *et al.*, 2009) by causing competition among different land users. Therefore, the Land use/cover change and future NCA pattern study are crucial for successful management strategies of ecosystem services in this World Heritage Site.

Different models have been established to forecast and simulate Land use/cover change, including artificial neural networks, statistical analysis, cellular automata, and Markov chain (Chen *et al.*, 2021; Koomen *et al.*, 2018; Subedi *et al.*, 2013). Several studies indicate that the CA–Markov model, when combined with RS and GIS; the combination creates a suitable method for studying the changes of land use/cover change (Aliani *et al.*, 2019; Li & Reynolds,

1997; Myint & Wang, 2006). The CA–Markov model is a robust method in modelling Land use/cover change, changes since RS can be well incorporated (Kamusoko *et al.*, 2011). The CA–Markov model understands the temporal succession and spatial projections of the Markov and CA theory, and it can be used to conduct pattern simulation (Sang *et al.*, 2011). The CA–Markov model similarly reflects the Land use/cover change, changes' suitability and the influence of natural, economic, and societal factors concerning land use/cover changes (Twisa & Buchroithner, 2019).

Numerous studies used CA-Markov, including Geographical Information System (GIS) and Remote Sensing (RS) techniques, in land use/cover modeling and simulation (Baja *et al.*, 2014; Kityuttachai *et al.*, 2013; Subedi *et al.*, 2013). Based on the previous investigation and the current trend toward land use/cover change projection, this study examined the Land use/cover change using the CA–Markov model. The CA-Markov approach is suitable for this study as it incorporate GIS and RS to quantitatively estimate the spatial and temporal land use/cover dynamic (Arsanjani *et al.*, 2013; Mishra & Rai, 2016). Application of GIS and remote sensing with the CA-Markov model reduce the cost and time needed for analysis (Arsanjani *et al.*, 2013). The output of this research will contribute to the existing or assist build a new scientific knowledge base on the spatial-temporal change of land use/cover change and link to ecosystem services of NCA. This will benefit the all stakeholders including natural resource professionals, policymakers, researchers as well as community regarding sustainable management and monitoring of land use and ecosystem services including water resources availability.

2.4 Impact of Climate Change and Land use/cover Change and Water Resources

Climate change is one of the major drivers that affect the energy and mass balance of the water resources, including the intensification of the water cycle (Huntington, 2006), which makes the hydrological patterns very likely to be different under different climates scenarios (Jarvie *et al.*, 2008). Under natural conditions, climate conditions are considered one of the major influences of hydrological variations with crucial social and economic implications for water resources (Bornschein & Pohl, 2018; Chang & Bonnette, 2016). Any water bodies like rivers, lakes, reservoirs, springs and swamps are considered a water sources (Chang & Bonnette, 2016). Climate change's impact on the water sources may include any changes in river discharges, lake levels and wetland due to changes in climate parameters such as precipitation, temperature (maximum and minimum), relative humidity and evapotranspiration (Chiew & Mcmahon, 2002).

There is considerable evidence underlining the decline in the volumes of water stored in lakes and rivers due to the decrease in long-term average precipitation and runoff and increased evaporation rates (Sharma *et al.*, 2021). These conditions necessitate the study on water sources and their interaction with climate change for development of water resources management plans. Better scientific understanding of the link between hydrological processes and climatic conditions and changes is thus a key issue for effective water resource management and its climate adaptation (Koutsouris *et al.*, 2010; Yira *et al.*, 2016). However, managing hydrological services cannot operate without monitoring or adaptive management.

Furthermore, land use/cover change is another driver that can have an impact on water resources and should be considered in hydrological studies. Changes in land use/cover have been shown to have a significant impact on regional hydrology (Näschen *et al.*, 2019). As a result, hydrological impact assessment studies may be unrealistic if the influence of land-use change is not included (Giertz *et al.*, 2005; Yira *et al.*, 2016). A significant increase in changes in several forms of land use/cover (e.g., urbanization, deforestation, and agriculture) has been reported as a result of global population growth posing difficulties to water resource availability (Abdulkareem *et al.*, 2018). Globally, water resources have been under intense stress to meet the requirements of an expanding population. As a result, in many locations, the future availability of appropriate quantities of water for agricultural and human purposes has become uncertain (Rosegrant *et al.*, 2009; Torbick *et al.*, 2006). Land use/cover change seriously affects water resources (Pervez & Henebry, 2015).

Land use/cover change is the most direct factor of the interaction between human activities and the natural environment that link directly to the hydrological processes (Liu *et al.*, 2014), which impact the condition of water resources' availability. Increased land use/cover changes impact water resources primarily through plant interception, evapotranspiration, runoff, surface infiltration, soil moisture status, and so on, influencing the process of watershed hydrology and water resource cycles (Zhu *et al.*, 2018).

Water resources are impacted by both climate change and land use/cover change regarding water quantity and quality. Therefore, research into the effects of climate change and land use/cover change on stream flow and water quality within a river basin has become a hot issue in hydrology and water resource studies (Liu *et al.*, 2017). Several studies have been done on this topic (Defries & Eshleman, 2004; Ed-Chaves *et al.*, 2020; Twisa *et al.*, 2020; Wang *et al.*,

2014; Zhu *et al.*, 2018). Currently, hydrological models are the most widely applied method to quantify the hydrological conditions of water sources (Zhao *et al.*, 2010).

2.5 Hydrological Models

Hydrological models are among the available tools used to predict water quantity and quality for decision makers (Chow *et al.*, 1988). Some of these models could also predict the impact of natural and anthropogenic changes on water resources and also quantify the spatial and temporal availability of resources. However, the challenges lie in the selection and use of these models for a specific basin and management plan (Maliehe & Mulungu, 2017). The hydrological models treat the water cycle as a system comprising its various components as inputs such as precipitation and outputs such as runoff, using a set of equations linking inputs and outputs (Chow *et al.*, 1988). When classifying models, stochastic and deterministic models are often considered to be at the top level of the classification tree, according to the way they treat the randomness of hydrological phenomena (Chow *et al.*, 1988).

Stochastic models use local hydrometric data to predict flows. These models allow for some randomness, leading to different outcomes, and are based on analysis of past events, typically rainfall and river discharge (Akhtar *et al.*, 2009; Tesfaye *et al.*, 2006). Deterministic models generally produce a single output of runoff for a given rainfall under identical physical environments. Deterministic models can be classified as; lumped models, in which a variable or parameter is assumed to have an average value for the entire catchment; and distributed models, in which all variables and parameters have different values that account for spatial variation in the catchment (Daggupati *et al.*, 2015; Zeng *et al.*, 2018).

Deterministic models can be further classified into empirical, conceptual, and physically based models. Empirical models, which are usually lumped together, are based on analyzes of parallel input-output time series without explicitly considering physical processes (Daniel *et al.*, 2011; Faiz *et al.*, 2018). One of the newer methods in this category is an Artificial Neural Network (ANN) model that can learn recursively from the data, also known as a data-driven model (Antar *et al.*, 2006; Govindaraju, 2000). Conceptual models, which can be aggregated or distributed, generally consist of mathematical descriptions of the processes of catchment response. These models represent the catchment as integrated conceptual components, but also include some aspects of physical processes. Some examples of conceptual models are the Soil

and Water Assessment Tool (Arnold *et al.*, 1998) and the HYDRUS 1D model (Šimůnek *et al.*, 2008).

2.6 Soil and Water Assessment Tool

The Soil and Water Assessment Tool model is a continuation of nearly 30 years of modeling efforts conducted by the USDA Agricultural Research Service (ARS). The Soil and Water Assessment Tool model (Arnold & Fohrer, 2005; Arnold *et al.*, 1998) has proven to be an effective tool for assessing water resource and non-point pollution issues for a variety of scales and environmental conditions around the world proven. The development of SWAT is a continuation of USDA Agricultural Research Service modeling experience spanning approximately 30 years.

The early origins of SWAT can be traced back to previously developed USDA-ARS models, including the Chemicals, Runoff, and Erosion from Agricultural Management Systems (CREAMS) model (Knisel, 1980), the Groundwater Loading Effects on Agricultural Management Systems (GLEAMS) model (Leonard *et al.*, 1987) and the Environmental Impact Policy Climate (EPIC) model (Izaurralde *et al.*, 2006), originally called the Erosion Productivity Impact Calculator (Williams, 1990).

The current SWAT model is a direct descendant of the Simulator for Water Resources in Rural Basins (SWRRB) model (Arnold & Williams, 1987), which was developed to calculate the effects of management on water and sediment movement for ungauged rural basins in to simulate the United States.

The SWRRB development began in the early 1980s with a modification of the CREAMS daily precipitation hydrology model. A major improvement was the extension of surface runoff and other calculations for up to ten sub-basins, as opposed to a single field, to predict the water yield of the basin (Arnold & Williams, 1987). Other improvements included an improved peak runoff rate method, calculation of transmission losses, and the addition of several new components: groundwater return flow, reservoir storage, the EPIC crop growth sub-model, a weather generator, and sediment transport (Arnold *et al.*, 1993). These modifications enhanced the model's ability to cope with a wide variety of water quality management problems in catchment areas.

Arnold *et al.* (1995), developed the Routing Outputs to Outlet (ROTO) model in the early 1990s to aid in evaluating the downstream impacts of water management on Indian reservation lands in Arizona and New Mexico; covering several thousand square kilometers, as required by the US Bureau of Indian Affairs. The analysis was performed by linking the results of multiple SWRRB runs and then routing the flows through channels and reservoirs in ROTO via a reach-routing approach (Arnold *et al.*, 1995). This methodology overcame the SWRRB restriction of only allowing ten sub-basins; however, inputting and outputting multiple SWRRB files was cumbersome and required significant computer memory.

To overcome the awkwardness of this arrangement, the SWRRB and ROTO were merged into a single SWAT model (Arnold *et al.*, 1998). The SWAT retained all of the features that made SWRRB such a valuable simulation model, while allowing simulations of very large areas. The SWAT has been continuously reviewed and expanded since its inception in the early 1990s (Arnold *et al.*, 1998). Important improvements for previous versions of the model (SWAT 94.2, 96.2, 98.1, 99.2 and 2000) are reported by Arnold and Fohrer (2005) and Neitsch (2005), including the incorporation of instream kinetics routines from the QUAL2E model (Brown & Barnwell, 1987). The latest version is SWAT 2012 and it source code is freely available online (https://swat.tamu.edu/). The SWAT model operates on a daily time step and is designed to predict the impact of land use and management on water, sediment, and agricultural chemical yields in unmeasured watersheds (Arnold *et al.*, 2010; Gassman *et al.*, 2010).

The SWAT model has been used to project the effects of climate and land use/cover change on streamflow in both small watersheds and large river basins (Arnold & Fohrer, 2005; Dosdogru *et al.*, 2020; Gassman *et al.*, 2014). In addition, SWAT has been used for urban and mixed-use watershed modeling (Dixon & Earls, 2012; Eshtawi *et al.*, 2016) and is capable of simulating flashy urban storm runoff using sub-hourly time steps (Arnold *et al.*, 2010; Jeong *et al.*, 2010).

Model performance has been comprehensively assessed over the last 30 years (Arnold & Fohrer, 2005; Gassman *et al.*, 2007). Despite having been designed for the U.S condition, studies have shown favorable results from many countries with differing site conditions across watersheds (Ghaffari *et al.*, 2010; Krysanova & Srinivasan, 2015). The SWAT supports varying applications ranging from simulating Land use/cover change impacts, climate change, best management practices for chemicals, irrigation and bacteria management, and sediment and nutrient loading on different watersheds (Lamba *et al.*, 2016; Milewski *et al.*, 2014).

Model calibration in SWAT involves altering or adjusting model parameters, within the recommended ranges, based on observed data to ensure the same response over time (Arnold *et al.*, 2012; Gashaw *et al.*, 2018; Vilaysane *et al.*, 2015). However, the validation involves checking the representation of the parameters by simulating the observed data with an independent data set without adjusting model parameters (Arnold *et al.*, 2010; Vilaysane *et al.*, 2015).

2.7 HYDRUS 1D Model

Over the years, various HYDRUS code software (e.g., SWMS-2D, CHAIN_2D, HYDRUS-1D, HYDRUS-2D, HYDRUS (2D/3D), UNSATCHEM, HP1, and CW2D) have been extensively used for evaluating the flow of water and movement of solute into the soil and groundwater (Šimůnek *et al.*, 2016). However, HYDRUS 1D users are significantly larger than those of HYDRUS (2D/3D) since HYDRUS-1D remains freely available in the public domain and can be downloaded from the HYDRUS website: **www.hydrus2d.com** (Šimůnek *et al.*, 2016).

At the same time, HYDRUS (2D/3D) is distributed commercially for a nominal fee. The HYDRUS-1D model may be used to simulate water flow and transport processes (as well as heat and carbon dioxide movement) in varying saturated mediums in a vertical, horizontal, or generally inclined direction (Šimunek *et al.*, 2012; Šimůnek *et al.*, 2016). For example, HYDRUS (2D/3D) simulates water flow and solute/heat transfer on two-dimensional vertical or horizontal planes, three-dimensional axisymmetrical domains, or completely three-dimensional variably saturated domains (Šimůnek *et al.*, 2008b).

The HYDRUS-1D follows its roots in the early work of SUMATRA and WORM models (Šimunek *et al.*, 2012). The HYDRUS 1D model was updated from time to time and came up with a different version of HYDRUS 1 D. Versions 1 and 2 of HYDRUS-1D (Šimůnek *et al.*, 1998a; Šimůnek *et al.*, 2016) was the first version that included both physical-nonequilibrium (dual porosity mobile-immobile water) and chemical nonequilibrium (two-site sorption model) solute transport. Version 3 of HYDRUS-1D included an option to consider dual-porosity water flow and solute transport.

The major development of HYDRUS 1D in version 4 included dual-permeability water flow and solute transport (Šimůnek & Van-Genuchten, 2008; Šimůnek *et al.*, 2008). Version 4 significantly improved the model's capabilities over Version 3. The HYDRUS 1 D Version

4.01 added vapour flow and fully coupled transport of water, vapour, and energy (Saito *et al.*, 2006). Version 4.01 also evaluates potential evapotranspiration using the FAO, Penman-Monteith combination equation (Smith *et al.*, 1992) or the Hargreaves equation (Hargreaves, 1994). The HYDRUS 1D Version 4.01 also generate intraday variations in evaporation and transpiration rates from daily values.

The HYDRUS versions 3 and 4 added modules for more complex biogeochemical processes than the baseline, which can consider mutual interaction independently between multiple solutes, contrary to versions 1 and 2, which involved a sequential first-order degradation chain (Šimunek *et al.*, 2012). Version 3 of HYDRUS 1D incorporates the UNSATCHEM module (Šimůnek *et al.*, 2007; Suarez & Šimůnek, 1997; Vaughan *et al.*, 1996). The UNSATCHEM module considers the transport of major cations (Na^+, K^+, Mg^{2+}, and Ca^{2+}) and anions (Cl^-, SO_4^{2-}, PO_4^{-3} and NO_3^-) in combination with most or all significant equilibrium and kinetic geochemical events, such as complexation, cation exchange, precipitation, and dissolution (e.g., of calcite, gypsum, and dolomite) (Šimůnek *et al.*, 2016).

Furthermore, Version 4 of HYDRUS-1D now includes the HP1 program (Jacques & Simunek, 2005), which resulted from coupling HYDRUS-1D with the biogeochemical program PHREEQC (Parkhurst & Appelo, 1999). The HYDRUS models are not confined to any specific geographical or temporal scale, as long as the governing equations are adequately written and can be applied at that scale. Many successful applications of HYDRUS-1D have been made at scales ranging from small laboratory soil columns to agricultural applications of soil profiles from one or several meters deep (Gärdenäs *et al.*, 2005; Hanson *et al.*, 2006) to soil profiles several hundred meters deep (Gärdenäs *et al.*, 2006; Scanlon *et al.*, 2003). The HYDRUS-1D model uses numerical methods to solve the Richards equation for variably saturated water flow and the convection dispersion equation for hydrochemical transport in the liquid phase (Šimůnek *et al.*, 2016).

2.8 Regression Analysis to Determine the Relationship between Climate Change, Land use/cover Changes and Movement of Hydrochemical

Water hydrochemical concentrations have frequently been linked to specific land use/cover characteristics using single and multiple regression analyses (Jones *et al.*, 2004; Mahaffey *et al.*, 2013; Noy-Meir, 1974). On the other hand, regression analyses are sensitive to missing data and rely on explanatory factors, and so cannot produce statistically significant findings

until the sample size surpasses the number of variables (Nash & Chaloud, 2011). However, Partial Least Squares (PLS) analysis has shown several advantages over more standard regression methods (De Jong, 1993; Frank *et al.*, 1983). The PLS has been found to generate significant results when the number of samples is minimal compared to the number of variables in chemo-metrics (Rigdon, 2012; Rönkkö *et al.*, 2016). Furthermore, PLS has been discovered to make accurate predictions and identify correlations between data sets with a high degree of collinearity (Chong & Jun, 2005; Pullanagari *et al.*, 2012).

In addition, the prediction error in PLS is lower than that in other multivariate approaches (Chen *et al.*, 2011; Swierenga *et al.*, 1998; Wang *et al.*, 2011). The benefits of PLS discussed above make it an appealing candidate statistical technique for developing landscape ecological models (Schulte & Mladenoff, 2001). Therefore, this study applied the PLS to determine the relationship between climate and land use/cover changes to the movement of hydrochemical (Cations and anions) to the groundwater as modelled by the HYDRUS 1D.

CHAPTER THREE

MATERIAL AND METHODS

3.1 Overview

This Chapter explains the applied methodologies for data analysis in this study. It includes the description of the study area and material and methods used to perform the required analysis for this study.

3.2 Study Area

The study area comprises the world heritage site of the NCA and surroundings covering about 33 452 km^2 area between latitude 2°0'00" to 5°0'00" S and longitude 34°0'00" and 37°0'00" E covering three sub-catchments as shown in Fig. 1. The area is characterized by moist and misty conditions, with the lowest temperatures of about 2°C in June/July. However, the highest temperature observed is 35°C during February in the semi-arid zones (Niboye, 2010). Rainfall in this area is seasonal and highly variable, ranging from 400 to 600 mm/year over the arid lowland plains in the west and 1000 to1200 mm/year over the highland forested areas in the east (Lawuo *et al.*, 2014). A bimodal seasonal variability characterizes the area, with two wet seasons from October to December and March to May, and two dry seasons from January to February (short dry season) and a between June and September (long dry period) (Żaba & Gaidzik, 2011a).

Ecologically, the area is divided into five zones: (a) the Crater highlands (b) Salei plains, (c) Gol Mountains, (d) Serengeti plains, and (e) Kakesio/Eyasi Mountains (Mkiramweni *et al.*, 2016). The area consists of a complex vegetation structure, ranging from montane forest and tussock grassland in the highlands to semi-arid woodlands and short grasslands in the lowlands (Niboye, 2010). Regarding land use, the protected area is mainly covered with natural and semi-natural vegetation, wildlife and tourism, pastures, and small-scale rainfed agriculture in the northern parts, whereas small-scale mechanized in the southern part farming is predominant (Ngana *et al.*, 2003). The volcanism and tectonic movements' active from the north to south of the East African Rift Valley system have influenced the area's geology. The system is responsible for forming the northern part and the Lake Manyara landscapes in the southern part of the study area (Żaba & Gaidzik, 2011b). Trachytic to Trachyandestic rock materials resulting from the volcano's pre-collapse occupy the Ngorongoro areas (Mollel & Swisher Iii, 2012). Neoproterozoic metamorphic rock forms the Mozambique belt and underlies

sedimentary and volcanic rocks at the Lake Manyara catchment (Dawson, 2008). The metamorphic rocks, mostly quartzite and gneiss covered by volcanic rocks and basalts, occupy the Lake Natron catchment (Schwartz *et al.*, 2012).

Lithological, the area is dominated by Olduvai beds with a maximum thickness of 140 m. The Olduvai beds are subdivided into seven layers above underlying basalts, including layers I-IV underneath the Masek, the Ndutu, and the Naisiusiu layers (Curtis & Hay, 1972; Walter *et al.*, 1991). Layers I and II are the earliest deposits with a thickness of 62 m (of which 20-30 m are covered by layer II), comprised of airfall tuffs, reworked tuffs, olivine, and ignimbrites. Layer III (7-9 m thick) and layer IV (2 m thick) are deposited on alluvial plains, which receive metamorphic and volcanic sediments, which are mainly consisted of claystone and sandstones containing illite and smectite (Hay & Kyser, 2001). The Maseck layer (12 m thick) overlies layers III and IV, followed by the Ndutu layer (18 m thick). The Masek layer comprises wind deposited Tephra and detrital sediments, while the Ndutu layers comprise small deposits of sands, conglomerates, and tuffs. The Naisusu layer (about 8 m thick) was deposited after the erosion of the Ndutu layers. The layer consists of Aeolian tuffs formed from the Olduvai gouge and Tephra developed from the Oldonyo Lengai volcanic eruptions. However, in the southern part of the study area, there are Manyara beds which consist of the upper and lower members. The upper member is covered by a thin (3-5 m) series of brown sandstone with breccia and Marls overly the volcanic rocks. Fine-grained greyish green deposits mainly cover this superimposed fluvial section. The lower member comprises 15 m of light grey to light greenish-grey mudstones, siltstones, diatoms, marls, and tuffs (Ring *et al.*, 2005). Furthermore, the lower member's lower 5- 6 m is covered by the deeper lacustrine facies, including mudstones (Ring *et al.*, 2005).

Hydrologically, the NCA is a protected semi-arid catchment bordered by a 600 m caldera wall that encloses surface water sources, including lakes, streams, springs, and swamps (Deocampo, 2004). In Lake Manyara, catchment area water sources include the shallow alkaline, saline lake Manyara with a depth of about 1.18 m (Deus *et al.*, 2013); with two main tributaries (Kirurumo and Mto wa mbu), and two seasonal rivers (Makuyuni and Simba) (Ngana *et al.*, 2003). Other water sources are the underground springs originating from crater highlands above the lake Manyara catchment (Schwartz *et al.*, 2012). In Natron, the area is covered by the transboundary lake Natron shared with Kenya in the northern part, and the area consists of freshwater springs and perennial rivers (Dawson, 2008). Looking at the groundwater, the area's water table differs in different locations based on catchment characteristics and interconnection with other

catchments. For instance, the NCA water table ranges between 2 to 39 m, while in Lake Manyara water table ranges between 3 m and 80 m, and at Natron, the water table could not be measured due to the lack of proper aquifer in the area (Ministry of Water [URT], 2014). However, these depths may not cover all aquifers in the NCA and surroundings; therefore, data collection and different exploration studies are required. Besides, water resources in these areas are subjected to depletion in terms of quantity and quality due to natural hazards such as climate change and anthropogenic activities (Deocampo, 2004). The quality deterioration is majorly due to volcanic lithology, mineral precipitation, dissolution, and agriculture activities (Ligate *et al.*, 2021).

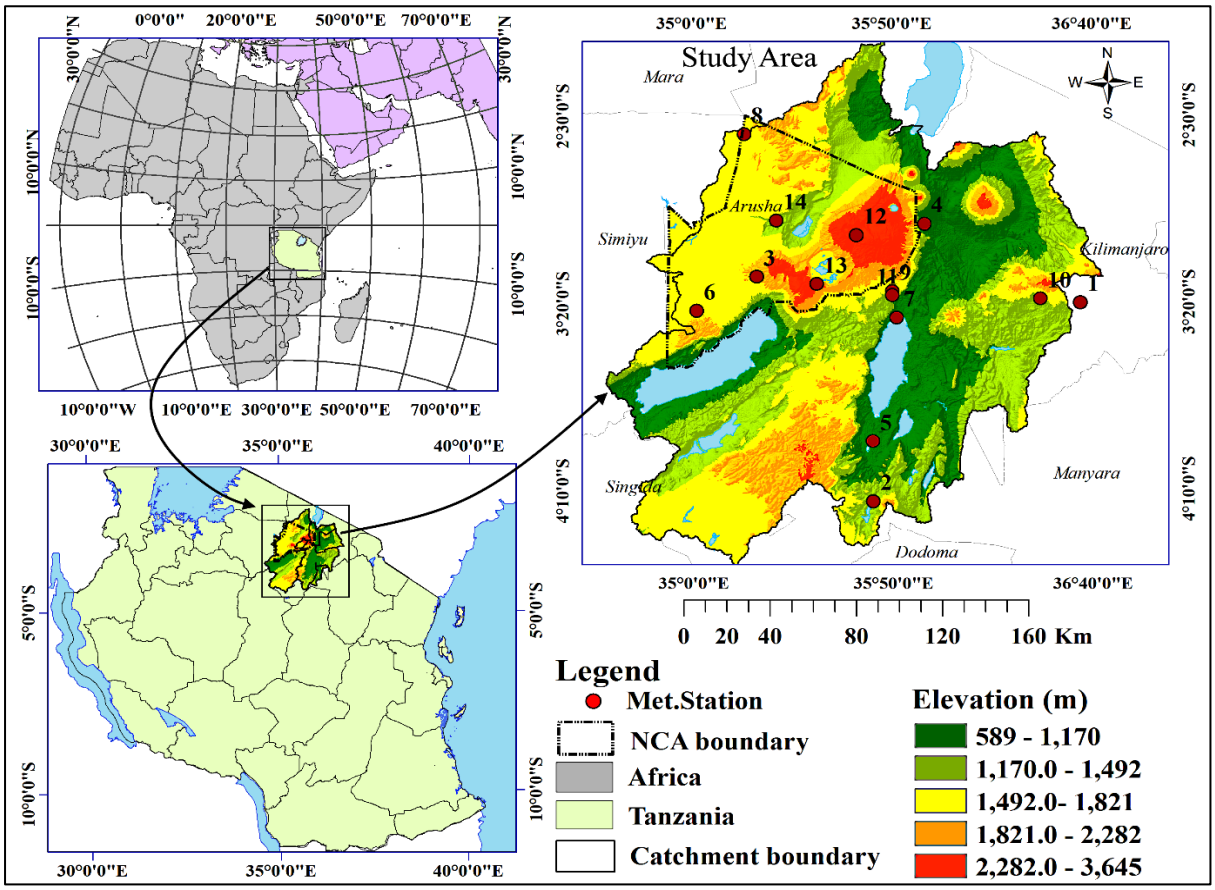

Figure 1: **Map of Africa (top left) indicating Tanzania (bottom left) and the Ngorongoro Conservation Area (NCA) and surroundings (right). The red dots on the NCA are the individual meteorological stations**

3.3 Materials

3.3.1 Data Acquisition, Quality Control, and Validation for the Downscaling and Analysis of the Climate Variability and Changes in Time and Space in the Study Area

(i) Observation Data

Historical daily rainfall, maximum and minimum temperature, and observed station data from 1982 to 2011 for four climate stations of Arusha, Babati, Enduleni, and Ngorongoro were obtained from the Tanzania Meteorological Authority (TMA). Data quality control was performed on the four climate stations to select the meteorological station with data gaps not exceeding 10% of the study period (Larbi *et al.*, 2018; Nkiaka *et al.*, 2017). Only the Arusha station passed this quality assurance test for rainfall and temperature data. Due to the historical data limitations and uneven spatial distribution of climate stations at the catchment, fourteen gridded daily rainfall point (Fig. 1) data from CHIRPS and MERRA-2 maximum and minimum temperature data for the period of 1982-2011 were extracted. In order to validate the applicability of the satellite-based climate products (i.e., CHIRPS precipitation and MERRA-2 maximum and minimum temperature), a comparison was made between the satellite-based data extracted for Arusha and historical daily precipitation and temperature data from the Arusha station. Arusha station data was used for validation as Arusha was the only station near the study area with less than 10% data gap. The statistical results of the CHIRPS precipitation data showed NSE = 0.51, PBIAS = -16.10 and RSR = 0.68 on the daily time scale and NSE = 0.78, PBIAS = -8.2 and RSR = 0.46 the monthly time scale. Therefore, the CHIRPS precipitation data for station Arusha can be compared very well with the observation data on a monthly time scale.

The validation of the MERRA-2 data for the Arusha station also showed good agreement with the observation data on daily and monthly timescales for both maximum and minimum temperature. The statistics showed that NSE = 0.82, PBIAS = -13.7 and RSR = 0.58 for the maximum temperature and NSE = 0.93, PBIAS = -12.7 and RSR = 0.39 for the minimum temperature for a daily time scale. For the monthly time scale, the indices showed that NSE = 0.88, PBIAS = -8.4 and RSR = 0.54 for maximum temperature and NSE = 0.96, PBIAS = -14.4 and RSR = 0.48 for the minimum temperature. The validation of the CHIRPS precipitation and the MERRA-2 maximum and minimum temperature on the point scale compared very well to the observation data from the Arusha station. Therefore, this study used CHIRPS

precipitation and MERRA-2 maximum and minimum temperature data on a point scale for 14 gridded points covering the study area (Fig. 1). The study CHIRPS and MERRA-2 data in a place and observed data for climate downscaling and climate change analysis (Gebrechorkos *et al.*, 2019; Larbi *et al.*, 2018; Molua, 2009; Mwabumba *et al.*, 2022).

(ii) National Centre for Environmental Prediction and Canadian Earth System Model Predictors for Statistical Downscaling

In the present study, twenty-six predictors (Table 1) obtained from the National Centre for Environmental Prediction (NCEP) covering the historical period (1961-2005) were used (Gebrechorkos *et al.*, 2019; Gulacha & Mulungu, 2017). The second-generation Canadian Earth System Model (CanESM2) predictors for RCP 4.5 and RCP 8.5 scenarios for the future (2006- 2050) with a spatial resolution of 2.81° were used for downscaling of the future rainfall and temperature. The selected scenarios have been principally used to run different models for the analysis based on medium- and high-range emission scenarios.

Table 1: National Centre for Environmental predictors used during the screening process

S/N	Predictors	S/N	Predictors
1	Mean sea level pressure	14	500 hPa divergence
2	1000 hPa wind speed	15	850 hPa wind speed
3	1000 hPa zonal velocity	16	850 hPa zonal velocity
4	1000 hPa meridional velocity	17	850 hPa meridional velocity
5	1000 hPa vorticity	18	850 hPa vorticity
6	1000 hPa wind direction	19	850 hPa geopotential height
7	1000 hpa divergence	20	850 hPa wind direction
8	500 hPa wind speed	21	850 hPa divergence
9	500 hPa zonal velocity	22	Total precipitation
10	500 hPa meridional velocity	23	500 hPa specific humidity
11	500 hPa relative vorticity	24	850 hPa specific humidity
12	500 hPa geopotential height	25	1000 hPa specific humidity
13	500 hPa wind direction	26	Air temperature at 2 m

(iii) Regional Climate Models Dataset

The RCMs datasets (Table 2) at 50 km resolution from the CORDEX-Africa experiment were used for this study. The four CORDEX-Africa RCMs (REMO2009, CanESM2-RCA4, NorESM1-RCA4 and KNMI-RACMO22T) are downscaled dynamically from GCMs. The RCM datasets used in this study at a daily scale consist of rainfall, minimum and maximum temperature for the RCM historical (1981–2005) and RCP 4.5 and 8.5 projected (2021–2050)

period. These RCMs were chosen because they were found to perform well over the sub-region with an acceptable range of biases (Kim *et al.*, 2014; Larbi *et al.*, 2020; López-Moreno *et al.*, 2011).

Table 2: Description of the Regional Climate Models used in this study

S/N	Institute	Forcing GCM	RCMs
1	Swedish Meteorological and Hydrological Institute, Rossby Centre (SMHI)	CCCma-CanESM2 CNRM-CERFACS- CM5 NCC-NorESM1-M	CanESM2-RCA4 and NorESM1-RCA4
2	Max Planck Institute-Computational methods in systems and control theory (MPI-CSC), Germany	ICHEC-ECEARTH	REMO2009
3	Koninklijk Nederlands Meteorologisch Instituut (KNMI)	ICHEC-ECEARTH	KNMI-RACMO22T

3.3.2 Data Acquisition and Quality Control for Analysis of Land use/cover Changes and Modeling of the Future Scenarios in the Study Area

This task involved the application of three Landsat images; Landsat-5 TM 1995, Landsat-5 TM (BUMPER) 2005, and Landsat-8 OLI_TIRS 2016 (Table. 3). The 30 m resolution images with less than 10% cloud cover were collected from U.S Geological Survey (USGS) Center for Earth Resources Observation and Science (EROS). The data were downloaded using Path/Row 168/62, 168/63, 169/62 and 169/63, which covered the study area by 19.6%, 10.8%, 40.6% and 29.1%, respectively.

Table 3: Detailed data on the Landsat images used in this study

Year	Satellite	Sensor	Path/Row	Acquisition Date	Cloud Cover (%)
1995	Landsat 5	TM (SAM)	168/62	30/01/1995	8
			168/63	27/09/1995	0
			169/62	02/06/1995	2
			169/63	17/10/1994	2
2005	Landsat 5	TM (BUMPER)	168/62	11/04/2005	3
			168/63	09/06/2005	2
			169/62	06/04/2005	0
			169/63	25/08/2004	1
2016	Landsat 8	OLI_TRIS	168/62	22/10/2016	4.82
			168/63	22/10/2016	1.9
			169/62	13/10/2016	0.16
			169/63	13/10/2016	0.53

3.3.3 Data Acquisition for SWAT Model, to Evaluate the Implications of Hydrological Response (Runoffs and Stream Flows) to Climate Change, Land Use/Cover Change and the Community in the Study Area

The input data for the SWAT model (soil, land cover, slope, and weather data) were pre-processed in ArcMap 10.7 to obtain the data format required for the ArcSWAT12 database. The 30 m long Shuttle Radar Topography Mission digital elevation mode (SRTM), Digital elevation model (DEM) (Fig. 2) of the study area was downloaded from the United States geological Survey (USGS) database at https://earthexplorer.usgs.gov/. The DEM was used to delineate the watershed and power grids of the study areas. The slope map was derived from the 30 m resolution DEM using the Spatial Analyst tool in ArcMap 10.7. For weather data, 14 gridded daily precipitation point data were extracted from CHIRPS and MERRA-2 maximum and minimum temperature data from NASA POWER for the period 1982-2011. The CHIRPS precipitation data is a product of the United States Geological Survey (USGS); and the University of California Santa Barbara (UCSB) with a spatial resolution of 0.05 (Funk *et al.*, 2015). For the maximum and minimum temperatures, MERRA-2 data with a spatial resolution of 0.5 were obtained from the NASA POWER project (Westberg *et al.*, 2013). The bias-corrected rainfall and temperature-simulated CORDEX RCMs, SDSM and LARS-WG ensembles was used for future period of 2021-2050 analysis.

The discharge data for the period of model calibration and validation (1982-1989) for the monitoring stations of the Hynu (2K47) and Mtowambu (2H3A) rivers were collected by the Office of the Internal Drainage Basin (IDB). However, the data had gaps of between six months and one year and mainly in the dry months where zero flow was observed during the site visit. The Hynu (2K47) data had a good series with few gaps compared to the Mtowambu (2H3A) data set. Therefore, the data from Mtowambu were used to fill gaps in the Hynu gauge station for the years 1986 and 1988 using simple interpolation and linear regression methods (Hyandye *et al.*, 2018; Koch & Cherie, 2013). Figure 2 represents the DEM, weather stations used to extract climate data and gauging stations for the stream flow data.

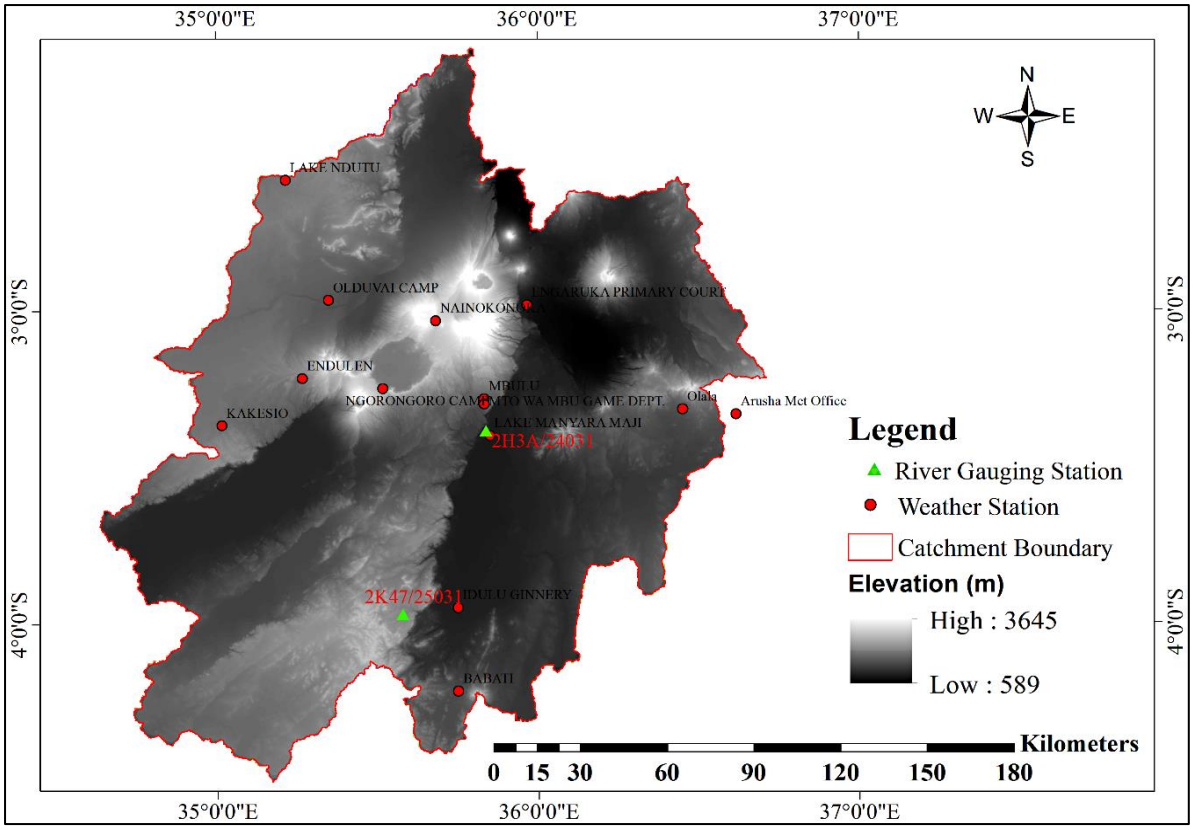

Figure 2: Digital Elevation Model for the NCA and surround catchments with location of weather station and river gauging stations used for the SWAT model data

Furthermore, the Soil data used in this study was downloaded from the FAO Harmonized Global Soils Database at **http://www.waterbase.org/download_data.html**. The watershed boundary was used to extract the soil data from the FAO soil database of the African soil slice. The attributes of these soils (Fig. 2 & Table 4) have been updated using Harmonize World Soil Database (HWSD) - Viewer software, version 1.21 (FAO/IIASA/ISRIC/ISS-CAS/JRC, 2012). The study area is dominated by 13 different soil types distribute over the entire study area with their soil mapping units as shown in the Fig. 2 and the description of their attributes are shown in the Table 4. Soils are essential components to the model because they influence hydrological processes such as surface runoff, infiltration, percolation, lateral subsurface flow, and plant water availability in the watershed.

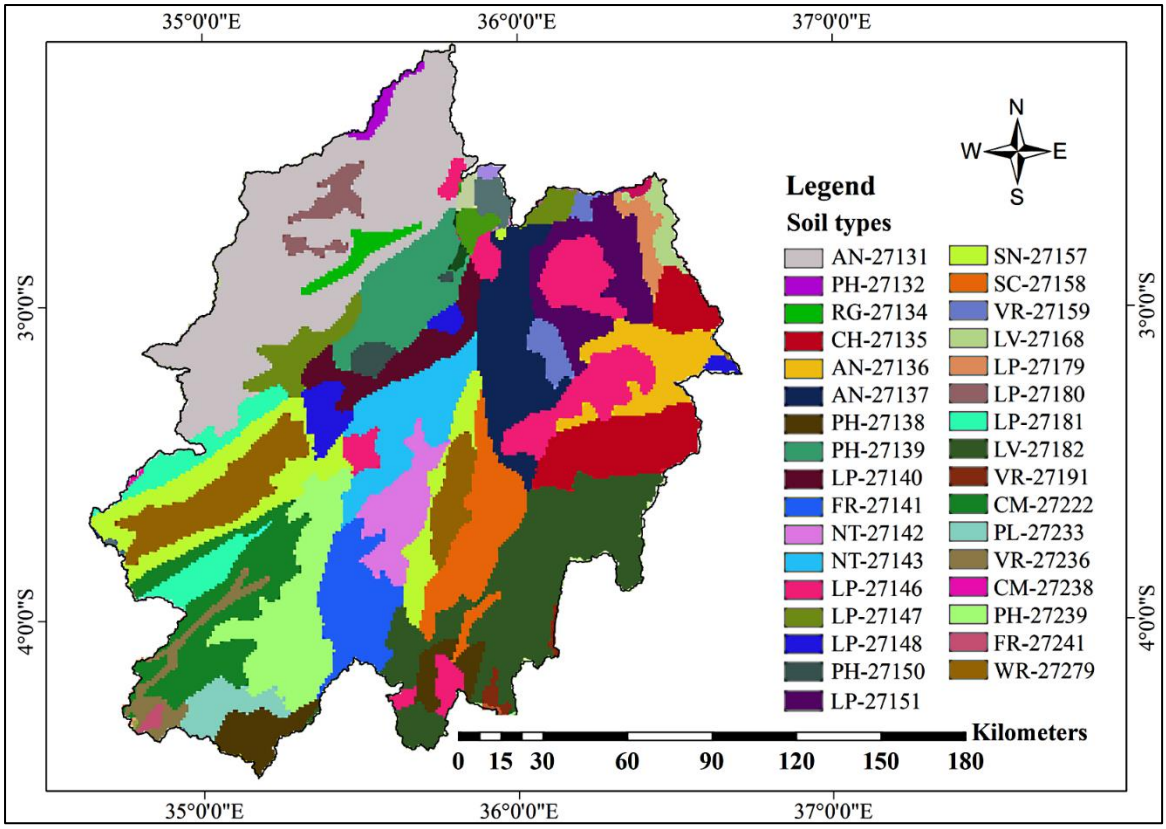

Figure 3: Soil characteristics of the NCA and surrounding catchments

For the land use/cover data, the 2016 baseline land use/coverage map (Fig. 4), was generated by classifying 30 m resolution Landsat-8 OLI_TIRS 2016 images with less than 10% cloud cover. The images were obtained from the U.S. Geological Survey (USGS) Center for Earth Resources Observation and Science (EROS) at Path/Row 168/62, 168/63, 169/62 and 169/63 covering the study area 19.6%, 10.8%, 40.6% and 29.1%, respectively. For the future simulation modelled Land use/cover map for 2025 and 2035 (Fig. 5 and 6) was used. CA – Markov model was used to simulate the future land use/cover maps used in this study (Mwabumba *et al.*, 2022). During the simulation, land use has a significant impact on surface erosion, runoff, and evapotranspiration processes in a watershed.

Table 4: Soil characteristics attributes for the NCA and surrounding catchments

SN	Acronym	Full Name	SN	Acronym	Full Name
1	AN	Andosol	8	SN	Solenetz
2	PH	Phaeozem	9	SC	Solonchak
3	RG	Regosol	10	VR	Vertisol
4	CH	Chernozem	11	LV	Luvisol
5	LP	Leptosol	12	CM	Cambisol
6	FR	Ferrasol	13	PL	Planosol
7	NT	Nitisol	14	WR	Waterbodies

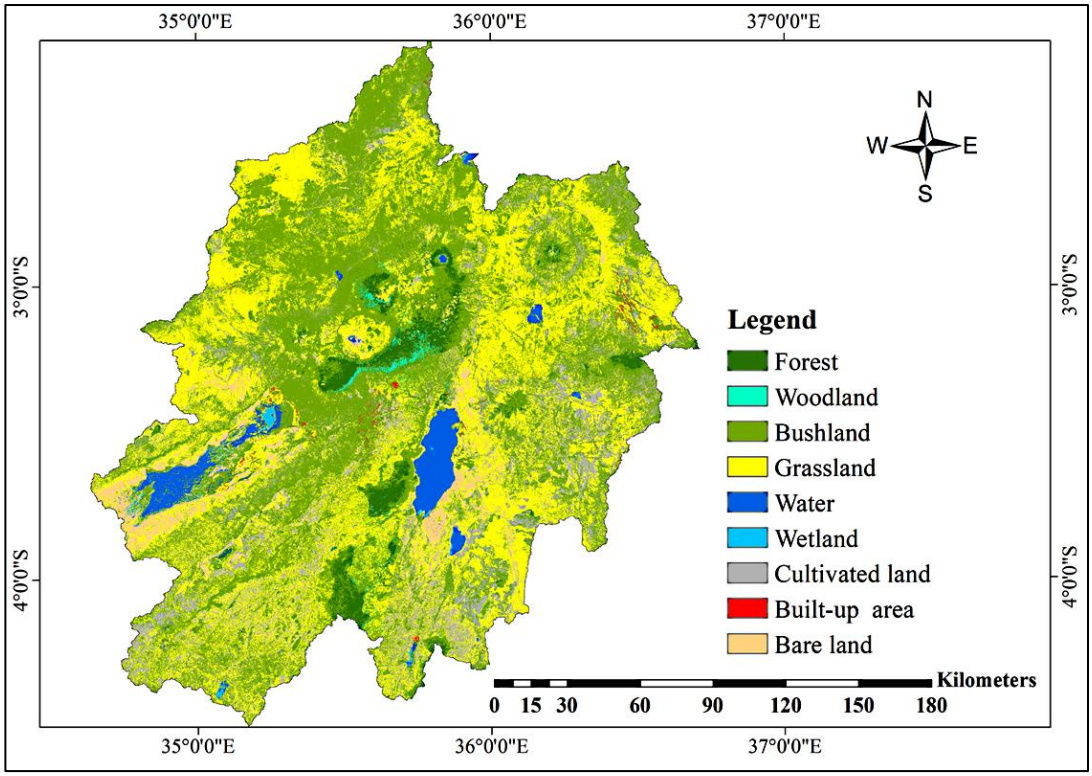

Figure 4: Simulated land use/cover of 2025 for the NCA and surrounding catchments

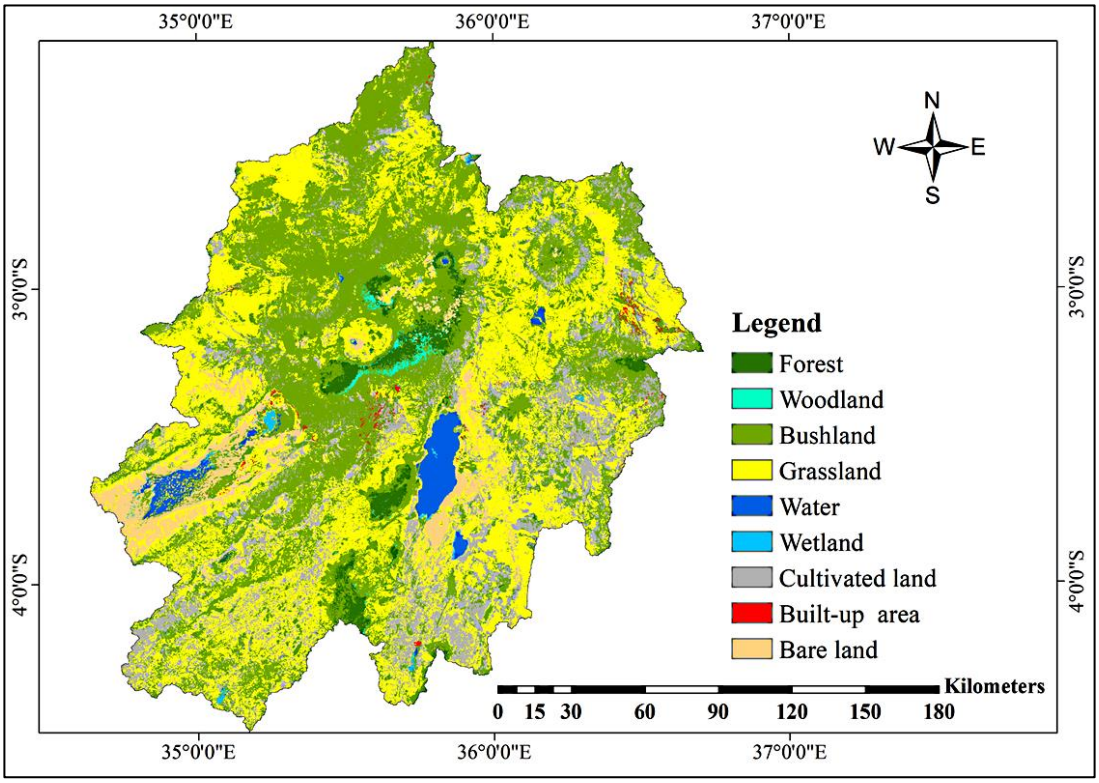

Figure 5: Simulated land use/cover of 2025 for the NCA and surrounding catchments

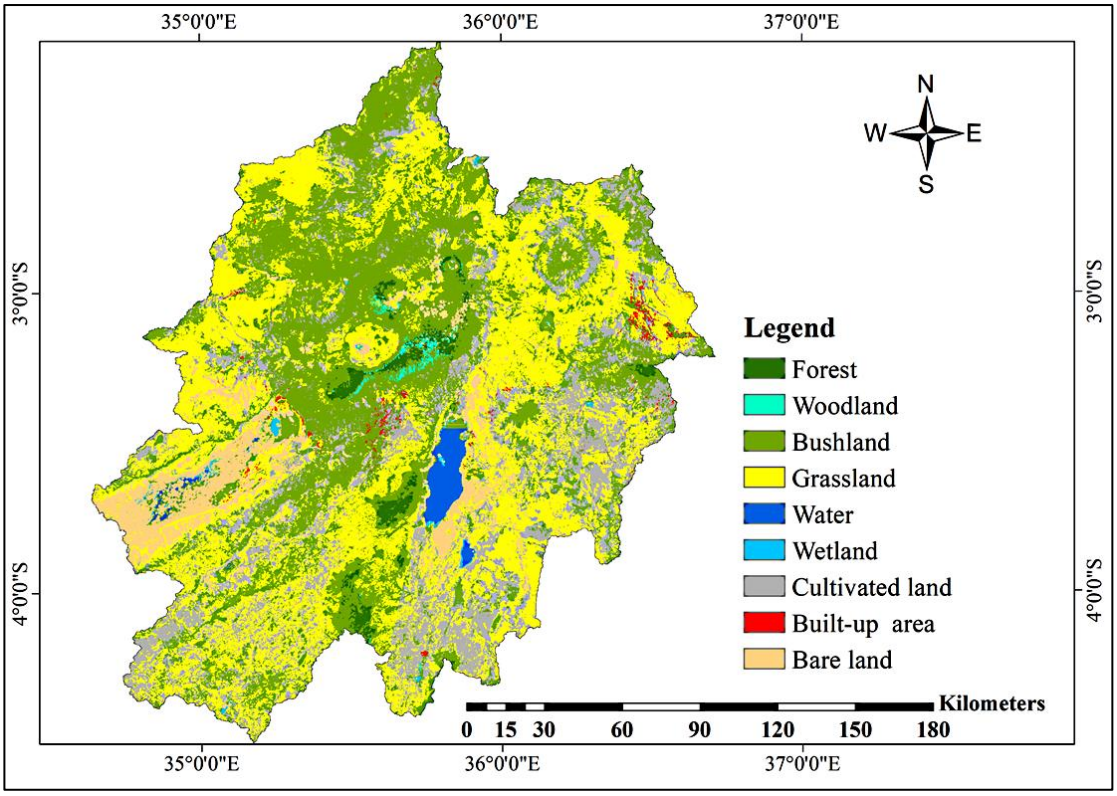

Figure 6: Simulated land use/cover of 2035 for the NCA and surrounding catchments

3.3.4 Data Acquisition for Characterizations of the Hydrochemical Composition of Water Resources in the Study Area and Monitoring of their Movement to the Groundwater around the Study Area

(i) Data for Characterizations of the Hydrochemical Composition of Water Resources in the Study Area

The water samples were collected from existing rivers, springs, and lakes from 30 locations in the three different sub-catchments (Lake Manyara, Natron, and Olduvai/NCA). Ten sample locations were chosen for each of the three sampling sub-catchments, as shown in red points in Table 5 and Fig. 7. Water samples were collected directly from sources using High-density polyethylene (HDPE) plastic bottles. A 0.45 µM pore size cellulose acetate was used to filter the turbid water samples before collecting them in the bottle. A multi-parameter probe HANNA instrument, model HI 9828 performed the on-site measurement of dissolved oxygen (DO), salinity, pH, temperature, and electrical conductivity (EC). The instrument calibration was performed according to the manufacturer's established procedures prior to making the measurements. Collected samples earmarked for the analyses of major cations, sodium (Na^+), potassium (K^+), magnesium (Mg^{2+}) and calcium (Ca^{2+}), were acidified using ultrapure

concentrated nitric acid, HNO_3 to a pH less than 2.0. All samples were stored in at 4°C to minimize microbial activity and unwanted physical-chemical reactions before laboratory analysis for other chemical parameters, including chloride (Cl^-), sulfate (SO_4^{2-}), nitrate (NO_3), phosphate (PO_4^{3-}) and bicarbonate (HCO_3^-) (Chacha *et al.*, 2018; Sundaram *et al.*, 2009).

Table 5: Location of sampling points for hydrochemical compositions for water resources in the study area

SN	Name of the water body	Type of waterbody	Eastings	Northings	Subcatchment
1	Takano spring	Spring	821506	9718646	Natron
2	Engarisero river	River	820116	9708510	Natron
3	Engong'was	Spring	821177	9725571	Natron
4	Marite	pond	819956	9674571	Natron
5	Marite Spring	Spring	817010	9674290	Natron
6	Ngopironi spring	Spring	820187	9675362	Natron
7	Engaruka river	River	833111	9668178	Natron
8	Lake Natron	Lake	821587	9728787	Natron
9	Empakaai spring 1	Spring	814250	9677555	Natron
10	Empakaai spring 2	Spring	815066	9679151	Natron
11	Munge river	River	797898	9665281	Olduvai/NCA
12	Mundus Hippo pool	Pool	783428	9650524	Olduvai/NCA
13	Mti Mmoja	Pond	783961	9648334	Olduvai/NCA
14	Lake Makat	Lake	779343	9647173	Olduvai/NCA
15	Ngoitok tok spring	Spring	789067	9644772	Olduvai/NCA
16	Gorgory swamp	Swamp	782025	9642541	Olduvai/NCA
17	Seneto	spring	777710	9648458	Olduvai/NCA
18	Olmoti Spring	Spring	797898	9665281	Olduvai/NCA
19	Oljoro Nyukie	River	793095	9650000	Olduvai/NCA
20	Mamahaw river	River	782660	9636478	Olduvai/NCA
21	Selela-Kapambe	Well	824620	9643735	Lake Manyara
22	Karuwasa borehole	Well	798885	9629754	Lake Manyara
23	Karatu well(Mbowe)	Well	798898	9629773	Lake Manyara
24	kigongoni river	River	806913	95460717	Lake Manyara
25	Mto wa mbu well	Well	818087	9628459	Lake Manyara
26	Majengo	Well	820070	9698027	Lake Manyara
27	Manyara hot spring	Hot spring	804166	9599774	Lake Manyara
28	Manyara cold spring	Cold spring	815101	9626606	Lake Manyara
29	mto wa mbu (River)	River	806913	95460717	Lake Manyara
30	Lake Manyara	Lake	787232	9620984	Lake Manyara

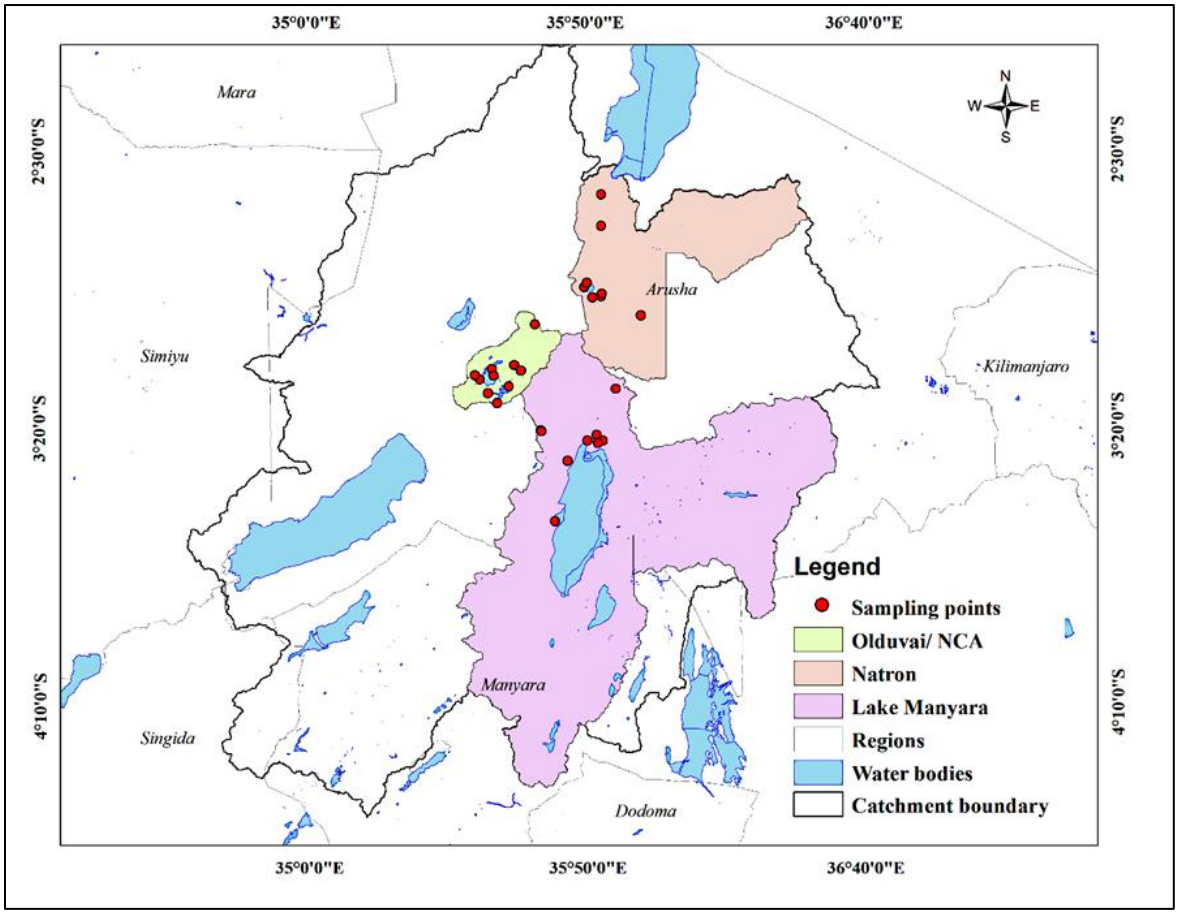

Figure 7: Water sampling locations in the three different sub-catchments (Lake Manyara, Natron, and Olduvai/NCA)

(ii) Data for Monitoring the Movements of Hydrochemical to Groundwater Surrounding the Study Area

The movement of hydrochemical to the ground was assessed by the HYDRUS 1D model. The HYDRUS 1D model requires Hydrochemical data, Soil type and soil hydrologic properties, climate data and Land Use data to model the movements of hydrochemical to groundwater. For the Hydrochemical data, the water sample data collected from different water sources in the study area were analysed in the laboratory at the Indian Institute of Technology, Roorkee, India. The output results for the analysed major anions (Chloride, Sulfate, Phosphate, Nitrate, and Bicarbonates) and cations (Calcium, Magnesium, Potassium, and Sodium) were used as inputs for the HYDRUS 1D Model. Tables 6 and 7 show the textural and hydraulic properties of the soil in the area. Soil texture information was obtained from the Harmonized World Soil Database (FAO *et al.,* 2012), and the soil hydraulic parameters were calculated using the Rosetta model (Schaap *et al.*, 2001).

Table 6: Soil characteristics for the studied sub-catchments

sub-catchment	Depth (cm)	Sand%	Silt%	Clay%	Bulk Density (g/cc)
Olduvai/NCA	0-30	49.5	35.2	15.3	1.6
	30- 4000	45.0	36.0	19.0	1.4
Lake Manyara	0-30	24.0	46.0	30.0	1.3
	30- 4000	37.0	35.0	28.0	1.4
Natron	0-30	46.0	35.0	19.0	1.4
	30-4000	32.0	35.0	33.0	1.4

Table 7: Soil hydraulic parameter obtained from Hydrus-1D using Rosetta model

Sub-catchment	Depth (cm)	Residual moisture content θr (-)	Saturated moisture content θs (-)	Parameter α in the soil water retention function Alpha(cm^{-1})	Parameter η in the soil water retention function η (-)	Saturated hydraulic conductivity K_s(cm/day)
Olduvai/NCA	0-30	0.0528	0.393	0.0145	1.447	16.69
	30-4000	0.0602	0.4003	0.0126	1.4583	10.57
Lake Manyara	0-30	0.0815	0.4469	0.0084	1.4966	12.32
	30-4000	0.0751	0.4227	0.0124	1.4281	6.51
Natron	0-30	0.0602	0.3994	0.0134	1.4492	11.2
	30-4000	0.0817	0.4375	0.0127	1.4015	7.17

3.4 Methods

3.4.1 Downscaling and Analysis of the Climate Variability and Changes in Time and Space in the Study Area

(i) The Climate Hazards Group Infrared Precipitation with Station Rainfall and Modern-Era Retrospective analysis for Research and Applications Data Validation

In order to validate the applicability of the satellite-based climate products (i.e. CHIRPS rainfall and MERRA-2), a comparison was made between the satellite-based data extracted for Arusha with historical daily rainfall and temperature data from the Arusha station. The Arusha station data was used for validation because Arusha was the only station in the vicinity of the study area with less than a 10% data gap. The validation for the CHIRPS rainfall and MERRA-2 maximum and minimum temperature was performed for the period 1982 to 2011 on a daily, monthly, and seasonal scale. Three standard valuation indices were used, namely: (a) Nash-Sutcliffe efficiency (NSE); (b) Percent bias (PBIAS) and (c) the RMSE observations' standard deviation ratio (RSR) (Moriasi *et al.*, 2015).

Nash–Sutcliffe efficiency (NSE) compares the magnitude of the residual variance relative to that of the measured data variance using normalized statistics as presented in Equation (1):

$$NSE = 1 - \left[\frac{\sum_{i-1}^{n}\left(Q_i^{obs} - Q_i^{sim}\right)^2}{\sum_{i-1}^{n}\left(Q_i^{obs} - Q^{mean}\right)^2}\right] \quad (1)$$

Where Q_i^{obs} is the ith observed discharge, Q^{mean} is the mean of observed rainfall data, and Q_i^{sim} is the ith modeled rainfall data.

The NSE can range from -∞ to 1. A value of 1 indicates a perfect fit between simulated and observed data. A value of 0 indicates that the average of the observed data would be a better fit than the model output (Nash & Sutcliffe, 1970). An NSE of 0.5 or higher is accepted as an indicator of satisfactory model performance for a monthly time step (Moriasi *et al.*, 2015).

Percentage bias (PBIAS) quantifies whether the average tendency of the simulated data is greater or less than the observed data and is expressed as a percentage, indicating a high or low bias in the modeled data. The PBIAS values were calculated using Equation (2).

$$PBIAS = \left[\frac{\sum_{i=1}^{obs}\left(Q_i^{obs} - Q_i^{sim}\right) * 100}{\sum_{i=1}^{n}\left(Q_i^{obs}\right)}\right] \quad (2)$$

Positive PBIAS values indicate that the simulated data is lower than the observed data on average, but negative values indicate the reverse: Simulated data is higher than the observed data on average. The A PBIAS value below 25% is considered satisfactory model performance, and a PBIAS value of 0 indicates a perfect simulation for a monthly time step (Moriasi *et al.*, 2015).

The RMSE observations' standard deviation ratio (RSR) standardizes the RMSE with regard to the observed records. The RSR values are the ratio of root mean square error (RMSE) to the standard deviation of observed data and were calculated using Equation (3).

$$RSR = \frac{RMSE}{STDEV_{abs}} = \left[\frac{\sqrt{\sum_{i=1}^{n}\left(Q_i^{obs} - Q_i^{sim}\right)^2}}{\sqrt{\sum_{i=1}^{n}\left(Q_i^{obs} - Q^{mean}\right)^2}}\right] \quad (3)$$

Where the RSR value of 0 indicates a perfect simulation, but values below 0.70 are considered satisfactory for model performance at a monthly time step (Moriasi *et al.*, 2015).

(ii) Regional Climate Models Performance Evaluation

The performances of the raw CORDEX-Africa RCMs (REMO2009, CanESM2-RCA4, NorESM1-RCA4, and KNMI-RACMO22T) in simulating the observed climatology over the study area were evaluated monthly and annual scale for the period 1982-2005 using statistics such as Nash-Sutcliff Efficiency (NSE) (Equation 1); percentage bias (PBIAS) (Equation 2) and Pearson correlation (r) (Equation 4). The *r* represents the temporal pattern of the models. The PBIAS describes the relative systematic error associated with the CMIP 6 models' data, where a positive and negative sign indicates overestimation and underestimation, respectively. At the spatial scale, the biases between the models and the observation were also estimated using the PBIAS statistical indicator.

$$r = \frac{n(\sum XY) - (\sum X)(\sum Y)}{\sqrt{\left[n\sum X^2 - (\sum X)^2\right]\left[n\sum Y^2 - (\sum Y)^2\right]}} \quad (4)$$

Where, X = Observed data, Y = Modeled data, and n = number of events.

(iii) Statistical Downscaling of Global Climate Model Outputs using Statistical Downscaling System Model

The SDSM is designed to statistically downscale simulated climate information from either coarse-resolution GCM output or large atmospheric variables to high-resolution forms needed for local impact studies using predictors and predictands (Gebrechorkos *et al.*, 2019). The SDSM uses multivariate linear regression to simulate future climate scenarios by combining stochastic weather generator and transfer function models (Wilby *et al.*, 2002). The stochastic data was included in the SDSM to improve the model's performance in reproducing the observed daily series by inflating the model output variance (Wilby *et al.*, 2002). In the present study, the SDSM was applied in the watersheds around the NCA to downscale the CanESM daily rainfall and temperature to a point-scale. Two datasets were involved in this process: (1) the predictands of interest, i.e., locally observed rainfall and temperature and (2) the corresponding large-scale predictors from NCEP and CanESM2 in the study area's grid box (Shukla & Singh, 2021; Shukla *et al.*, 2015). Model calibration and respective downscaling were performed through the steps as suggested by Wilby *et al.* (2002):

(i) Screening of the 26 large-scale NCEP predictors based on the correlation matrix, partial correlation, and *p*-value indicators between the predictors and local-scale predictands as practised in previous studies (Gebrechorkos *et al.*, 2019; Gulacha & Mulungu, 2017). Highly correlating predictors at a 95% confidence level (p-value < 0.05) were selected. For regression analysis between the selected NCEP predictors and predictands during model calibration for each station, a minimum of three large-scale variables was recommended for calibration at each station (Gebrechorkos *et al.*, 2019; Huang *et al.*, 2012).

(ii) The SDSM model calibration and validation were performed for the periods of 1982-1996 and 1997-2005, respectively, under 'conditional' for the rainfall and 'unconditional' for the temperature on a monthly scale. Several studies have applied this method of splitting the data into two for SDSM calibration and validation, such as (Gebrechorkos *et al.*, 2019; Huang *et al.*, 2012; Osman & Abdellatif, 2016) with SDSM indicating satisfactory results.

(iii) Generation of daily synthetic data series for rainfall, maximum and minimum temperatures for the period of 1982-2005 was performed by the weather generator

(WG) using the calibrated SDSM. The WG was applied to produce the weather series with similar statistical properties to those of the observed location-based data (Li & Babovic, 2019).

(iv) The SDSM performance was evaluated using statistical indicators including Nash-Sutcliffe efficiency (NSE), Percent bias (PBIAS), and RMSE observation's standard deviation ratio (RSR), which were also used to evaluate the SDSM performance at a daily, monthly, and seasonal timescale.

The model scenario generator, which follows a similar process as step (iii), was applied to downscale the CanESM2 daily rainfall and temperature for the future period of 2006-2050 under RCP 4.5 and RCP 8.5 scenarios.

(iv) Statistical Downscaling of Global Climate Model Outputs using Long Ashton Research Station Weather Generator

The LARS-WG is a stochastic weather generator designed to simulate the daily climate data at a station scale for climate change impact studies (Chen *et al.*, 2013; Osman *et al.*, 2014). The LARS-WG synthesizes daily series data through three processes:

(i) The LARS-WG use statistical properties of the station data on a monthly scale to generate the probability distribution of the climate parameters for a particular station on the ground.

(ii) The LARS-WG use the generated parameters files to synthesize data with the same statistical properties as the station data. Furthermore, observed and simulated average monthly weather statistical indices calibrate LARS-WG using calculated relative change factors from the GCMs outputs for each month.

(iii) Finally, LARS-WG uses the calibrated parameters and relative change factors to project daily time-series data (Chen *et al.*, 2013).

This study applied LARS-WG6 to downscale rainfall and temperature for each station individually by incorporating 20 years (1982-2001) to generate model calibration parameters. For model validation, a ten-year extended time series (2002-2011) was generated and examined using a statistical test at a 5% significance level to determine the significant difference between the simulated and observed data. After the calibration and validation process of LARS-WG,

the model generated future weather data series by updating model output parameters with selected RCMs and RCPs. This study applied LARS-WG to downscale rainfall and temperature data series for future 2021-2050 from four GCMs (CanESM2-RCA4, NorESM1-RCA4, CSIRO-CMS and HadGEM2-ES) under RCP 4.5 and 8.5.

(v) Climate Change Analysis

Temporal and spatial changes in rainfall and temperature at an annual and seasonal scale for the observed historical period of 1982-2011 and the future periods of 2021-2050 were analyzed using the bias-corrected rainfall and temperature-simulated CORDEX RCMs, SDSM and LARS-WG ensembles. The percentage changes in rainfall at seasonal and annual scales and the projected relative changes in the mean annual temperature were estimated for each station and over the entire basin. The significance of the projected changes was assessed at a 95% confidence level using the *t*-test. For the spatial analysis, the Inverse Distance Weighted (IDW) interpolation method was used to generate the distribution of seasonal and mean annual changes in rainfall and temperature between the future and historical periods.

3.4.2 Analysis of Land Use/Cover Classification, Change Detection and Modeling of the Future Scenarios in the Study Area

(i) Land use/cover Classification and Change Detection

Land use/cover maps were produced using three Landsat images; Landsat-5 TM 1995, Landsat-5 TM (BUMPER) 2005, and Landsat-8 OLI_TIRS 2016 (Table 3) using Path/Row 168/62, 168/63, 169/62 and 169/63 which covered study area by 19.6%, 10.8%, 40.6% and 29.1%, respectively. The 30 m resolution images with less than 10% cloud cover were collected from U.S Geological Survey (USGS) Center for Earth Resources Observation and Science (EROS). The hybrid classification method (Solomon *et al.*, 2019; Teferi *et al.*, 2010), which includes unsupervised and supervised classification methods, was used to classify the images. The Iterative, Self-Organizing Data Analysis (ISODATA) clustering algorithm, performed the unsupervised classifications (Boakye *et al.*, 2008; Teferi *et al.*, 2013); while the Maximum Likelihood Classification (MLC) algorithm executed the supervised classifications (Gashaw *et al.*, 2017; Larbi *et al.*, 2019; Solomon *et al.*, 2019). The Land use/cover classes formed include forest, woodland, bushland, grassland, water, wetland, cultivated land, built-up area, and bare land (Table.8).

For accurate assessment of Land use/cover maps produced from the satellite images, the stratified random method for each of the three classified Land use/cover maps was used to represent the different Land use/cover classes of the study area. The accuracy was assessed using 90 pixels per category and was based on visual interpretation and ground truth data. The reference data for ground-truthing was obtained from a high-resolution Google Earth and field visit using GPS (Larbi *et al.*, 2019) and previously classified Land use/cover (Masao *et al.*, 2015). A cross-tabulation was achieved between the class values and the ground truth, and the results were as an error matrix. In addition, the non-parametric Kappa test was performed to measure the magnitude of the classification accuracy to account for diagonal elements and in the confusion matrix (Rosenfield & Fitzpatrick-Lins, 1986).

Table 8: Land use/cover classes descriptions

Class	Descriptions
Bushland	Mainly comprised of plants that are multi-stemmed from a single root base.
Woodland	An assemblage of trees with canopy ranging from 20% to 80% but which may, on rare occasions, be closed entirely.
Wetland	The low-lying, uncultivated ground where water collects; is a bog or marsh.
Cultivated land	Crop fields and fallow lands.
Built-up area	Residential, commercial, industry, transportation, roads, mixed urban.
Grassland	Mainly composed of grass.
Forest	The continuous stand of trees, many of which may attain a height of 50 m, include natural forest, mangroves and plantation forest.
Water	River, open water, lakes, ponds and reservoirs.
Bare land	The land area of exposed soil and the barren area is influenced by a human.

(ii) Land use/cover Prediction

The study applied Cellular Automata-Markov (CA-Markov) model to predict the 2025 and 2035 Land use/cover status. The CA-Markov is a robust model for predicting the patterns and the spatial arrangement of different Land use/cover change categories, which is available in IDRISI 17.0 (Arsanjani *et al.*, 2011; Wang *et al.*, 2012). The model operates with reference to the historical Land use/cover status image, transition probability matrix, and suitability images as a group file (Eastman, 2012). The model is also commonly realistic in several countries (Mosammam *et al.*, 2017; Omar *et al.*, 2014; Singh *et al.*, 2018) and comprises two

components, the Cellular Automata model and the Markov model. The mathematical expression of the Markov model is as presented in Equation 5.

$$\mathbf{S(t+1) = P_{ij} \times S(t)} \quad (5)$$

Where, $\mathbf{S(t+1)}$ represents the status of land use/cover at a time$\mathbf{(t+1)}$, $\mathbf{P_{ij}}$ represent a Transitional Matrix:

$$P_{ij} = \begin{bmatrix} P_{11} & P_{12} & P_{13} & \dots & P_{1n} \\ P_{21} & P_{22} & P_{23} & \dots & P_{2n} \\ P_{31} & P_{32} & P_{33} & \dots & P_{3n} \\ \dots & \dots & \dots & \dots & \dots \\ P_{n1} & P_{n2} & P_{n3} & \dots & P_{nn} \end{bmatrix}$$

$\mathbf{(0 \leq P_{ij} < 1)}$, and $\mathbf{\sum_{j=1}^{n} P_{ij} = 1}$. Where$\mathbf{(i, j = 1, 2, \dots, n)}$. **i and j**, are the land uses and $\mathbf{P_{ij}}$ represents the transition probability between any pair of land uses. From the matrix, the rows and columns represent historical and current land use/cover classes, respectively. Furthermore, the mathematical expression of the cellular automata is as presented in Equation 6.

$$\mathbf{S(t, t+1) = f(S(t), N)} \quad (6)$$

The CA Markov model is a combination between the Markov model and cellular automata, which predicts land use/cover; by adding the spatial distribution element and possible land use/cover transition and distribution (Myint & Wang, 2006). The CA-Markov applies a standard filter with a 5 × 5 size Kernel pixel and Multi-Objective Land Allocation (MOLA) dynamic procedures for land use/cover prediction. The process then accomplishes the cellular automata component by reducing the weight of the suitability of pixels that are far from the considered land use/cover types. However, the reduced weighted suitability should not exceed 90% of the original value to ensure the proximate areas' conditional probability (Roose & Hietala, 2018). In this study, the 2025 and 2035 land use/cover maps were predicted using the 2016 land use/cover classified map as a base map and a transition potential map. The transition potentials were generated based on the main transitions that occurred between the years 2005 and 2016 among the land use/cover classes. The model validation was performed by comparing the simulated 2016 land use/cover map, which was based on the 1995 and 2005 classified images, with the classified 2016 land use/cover map. The "Relative Operating Characteristic

(ROC)" and "Kappa indexes" were used to compare the agreements between the simulated and classified 2016 land use/cover status maps. The kappa indexes used include Kappa for no information (Kno), Kappa for location (Klocation), Kappa for location stratum level (KlocationStrata), and Kappa for standard (Kstandard) (Eastman, 2012; Mosammam *et al.*, 2017; Pontius & Schneider, 2001). Change analysis was carried out using the classified (1995, 2005 and 2016) and the predicted Land use/cover (2025 and 2035) maps to establish the pattern of Land use/cover changes. However, to calculate the extent of changes that occurred during the subsequent periods, 1995-2005, 2005-2016, 2016-2025 and 2025-2035, the percentage change was computed.

(iii) The SWAT Model, to Evaluate the Implications of Hydrological Response (Runoffs And Stream Flows) to Climate Change, Land use/cover Change and The Community in the Study Area

The SWAT model simulates the hydrological division of watersheds using the water balance approach. The water balance approach of the SWAT model simulates surface runoff, infiltration, seepage, channeling, shallow and deep aquifer flow (Neitsch *et al.*, 2011). The SWAT model's hydrologic procedures are built on Equation 7 of the water equilibrium.

$$\mathrm{SW_t} = \mathrm{SW_0} + \sum_{\mathrm{i=1}}^{\mathrm{t}}\left(\mathrm{P_{day}} - \mathrm{Q_{sur}} - \mathrm{E_a} - \mathrm{W_{seep}} - \mathrm{Q_{gw}}\right) \quad (7)$$

Where, SW_t is final soil water content; SW_0 is initial soil water content day i (mm); P_{day} precipitation amount on a day i (mm); Q_{sur} is surface runoff on day i (mm); E_a is Evapotranspiration amount on day i (mm); W_{seep} is the amount of water entering the vadose zone from the soil profile on the day i (mm) and $\mathrm{Q_{gw}}$ is the amount of return flow or base flow on the day i (mm).

This study used the ArcSWAT (2012 version) modeling software (Arnold *et al.*, 2012) to simulate baseline and future streamflow dynamics. The SWAT model delineates a watershed using a digital elevation model (DEM) and then divides the watershed into subbasins or sub-watersheds based on the drainage area of the tributaries. Each subwatershed is subdivided into hydrologic response units (HRUs), grouped upon land use, soil, and topography combinations. The SWAT model simulated the Evapotranspiration (ET) using the Penman-Monteith option (Monteith, 1965), surface runoff, lateral flow in the soil profile, groundwater flow, channel

routing (Manning's equation for uniform flow in a channel), and reservoir storage (Arnold *et al.*, 2012).

(iv) The SWAT Model Set-up and Evaluation

The SWAT delineated the catchment into 66 sub-watersheds (Fig. 8) within a total watershed area of 32 779.8 km. The outlet for this watershed is located at the 2K47 gage on the Hynu River and 2H3A on Mtowambu River. The 66 sub-watersheds were further delineated into 919 HRUs classified based on homogeneous land use types, soil types, and topography. The HRUs were defined by using per cent thresholds of land use, soils, and slope of 5, 20, and 10%, respectively, within each of the 66 sub-watersheds. The SWAT model was calibrated and validated using a split data approach that covered high and low flow periods in each of the two. Daily flow data from the 2K47 gage on the Hynu River, were used for model setup using eight (8) years (1982-1989) of daily observed flow data. The data was divided into warm-up (1982-1984), calibration (1985-1987) and validation (1988-1989) periods. The study used this gauge locations because they are only gauging stations around the study area with historical records that are good for calibration/validation of the model. The Nash Sutcliffe efficiency coefficient (NSE), the ratio of root mean square error to the standard deviation (RSR), and percentage bias (PBIAS) were calculated and represent measures of model performance.

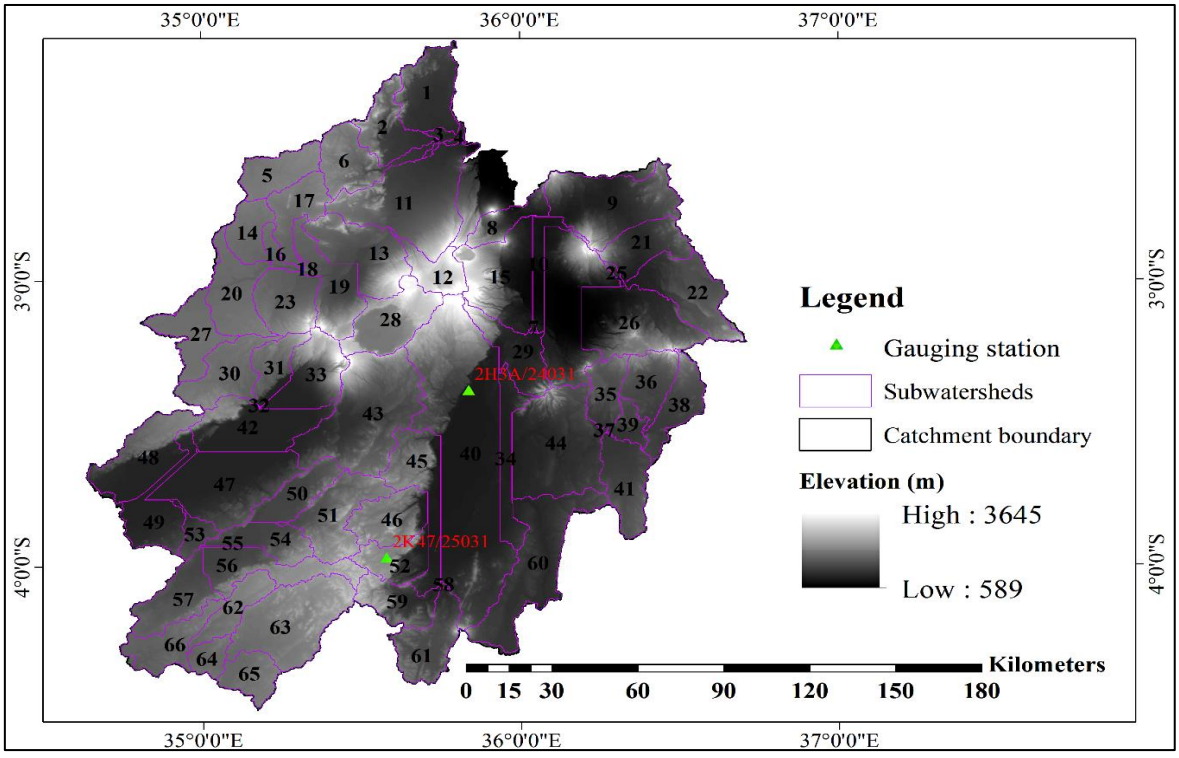

Figure 8: The 66 sub basin delineated from SWAT model within total watershed area of 32 779.8 km^2

(v) Model Sensitivity Analysis

Sensitivity analysis identifies the most important parameters for calibration and validation of the SWAT model (Arnold *et al.*, 2012; Moriasi *et al.*, 2007; Tang *et al.*, 2012). However, to identify the most important SWAT parameters, 14 flow parameters (Table 9) were selected from literature (Assfaw, 2019; Gebremicael *et al.*, 2013; Gyamfi *et al.*, 2016; Tang *et al.*, 2012). For this purpose, global sensitivity analysis (Begou *et al.*, 2016; Khalid *et al.*, 2016), which allows changing each parameter at a time (Arnold *et al.*, 2012), was employed in SWAT-CUP 2012 version 5.1.4. Indices such as t-Stat and p-value were used to provide a measure and significance of sensitivity, respectively (Begou *et al.*, 2016; Khalid *et al.*, 2016; Narsimlu *et al.*, 2015). Hence, a higher t-test in absolute values measures high sensitivity while a p-value of 0 is more significant (Abbaspour, 2013; Khalid *et al.*, 2016; Narsimlu *et al.*, 2015).

(vi) Model Calibration and Validation

In this study calibration and validation were performed between January 1, 1985, to December 31, 1987, and from January 1, 1988, to December 31, 1989, respectively. Calibration and validation were carried out in SWAT-CUP 2012 version 5.1.4 using the Sequential Uncertainty Fitting (SUFI-2) algorithm, based on the SWAT-CUP user manual (Abbaspour, 2013). The SUFI-2 is a semi-automated calibration and uncertainty analysis algorithm (Zhou *et al.*, 2014) that accounts for all sources of uncertainty, including uncertainty in the driving variables (e.g. rainfall), conceptual model, parameters and measured data (Tang *et al.*, 2012; Vilaysane *et al.*, 2015; Zhou *et al.*, 2014). Table 9 represents flow parameters considered for calibration and validation of the SWAT model.

Table 9: Flow parameters for calibration and validation of the SWAT model

Parameter	Parameter Definition
ALPHA_BF.gw	Baseflow alpha factor for bank storage
CN2.mgt	SCS runoff curve number
ESCO.bsn	Soil evaporation compensation factor
GW_DWLAY.gw	Groundwater delay (days)
GW_REVAP	Groundwater "revap" coefficient
GW_SPYLD (m)	Specific yield of the shallow aquifer
GWQMN.gw	Threshold depth of water in the shallow aquifer required for return flow to occur
HRU_SLP	Average slope steepness
OV_N.hru	Manning "n" value for overland flow
R_EPCO.HRU	Plant uptake compensation factor
RCHRG_DP.gw	Deep aquifer percolation fraction
REVAPMN	Threshold depth of water in shallow aquifer for revap to occur
SLSUBBSN	Average slope length
SURLAG	Surface runoff lag coefficient

(vii) Simulating Land Use snd Climate Scenario

The SWAT model simulations were performed for two time periods: baseline (1982–2016) and future (2021–2050). These time periods bracket the land use descriptions of 2016, projected 2025 and 2035. However, to simulate the effects of land-use change and climate change, the study created three scenarios with the following input datasets:

(i) Baseline 2016 land use and historical climate data (1982–2011)

(ii) Land use only scenarios: Historical climate data (1982–2011) with corresponding land use 2025 and 2035.

(iii) Climate only scenarios: Baseline 2016 land cover with corresponding 2021- 2050 future climate scenarios (RCP 4.5 and RCP 8.5) and

(iv) Combined scenarios: Land use 2025 with future climate scenario 2021-2050 (RCP 4.5 and RCP 8.5) and land use 2035 with future climate scenario 2021-2050 (RCP 4.5 and RCP 8.5).

3.4.3 Characterizations of the Hydrochemical Groundwater around the Study Area

(i) Characterization of Hydrochemical Composition of Water Resources in the Study Area

In this study, water samples were collected from 30 different locations within the study area and analyzed for the laboratory's major cations and anions concentrations. The National Institute of Hydrology (NIH) Laboratory at the Indian Institute of Technology Roorkee (IITR), India, analyzed the sample for key cations (Na^+, K^+, Mg^{2+}, Ca^{2+}) and anions (Cl^-, SO_4^{2-}, NO_3^-, PO_4^{3-}). The water samples were analyzed using an ion chromatograph instrument (930 Compact IC Flex model). The concentration of major cations and anions characterize the hydrochemical composition of water resources in the study area). Furthermore, the laboratory results for the concentration of anions and cations were used as inputs for the HYDRUS 1D Model to monitor the movement of hydrochemical to the groundwater around the study area. In addition, water quality standards for maximum drinking water limit values for aquatic contaminants (WHO, 2008, 2011) and (Tanzania Bureau of Standards, 2005) were used to analyze the water quality in the study area.

(ii) The HYDRUS 1D Modeling Procedure to Monitor the Movement of Hydrochemical to Groundwater around the Study Area

The flow chart of the methodology adopted to achieve the objectives of this study is shown in Fig. 9. The laboratory results of the surface water resource and varying climate conditions are used as the top boundary condition for running the Hydrus 1D for the simulating movement of hydro-chemicals to the underlying groundwater of the area. The model results for hydro-chemicals to the groundwater were analyzed for spatial distribution, temporal trends, and correlations, using QGIS 3.18 and Origin Pro 9.0 and R software. A Pearson correlations matrix determined a relationship between climate variables and hydro chemicals contaminations to the groundwater in this study. The study applied the Guildford's classification techniques to interpret the obtained correlation outputs as 0.0-0.29 (little/negligible correlation); 0.3-0.49 (low correlation); 0.5-0.69 (marked/moderate

correlation); 0.7-0.89 (high correlation); 0.9-1.0 (very high correlation) (Guilford & Lacey, 1947).

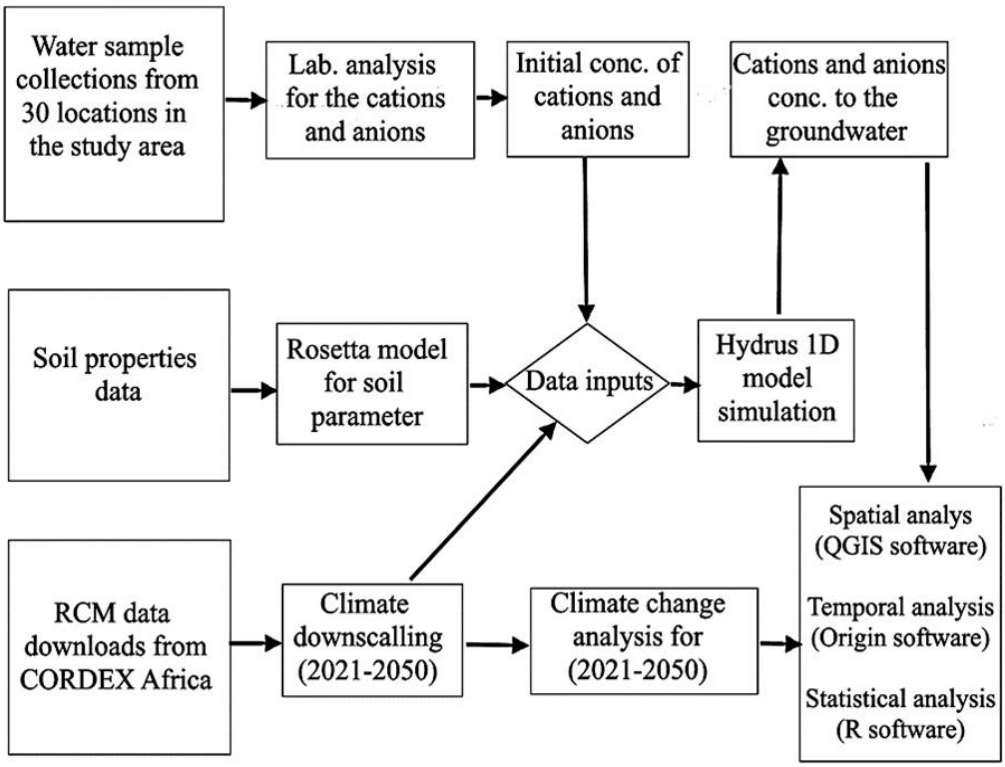

Figure 9: The overall methodology for the numerical model used for hydro-chemical transport to the groundwater

The HYDRUS 1D model uses the modified one-dimensional Richards' equation to simulate the movement of water and its dissolved chemicals through a variably saturated zone. The equation can be derived by integrating Darcy's law with mass balance (Mathur & Yadav, 2009) as:

$$\frac{\partial \theta}{\partial t} = \frac{\partial}{\partial z}\left[K(h)\frac{\partial h}{\partial z} - K(h)\right] - S \qquad (8)$$

where θ is the volumetric water content (dimensionless), h, is the soil water pressure head [L], t is time [T], z is the vertical coordinate [L], S is the sink term [T^{-1}], and $K(h)$ is the unsaturated hydraulic conductivity [LT^{-1}]. The unsaturated hydraulic conductivity, $K(h)$, and the water content θ depend on the soil water pressure head. This makes Richards' equation a highly nonlinear equation that needs to be solved numerically. The HYDRUS-1D is used for solving this equation numerically by using five different analytical models to describe the soil hydraulic properties (Abbasi *et al.*, 2004; Brooks & Corey, 1964; Van Genuchten, 1980).

The HYDRUS-1D model (Šimůnek *et al.*, 2016) simulates hydrochemical transport in variably saturated porous media using the standard advection-dispersion reaction as:

$$\frac{\partial \theta c}{\partial t} + \rho \frac{\partial s}{\partial t} = \frac{\partial}{\partial z}\left(\theta D \frac{\partial c}{\partial z}\right) - \frac{\partial qc}{\partial z} - \phi \quad (9)$$

Where c is the solution concentration [ML^{-3}], s is the sorbed concentration [MM^{-1}], D is the dispersion coefficient [L^2T^{-1}], ρ is the bulk density of the porous medium [ML^{-3}], θ is the volumetric water content (dimensionless), q is the volumetric flux density [LT^{-1}], which is obtained using the Darcy-Buckingham law, and ϕ is a sink-source term accounting for various zero- and first-order or other reactions [$ML^{-3}T^{-1}$]. The governing flow and transport equations are solved numerically using Galerkin-type linear finite element schemes (Šimůnek & Van Genuchten, 2008).

(iii) The HYDRUS-1D Model Settings: Initial Condition and Boundary Condition

The flow and transport are analyzed at 30 locations (marked in Fig. 7) by considering 30 lithologs. A constant depth of 40 m represents the average level of the groundwater table in this area. Two different soil layers, soil 1 (0 to 30 cm) and soil 2 (3 cm to 40 m), are shown in Fig. 10 (In the simulation domain, soil materials represent actual lithological conditions at the selected sites). The observation points at the water table are also marked in this figure. The soil hydraulic properties are described using van Genuchten-Mualem type analytical functions. Soil hydraulic parameters obtained from the Rosetta model given in Table 7 are used for the simulation. For the water flow simulations, atmospheric boundary conditions (rainfall, potential evapotranspiration) with surface water status are taken as the upper boundary condition, and a free drainage boundary condition is considered at the lower boundary. The Penman-Monteith equation calculates the potential evapotranspiration using the minimum/maximum temperatures, relative humidity, and wind speed. The model uses a concentration flux (Cauchy or third-type) type of the boundary condition at the surface and a zero concentration gradient boundary condition at the bottom for hydrochemical transport. The hydrochemical concentration analyzed from water samples collected from the various surface sources (30 locations) is taken as the concentration flux at the surface. The study assumed the same concentration of hydrochemical on the surface for the entire simulation period as the source of the pollutants are volcanic lithology, mineral precipitation, dissolution, and agriculture activities. The initial pressure heads in all the HYDRUS-1D columns are

assumed to be in hydrostatic equilibrium, with the pressure head equal to zero at the water table. Therefore, the HYDRUS-1D columns are discretized into a finite element with relatively small elements at the surface where large hydraulic gradients are expected, as Fig. 3 depicts.

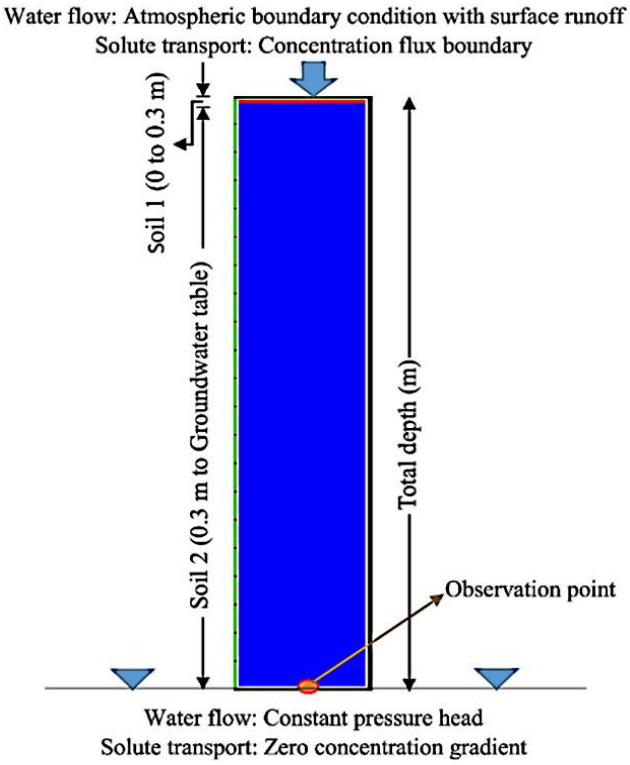

Figure 10: Schematic representation of the simulation domain in HYDRUS-1D with hydro-chemical and water flow boundary conditions

3.4.4 The Analysis of the Impacts of Climate and Land use/cover Change on Hydrochemical Movement to the Groundwater as Influenced by Future Climate around the Study Area

The impact of climate and land use/cover change on the movement of hydrochemical, cations (Na^+, Ca^{2+}, Mg^{2+}, and K^+) and anions (Cl^-, SO_4^{2-}, PO_4^{3-}, NO_3^{-1}, HCO_3^-) to the groundwater was determined using the pairwise Pearson correlation (Nie *et al.*, 2011; Twisa *et al.*, 2020; Woldesenbet *et al.*, 2017). The Pearson correlation analysis was applied to determine the linear relationship between land use/cover changes (Independent variable) and movement of hydrochemical (Cations and Anions) to groundwater (dependent variables). The significant correlation between variables was determined at a 95% confidence interval. Thus, the land use/ cover change highly influences the hydrochemical movements to groundwater as the Pearson correlation coefficient value approaches 1. Furthermore, the study investigated the hydrological response of individual climate parameters and land use/cover type to the

movement in relation to the movements of hydrochemical to groundwater, using correlation analysis by the Partial Least Squares Regression (PLSR) model (Equation 10).

$$y = b_0 + b_1x_1 + b_2x_2 + b_3x_3 + \cdots + b_ix_i \quad (10)$$

Where, y is the dependent variable, b_0 is the intercept, x is the independent variables from 1 to i, and b is the coefficients of the x variables.

The PLSR is an approach that analyses, integrate, and generalizes characteristics from primary element analysis and multiple regression. The PLSR is a robust multivariate regression approach that is useful when the predictors are collinear and have many independent variables (Song *et al.*, 2013; Wold *et al.*, 2001). The advantage of PLSR is that it can deduce the relationships between the dependent and independent variables from a single dependent variable's weights (w*) and regression coefficients in the subsequent independent components (Ma *et al.*, 2015; Shi *et al.*, 2019; Zhu *et al.*, 2019). The predictors in this study are the climatic variables and land-use/cover classes, whereas the response function is the annual hydrochemical (cations and anions) concentration. The number of relevant components to maintain is generally determined using a criterion that includes cross-validation. Model validity and strength are measured using two indices: (a) The goodness of fit (R^2), which is the proportion of variation in the dependent variable explained by the model, and (b) The R^2_{cross} (cross-validated R^2; goodness of prediction), which is the proportion of variation in the dependent variable that the model can predict. The R^2 and R^2_{cross} are used to determine the number of components in each PLSR model (Yan *et al.*, 2013). The PLSR regression model provides significant and good predictions when R^2 is > 5 and when R^2_{cross} is > 0.0975 (Trap *et al.*, 2013).

The study applied multiple regression analysis to determine the movements of cations and anions composition in groundwater between two climate periods (2021-2035) and (2036-2050) due to individual climate variables (rainfall, Tmax, Tmin, RH and wind speed). Furthermore, the study used a land-use/cover map of 2016 and projected 2025 and 2035 to determine land use/cover change and quantify the effect of individual land use/cover on the movement of cations and anions to groundwater at the basin scale. In analysing climate change impacts, independent variables were the changes of seven climate parameters (Rainfall, Tmax, Tmin, Tmean, RH, Wind speed (WS) and ET). However, land use/cover classes (i.e., natural forest, woodland, bushland, grassland, water, wetland, cultivated land and built-up area) were

independent variables to determine individual land use/cover change impacts. The PLSR models were created to recognize the key Climate parameters and land use/ cover types that control the movement of cations and anions to groundwater. The study further applied the cross-validation technique to determine the suitable number of components of individual PLSR models and obtain an optimum balance between the described variation in the response and the projecting ability of the model (goodness of prediction: Q_2). Also, it reduces the drawback of overfitting.

In PLSR modelling, the variable importance of the projection (VIP) and regression coefficients (RCs) was utilized to describe the relative effect of each independent variable. Thus, it is feasible to discover which climate parameter or land use/cover types interact the most strongly with the hydrochemical. An independent variable with a VIP value greater than 0.8 is important and significant for explaining the dependent variable (Wold, 1995). In contrast, a value less than 0.5 suggests that the variable does not explain the dependent variable significantly (Woldesenbet *et al.*, 2017). The RCs of the PLSR models determine the direction and degree of each independent variable's influence in the PLSR model. For example, an independent variable may have a low RC but a high VIP, which is relevant and contributes considerably to the prediction. Thus, the model must maintain it. If the VIP and RC values are small, the variable may be removed from the model. However, to avoid model's over-fitting, the number of components in each PLSR model was chosen using cross-validation to establish an ideal balance between the explained variance in the response (R^2) and the model's predictive performance (goodness of prediction: R^2_{cross}). Further, the study defined the percentage of variance and cross-validated goodness of prediction (Q_2) for the dependent variables (cations and anions composition in groundwater) for each model. The cross-validated RMSE as the difference between each pass's predicted and observed values were analyzed. Finally, the PLSR models' regression coefficients were applied to represent the direction of the link between changes in different climate parameters and land use/cover categories and cations and anions composition to groundwater. The statistical analysis of the dataset was carried out using XLSTAT (Yan *et al.*, 2013).

3.4.5 The Analysis of Climate Change Impacts on Water Resources and the Communities

This exercise used the GPS, field survey and focus group discussion with key informants to determine the community experience on the impact of climate change and Land Use/ cover

change in water resources around the study area. The study used the information from the focus group discussion to evaluate the implication of climate and land use/ cover change on the water resources in the NCA. The survey included stakeholders residing in the area through a random selection of Individuals from populated areas. Respondents were asked to participate in the study and provide their knowledge of the water resources, the benefits they receive from the existing water sources and how that benefit changed due to an anticipated climate and land use/cover changes. They were informed that all responses were anonymous.

CHAPTER FOUR

RESULTS AND DISCUSSION

4.1 To Evaluate Temporal and Spatial Changes of Climate in the Study Area for the Future Period, 2021-2050 Compared to Baseline 1982-2011

The evaluation of temporal and spatial change in climate, involved the climate downscaling process and climate change analysis. The downscaling process involved the evaluation of dynamically downscaled RCMs downloaded from CORDEX-Africa, bias correction of the RCMS, followed by the statistical downscaling. The CHIRPS and MERRA -2 data were used as the predictors for the statistical downscaling process using SDSM and LARS-WG. Furthermore, the bias-corrected RCMS was used in the generation of the ensemble mean dataset between bias-corrected RCMs, SDSM and LARS-WG for climate change analysis.

4.1.1 Climate Downscaling in Time and Space in the Study Area

(i) Performance Evaluation Statistics of Regional Climate Models over the Catchment

The statistical tests for comparing the observed (CHIRPS) data and the RCMs (REMO2009, CanESM2-RCA4, NorESM1-RCA4, and KNMI-RACMO22T) simulating the rainfall and temperature for the period 1982 to 2005 are presented in Table 10. A high correlation (r) greater than 0.9 was found for all the RCMs for rainfall and Temperature. Three RCMs (REMO2009, KNMI-RACMO22T and CanESM2-RCA4) overestimated rainfall in the area in the range of 13% to 16.7%, while NorESM1-RCA4 shows an underestimation of rainfall with PBIAS of -2.5%. A similar rainfall result of a higher correlation between the RCMs and the observed (MERRA-2) was found for temperature. Unlike rainfall, all the RCMs show overestimation in the case of temperature with biases in the range of 0.2 to 1.4^{o}C. In addition, Fig. 11 and 12 (a, b, c & d), respectively indicate the spatial biases between observed (CHIPRS) data and RCMs for rainfall and temperatures. The spatial PBIAS was found to range between +20.3% and -28.9% for rainfall. In the case of temperature, all the RCMs show overestimation with biases in the range of 0.01 to 1.98^{o}C. The biases across the basin found in NorESM1-RCA4, and KNMI-RACMO22T models were relatively low compared to REMO2009 and CanESM2-RCA4. Therefore, the evaluation results of CORDEX RCMs (REMO2009, CanESM2- RCA4,

NorESM1-RCA4, and KNMI-RACMO22T) indicate good performance of the RCMs in simulating monthly rainfall and temperatures, as shown in Table 10.

Table 10: Statistical analysis between the raw RCMs and Observed (CHIRPS/MERRA-2) for the mean monthly rainfall and temperature of the catchment for the period 1981-2005

Models	Rainfall			Temperature		
	r	PBIAS	NSE	*r*	BIAS	NSE
REMO2009	0.96	13.0	0.86	0.97	1.4	0.88
CanESM2-RCA4	0.92	16.0	0.71	0.94	0.8	0.75
NorESM1-RCA4	0.9	-2.5	0.95	0.92	0.2	0.91
KNMI-RACMO22T	0.94	16.7	0.84	0.95	0.9	0.81

Note: *r* indicates correlation; NSE indicates Nash-Sutcliffe Efficiency

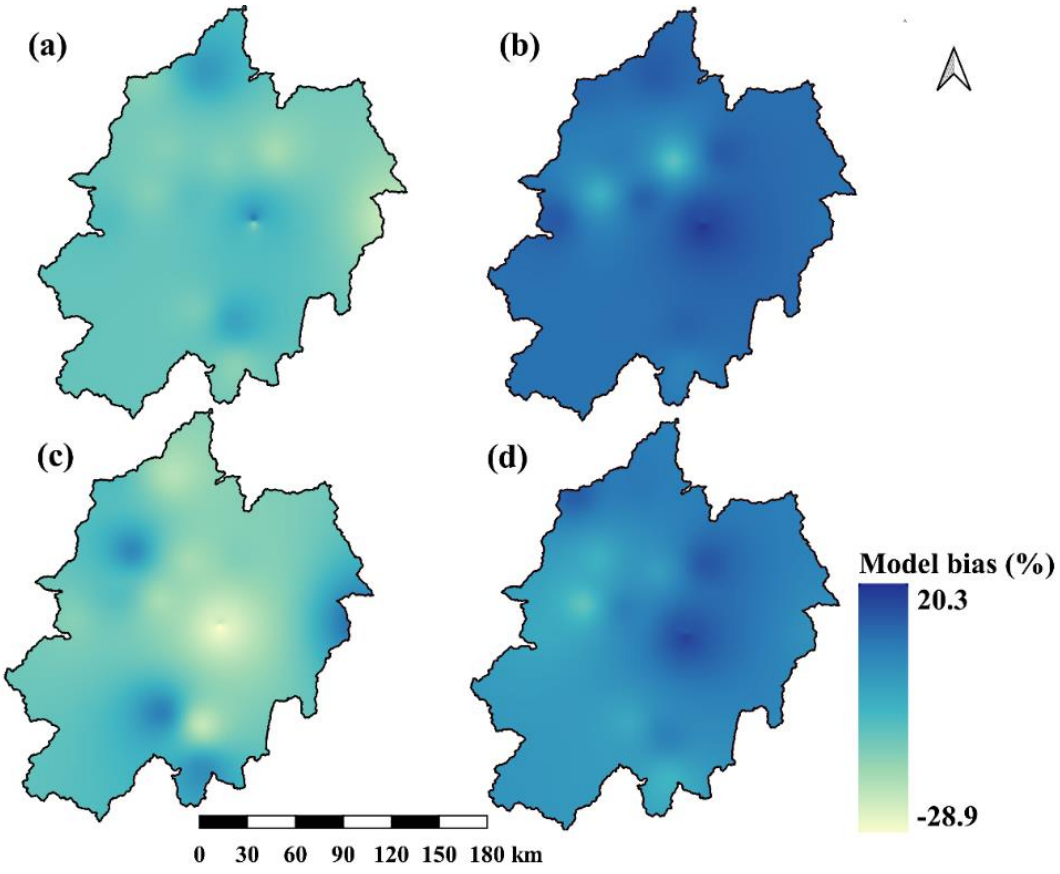

Figure 11: Spatial biases for rainfall data between observed (CHIRPS) and CORDEX RCMs: (a) REMO2009, (b) CanESM2-RCA4, (c) NorESM1-RCA4 and (d) KNMI-RACMO22T

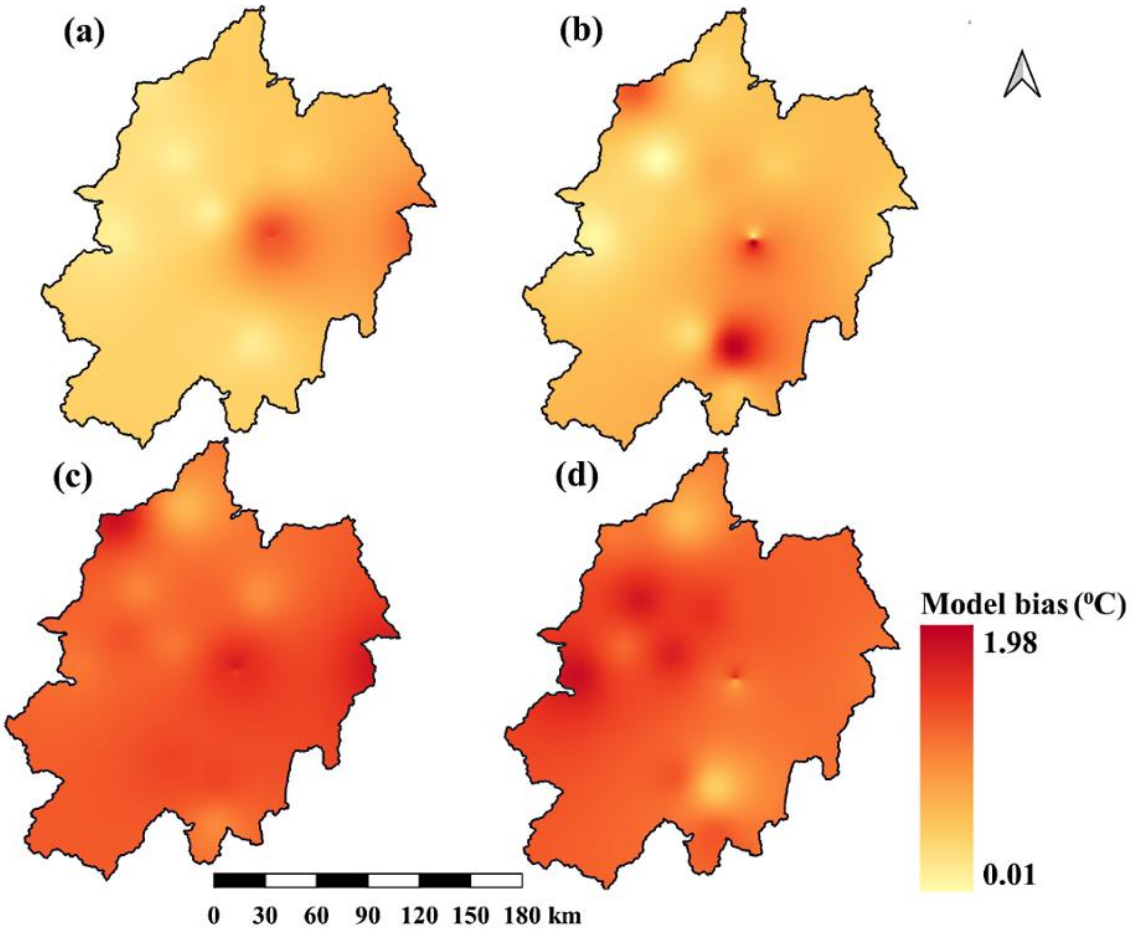

Figure 12: Spatial biases (°C) for temperature data between observed (MERRA-2) and CORDEX RCMs: (a) REMO2009, (b) CanESM2-RCA4, (c) NorESM1-RCA4, and (d) KNMI-RACMO22T)

(ii) Screening of the Predictors for Statistical Downscaling using the Statistical Downscaling System Model

The screening of suitable predictor variables is an important process in statistical downscaling. The power of each predictor is distinguishable in space and time, making the choice of predictors differ according to the geographical location and the relationship between predictors and predictands to be downscaled. With reference to the coefficient of correlation (*r*) and partial correlation (partial-*r*), among the individual best performed NCEP predictors in the SDSM, the selected suitable predictors for downscaling of rainfall and temperatures are listed in Table 11.

Table 11: Selected predictor variables from National Centre for Environmental Prediction

Parameter	Predictors	*r*	*p*-value	Partial-*r*
Rainfall(mm)	Mean sea level pressure	0.38	0.0047	0.247
	850 hPa geopotential height	0.36	0.0047	0.144
	1000 hPa specific humidity	0.39	0.0081	0.281
Tmax. (ºC)	Mean sea level pressure	0.42	0.0000	0.180
	1000 hPa meridional velocity	0.40	0.0000	0.381
	850 hPa geopotential height	0.40	0.0000	0.325
	Air temperature at 2 m	0.50	0.0000	0.380
Tmin. (ºC)	Mean se level pressure	-0.60	0.0000	-0.137
	1000 hPa meridional velocity	-0.50	0.0008	-0.239
	850 hPa geopotential height	0.60	0.0000	0.503
	1000 hPa specific humidity	0.60	0.0000	0.469
	Air temperature at 2 m	0.40	0.0000	0.297

(iii) Performance Evaluation of the Statistical Downscaling System Model and Long Ashton Research Station Weather Generator Outputs

The SDSM validation results for the simulated rainfall and maximum and minimum temperatures for all stations are shown in Tables 12, 13 and 14. The SDSM indicated poor performance in simulating the daily rainfall with Nash-Sutcliffe efficiency (NSE), Percent bias (PBIAS), and RMSE observation's standard deviation ratio (RSR) ranging from 0.12 to 0.25, -56.30 to -26.10, and 0.63 to 0.87, respectively (Table 12). However, the model performed relatively well in reproducing maximum and minimum temperatures at the daily timescale (Tables 13 and 14). The model had NSE, PBIAS, and RSR ranging from 0.70 to 0.89, -17.8 to 11.8 and 0.39 to 0.58, for the maximum temperature; 0.67 to 0.97, -17.8 to 7.8, and 0.35 to 0.59, for minimum temperature, respectively.

At monthly and seasonal timescales, the model performed well in simulating both rainfall and maximum and minimum temperatures. For rainfall at a monthly timescale, the model had NSE, PBIAS, and RSR that ranged from 0.76 to 0.98, -13.8 to 1.70, and 0.04 to 0.58, respectively. For the maximum and minimum temperatures at a monthly timescale, the model performance showed NSE, PBIAS and RSR ranging from 0.78 to 0.96, -14.60 to 11.30, and 0.42 to 0.64; and 0.78 to 0.96, -15.10 to 9.60, and 0.48 to 0.56, respectively. Besides, the model performed well in simulating rainfall and maximum and minimum temperatures on a seasonal scale. The model performance showed NSE, PBIAS, and RSR ranging from 0.62 to 0.99, -13.20 to 1.90, and 0.33 to 0.61; 0.78 to 0.92, -16.20 to 9.60, and 0.41 to 0.59; and 0.78 to 0.92, -13.90 to 8.70 and, 0.42 to 0.58, respectively, for the rainfall, maximum temperature, and minimum

temperature. Therefore, for monthly and seasonal timescales, the SDSM could be used as a tool to simulate rainfall data. Moreover, the model simulated temperature data with good precision for daily, monthly and seasonal timescales.

Table 12: Model performance for the rainfall (mm) simulation for daily, monthly, and seasonal timescales during the validation period from 1997to 2005

S/N	Station	Daily			Monthly			Seasonal		
		NSE	PBIAS	RSR	NSE	PBIAS	RSR	NSE	PBIAS	RSR
1	Arusha	0.24	-26.10	0.68	0.98	-4.40	0.10	0.78	-6.40	0.54
2	Babati	0.18	-28.30	0.87	0.88	-13.80	0.57	0.97	-11.80	0.48
3	Enduleni	0.22	-34.60	0.73	0.95	-1.60	0.05	0.95	-9.60	0.42
4	Engaruka	0.25	-27.20	0.68	0.94	-0.70	0.06	0.79	-10.70	0.58
5	Idulu	0.16	-29.50	0.72	0.97	-0.90	0.04	0.99	-5.90	0.34
6	Kakesio	0.23	-32.70	0.86	0.76	0.80	0.04	0.91	1.80	0.51
7	Manyara	0.18	-56.30	0.74	0.88	-12.30	0.45	0.94	-13.20	0.33
8	Mbulu	0.21	-27.20	0.63	0.90	-13.30	0.96	0.64	-12.30	0.52
9	Mtowambu	0.24	-35.60	0.67	0.83	1.70	0.06	0.91	1.90	0.57
10	Nainokanoka	0.15	-44.20	0.72	0.76	-1.20	0.05	0.83	-4.20	0.39
11	Ndutu	0.24	-32.40	0.77	0.86	-1.20	0.05	0.62	-7.20	0.51
12	Ngorongoro	0.22	-47.30	0.81	0.91	-12.10	0.16	0.81	-11.10	0.56
13	Olala	0.12	-28.20	0.70	0.86	-9.30	0.08	0.77	-8.30	0.44
14	Olduvai	0.20	-31.60	0.68	0.82	-3.20	0.58	0.83	-2.70	0.36

Table 13: Model performance for the maximum temperature (ºC) simulation for daily, monthly, and seasonal timescales during the validation period of 1997- 2005

SN	Station	Daily			Monthly			Seasonal		
		NSE	PBIAS	RSR	NSE	PBIAS	RSR	NSE	PBIAS	RSR
1	Arusha	0.82	-13.70	0.58	0.88	-8.40	0.54	0.81	-11.05	0.52
2	Babati	0.87	-17.80	0.48	0.78	-14.60	0.53	0.83	-14.20	0.58
3	Enduleni	0.75	-12.60	0.52	0.85	-11.60	0.49	0.84	-12.10	0.59
4	Engaruka	0.89	-14.70	0.57	0.95	-6.70	0.52	0.86	-10.70	0.47
5	Idulu	0.79	-15.90	0.44	0.93	-10.90	0.64	0.79	-13.40	0.58
6	Kakesio	0.81	11.80	0.51	0.86	6.80	0.48	0.83	9.30	0.54
7	Manyara	0.84	-14.20	0.39	0.78	-14.30	0.42	0.81	-14.25	0.56
8	Mbulu	0.74	-10.30	0.55	0.82	-11.60	0.62	0.78	-10.95	0.50
9	Mtowambu	0.81	7.90	0.47	0.81	11.30	0.57	0.79	9.60	0.51
10	Nainokanoka	0.87	-6.20	0.49	0.78	-13.20	0.47	0.85	-9.70	0.54
11	Ndutu	0.72	-5.20	0.56	0.96	-9.20	0.51	0.82	-7.20	0.54
12	Ngorongoro	0.77	-12.10	0.51	0.94	-12.70	0.44	0.80	-12.40	0.49
13	Olala	0.70	-6.30	0.54	0.88	-10.30	0.61	0.92	-8.30	0.41
14	Olduvai	0.73	-12.70	0.47	0.84	-13.40	0.57	0.86	-13.05	0.58

Table 14: Model performance for the minimum temperature (ºC) simulation on the daily, monthly, and seasonal timescale during the validation period from 1997 to 2005

SN	Station	Daily			Monthly			Seasonal		
		NSE	PBIAS	RSR	NSE	PBIAS	RSR	NSE	PBIAS	RSR
1	Arusha	0.93	-12.70	0.39	0.96	-14.40	0.48	0.81	-13.55	0.44
2	Babati	0.97	-15.80	0.57	0.94	-9.60	0.56	0.83	-12.70	0.56
3	Enduleni	0.86	-11.60	0.45	0.88	-10.80	0.51	0.84	-11.20	0.48
4	Engaruka	0.82	-12.70	0.59	0.84	-15.10	0.53	0.86	-13.90	0.56
5	Idulu	0.89	-10.90	0.47	0.82	-8.90	0.56	0.79	-9.90	0.52
6	Kakesio	0.91	7.80	0.43	0.81	9.60	0.48	0.83	8.70	0.46
7	Manyara	0.88	-11.20	0.49	0.78	-9.70	0.49	0.81	-10.45	0.49
8	Mbulu	0.76	-14.30	0.35	0.96	-7.20	0.49	0.78	-10.75	0.42
9	Mtowambu	0.71	5.90	0.48	0.94	-12.40	0.52	0.79	-3.25	0.50
10	Nainokanoka	0.77	-13.30	0.59	0.84	-10.70	0.53	0.85	-12.00	0.56
11	Ndutu	0.82	-7.20	0.46	0.86	-13.40	0.50	0.82	-10.30	0.48
12	Ngorongoro	0.67	-13.10	0.52	0.79	-12.30	0.48	0.80	-12.70	0.50
13	Olala	0.90	-12.30	0.44	0.83	-11.25	0.49	0.92	-11.78	0.46
14	Olduvai	0.78	-11.70	0.39	0.81	-10.40	0.51	0.86	-11.05	0.45

(iv) Performance of Long Ashton Research Station Weather Generator in Statistical Downscaling of Global Climate Models

The LARS-WG performance is shown in Fig. 13 (calibration) and Table 15 (validation). Figure 13 a and c indicate the monthly mean rainfall and standard deviations of the synthesized LARS-WG data compared to the observed data during the calibration period (1982-2001). However, Fig. 13 b and d indicates the comparison between observed and synthesized monthly mean maximum and minimum temperature. Four GCMs (i.e. CanESM2-RCA4, NorESM1-RCA4, CSIRO-CMS and HadGEM2-ES) were used to generate daily rainfall and temperature data for RCP 4.5 and 8.5 using the LARS-WG model. Furthermore, the statistical test to validate the LARS-WG output was performed and indicated in Table 15

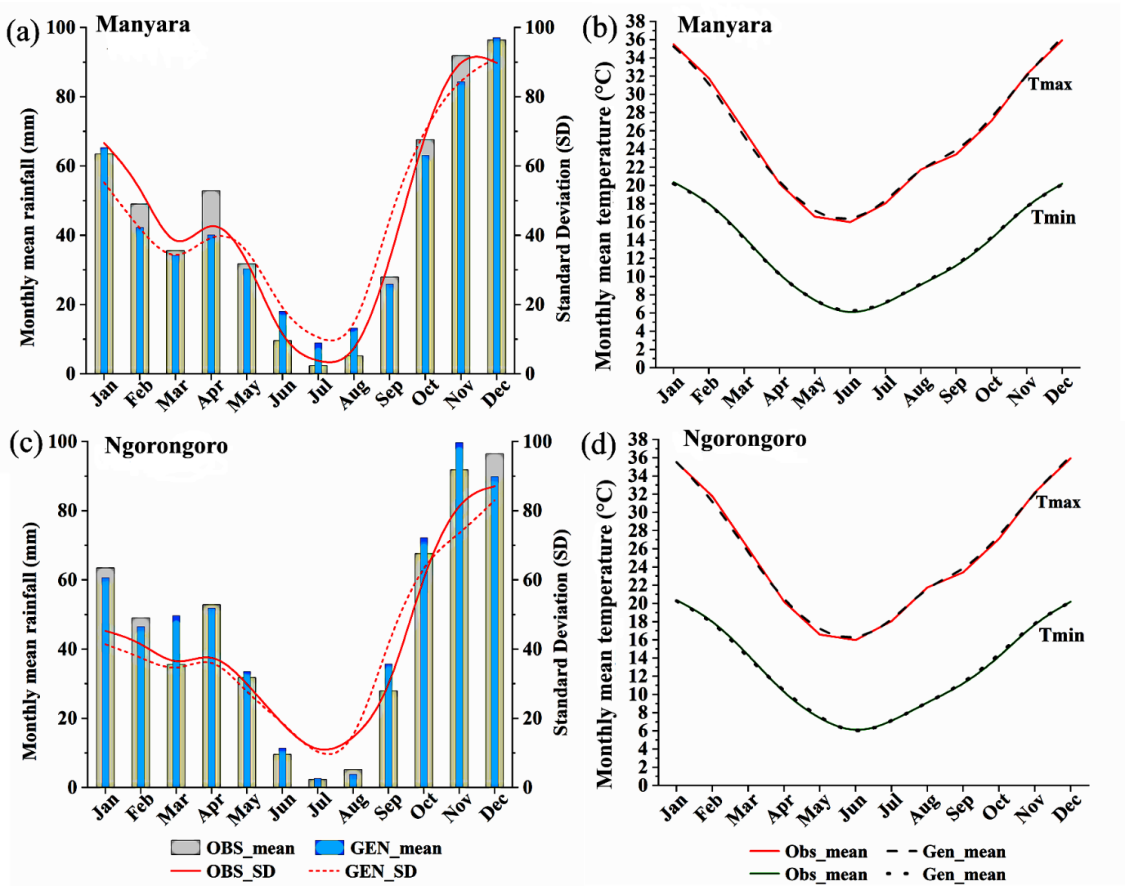

Figure 13: Calibration of Long Ashton Research Station Weather Generator for mean monthly rainfall (mm) and temperatures for Manyara (a and b), and Ngorongoro (c and d), respectively

Table 15: Model performance for the rainfall (mm), Maximum temperature (ºC) and minimum temperature (ºC) at a daily and monthly timescale during the validation period of 2002 -2011 for the entire basin

Scale	Parameter	NSE	RSR	RMSE	PBIAS	R^2
Daily	Rainfall	-0.80	1.34	7.94	-1.10	0.00
	Tmax	-0.70	1.30	10.05	14.90	0.52
	Tmin	0.89	1.38	8.05	26.20	0.47
Monthly	Rainfall	0.78	0.81	14.58	-8.50	0.53
	Tmax	-0.80	1.29	9.15	15.10	0.64
	Tmin	-1.15	1.41	7.43	26.5	0.91

The results show good performance in synthesizing data series daily and monthly time scales for the entire basin during validation. The LARS-WG performed well in reproducing the rainfall and temperature data on daily and monthly scales. These results are consistent with other studies (Bessah *et al.*, 2021; Chen *et al.*, 2013) which indicated a good performance of LARS-WG in generating daily and monthly rainfall and temperature data. Therefore, the output

from LARW-WG could be used for the climate change analysis and climate change impact studies in and around the NCA. However, to minimize model uncertainties, the study applied the bias-corrected rainfall and temperature-simulated CORDEX RCMs, SDSM and LARS-WG ensembles to analyze the change in climate around the NCA by comparing the future projection for 2021-2050 with historical data from the period 1982-2011.

4.1.2 Analysis of Climate Variability and Changes in Time and Space in the Study Area under Representative Concentration Pathways 4.5 and Representative Concentration Pathways 8.5 Scenarios

(i) Spatial-Temporal Change in Climate Variables

Table 16 represents the annual statistical summary for the average rainfall and temperature for the baseline period (1982-2011), which was used as a reference to determine the future (2021-2050) changes in climate over the study area.

Table 16: Annual statistics for the baseline (1982 – 2011) climate variables

	Rain(mm)	Tmax (°C)	Tmin(°C)	Tmean(°C)
Mean	812.28	26.87	14.26	20.56
Std. Deviation	178.90	0.59	0.32	0.40
Minimum	486.42	25.64	13.61	19.69
Maximum	1230.29	28.02	14.85	21.32
Percentiles				
25	718.59	26.49	14.08	20.34
50	790.65	26.84	14.37	20.55
75	906.62	27.22	14.45	20.85

Generally, the annual change in climatic variables for 2021-2050 compared to the mean climate variable at the baseline (1982-2011) is presented in Fig. 14. The results include percentage change in annual mean rainfall (mm) and maximum and minimum temperature anomalies. In addition, the study analysed the percentage changes in the mean seasonal (JF, MAM, JJAS, and OND) and annual rainfall for the future (2021-2050) period by considering RCP 4.5 and RCP 8.5 scenarios compared to the historical (1982-2011) period. The results of the temporal analysis are presented in Fig. 15.

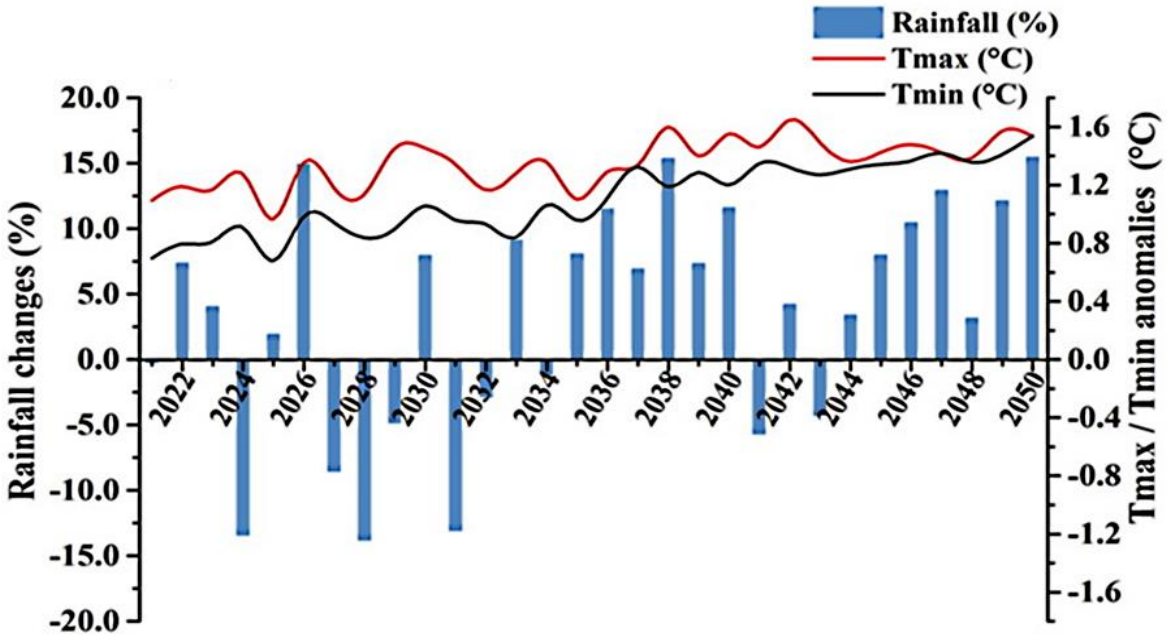

Figure 14: **The percentage change in annual mean rainfall (mm), maximum and minimum temperature anomalies for 2021-2050 compared to the baseline (1982-2011)**

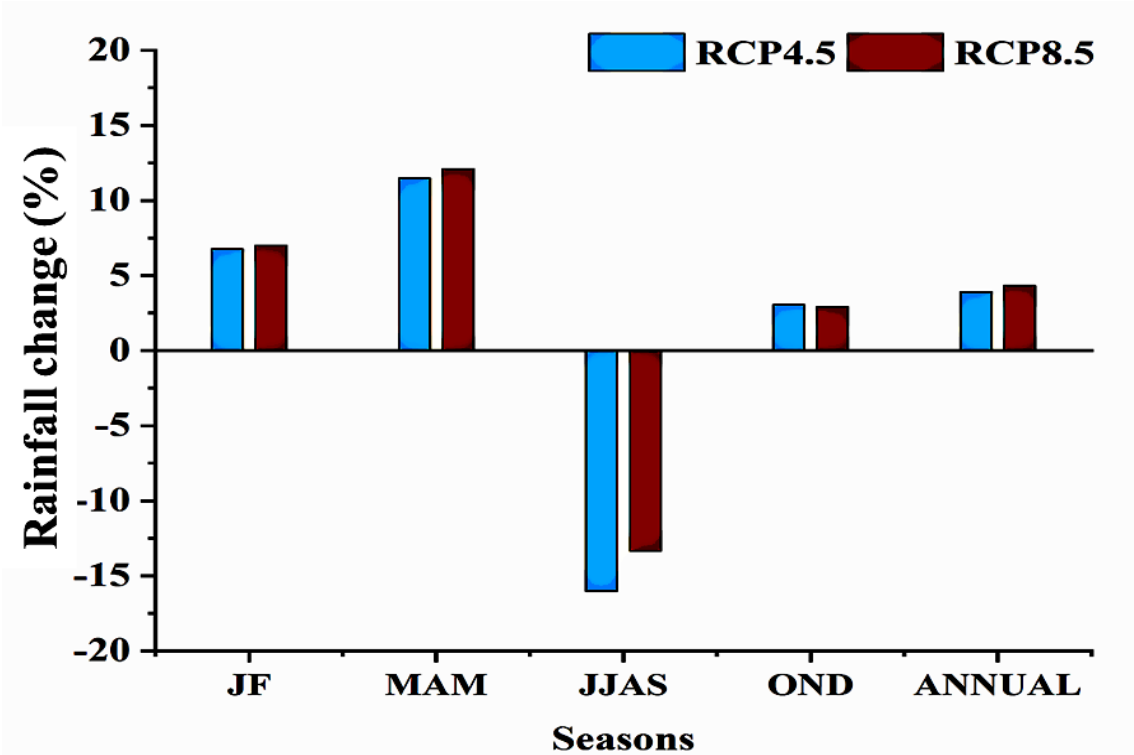

Figure 15: **Percentage change in seasonal and annual mean rainfall for the future period (2021-2050) under RCP 4.5 and RCP 8.5, compared to the simulated historical period (1982-2011)**

The results for the future period 2021-2050 indicated an increasing trend of annual mean rainfall and maximum/minimum temperatures. However, between 2021 and 2035, the results

show a decreasing rainfall trend, with the highest decrease of 13.8% in 2024. A more significant increase is observed between 2036 and 2050, with a maximum rise of 15.4% in 2038 (Fig. 14). Seasonally, the rainfall data shows an increase in all seasons except the JJAS season, which decreases 13 and 16% under RCP 4.5 and RCP 8.5, respectively. The annual rainfall indicates an increase with an average of 4% under RCP 4.5 and 5% under RCP 8.5. The comparison between future projections and the historical data showed increasing rainfall for all seasons except JJAS, which showed a decreasing trend for both RCPs. However, the annual rainfall showed a significantly increasing pattern for the periods of 2021-2050 for both RCPs. Similarly, for maximum and minimum temperatures, the annual temperature rise would occur in future periods, with a higher rise expected under RCP 8.5. Other research findings in Tanzania (Cooper *et al.*, 2008; Luhunga *et al.*, 2018; Mtongori *et al.*, 2016) also anticipated an increase in rainfall across Tanzania's northeastern highlands. The studies correspondingly showed an increase in maximum and minimum temperature for all future periods and RCPs but with the highest rise under RCP 8.5.

The spatial distribution of the changes in annual rainfall for 2021-2050 under RCP 4.5 and RCP 8.5 are depicted in Fig. 16 a and b. Spatially, the rainfall would increase over the entire study area during the period of 2021-2050 under both RCPs, with the highest increase over the Eastern, Southern parts and some areas in the West. The study area's central, western, and northern parts would experience a low percentage increase in rainfall with the lowest percentage of 2 % under both RCPs. Both RCPs indicate similar patterns over the area for the future 2021-2050; however, RCP 4.5 outputs show higher increases compared to the RCP 8.5.

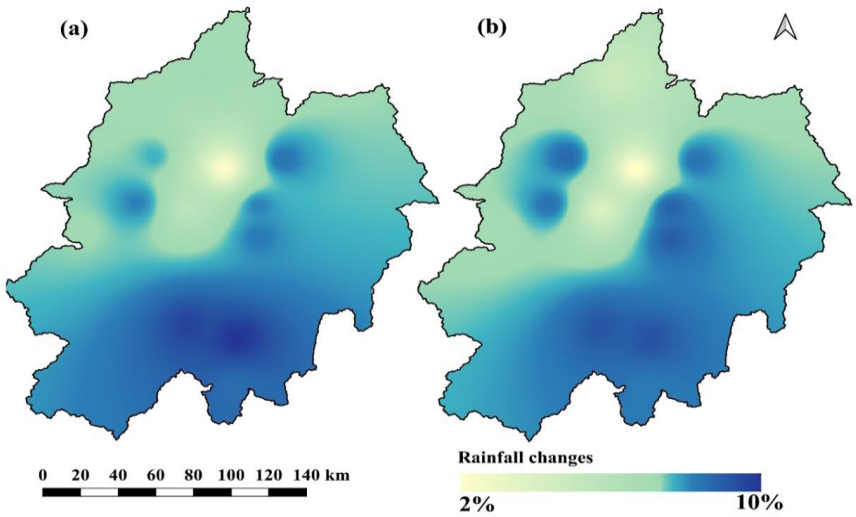

Figure 16: Spatial distribution of changes in the mean annual rainfall under RCP 4.5 (a) and RCP 8.5 (b) for the period of 2021-2050 compared to the historical period of 1982-2011

(ii) Projected Changes in Temperature

Results also indicate maximum and minimum temperature anomalies rise between 2036 and 2050, with the highest rise of 1.7°C and 1.5°C) in 2042 and 2050, respectively (Fig. 14). However, for the annual mean maximum, minimum and mean temperature change under RCPs 4.5 and 8.5 as presented in Table 18. The results indicate an increase in maximum, minimum, and mean temperatures. The maximum, minimum, and mean temperature have increased respectively by 0.4°C, 0.5°C, and 0.5°C under RCP 4.5 and 0.6°C, 0.6°C, 0.6°C under RCP 8.5 during the future 2021-2050.

Table 17: Temperature (°C) projections and change signal for the (2021-2050) future under RCP 4.5 and RCP 8.5 scenarios relative to the historical (1982-2011) period, the ensemble mean

Temperature	Historical (1982-2011)	RCP4.5 scenario	RCP8.5 scenario
Maximum	26.9	27.3 (+0.4) *	27.5 (+0.6) *
Minimum	14.3	14.8 (+0.5) *	14.9 (+0.6) *
Mean	20.6	21.1 (+0.5) *	21.1 (+0.6) *

Values in brackets indicate the projected changes. *Indicates the significance of the projected changes at a 95% confidence level

(iii) Spatial Distribution of Temperature Change

Spatial distribution for the maximum and minimum temperature change for the future periods of 2021-2050 under RCP 4.5 and RCP 8.5 emission scenarios as captured by the SDSM and RCMs ensembles are presented in Fig. 17 a and b and Fig. 18 a and b, respectively. The results for the maximum temperature change indicate warming over the study area with spatial variations. The maximum temperature increase during the period of 2021-2050 is expected to be in the range of 0.1 to 0.8°C under RCP 4.5. The highest increase is in the central and southern parts, and the lowest increase is over the western and northwestern areas and a few parts in the east of the study area. The maximum temperature rises for the same period, under RCP 8.5, would be between 0.1°C and 0.9°C, with the highest value in the central and the southern parts; most of the areas would be warmer by a range of 0.2°C to 0.8°C during the 2021-2050 period under both RCPs as captured in (Fig. 17 a-b).

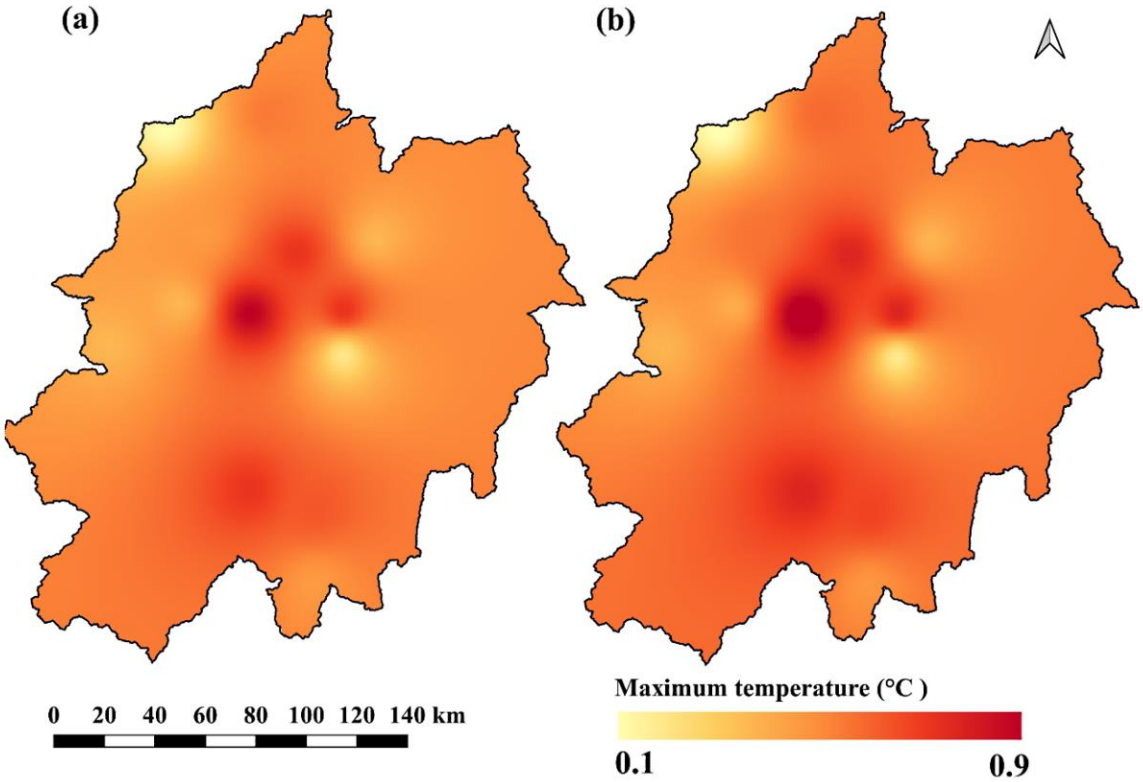

Figure 17: Spatial distribution for the annual maximum temperature anomalies (°C) under RCP 4.5 (a) and RCP 8.5 (c) for the period of 2021-2050 compared to the historical period of 1982-2011

The results for the minimum temperature change (Fig. 18 a & b) also show a warming regime over the study area with variations in spatial distribution. The minimum temperature rises during 2021-2050 are expected to range from 0.1°C to 1.0°C under RCP 4.5. The highest increases are in the central and south of the study area, while northwestern areas and part of the central area would experience the lowest rise as captured by the ensemble mean of LARS-WG, SDSM and RCMs. The minimum temperature rises for the same period, under RCP 8.5, would be between 0.1 and 0.9°C, with the highest value covering a large part of the central and south of the study area and the lowest found in the northwestern areas and parts of central areas. Generally, most of the areas would be anomalously warmer by 0.2°C to 0.8°C under both RCPs, as shown in Fig. 18 a and b.

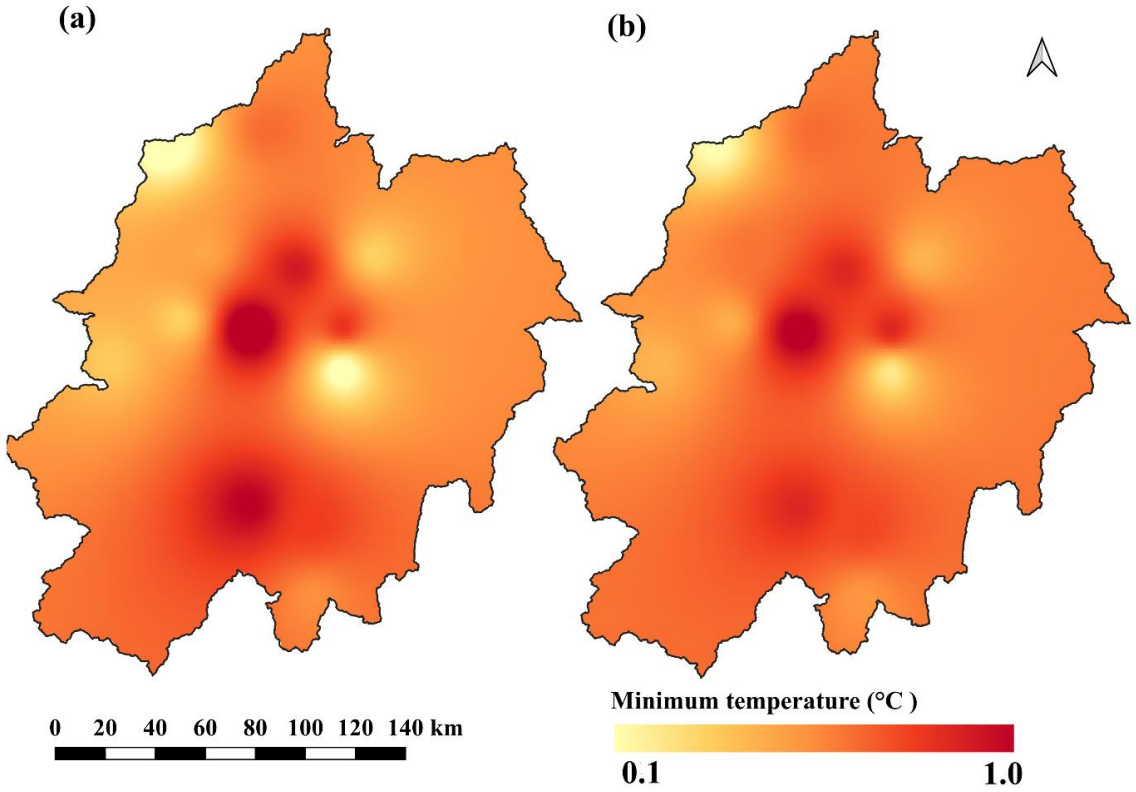

Figure 18: Spatial distribution for the annual minimum temperature anomalies (°C) under RCP 4.5 (a) and RCP 8.5 (c) for the period of 2021-2050 compared to the historical period of 1982-2011

The projected rise in rainfall and temperature can affect water resources, their services, and the prevalent social-economic activities in the study area (Obuobie *et al.*, 2012). The Government of Tanzania has reported climate change impacts in several places, including in the protected areas of conservation importance (United Republic of Tanzania [URT], 2008). The Government has shown concerns about the increase in drought and flood events in its protected areas. As the findings of this study projected an increase in rainfall and temperature in NCA and its surroundings, severe climatic events are expected. The severity of climatic events may lead to encroachment problems in local communities where communities are increasingly forced to expand their activities into conserved areas. The projected increase in rainfall in the present study agrees with the findings of Donat *et al.* (2016) who projected that the world's dry places like the tropics would experience more extreme precipitation. However, the projected increase in rainfall will have the advantage of a constant water supply to the biodiversity and ensure food security for the expanding human population in the Ngorongoro Conservation Area and its surroundings. Due to the possibility of human activities expansion and encroachment to the conserved areas, the study also analysed the Land use/ cover changes and modelled the

future land use/cover scenarios in the study area to determine the impact of climate and land use/ cover change to water resources.

4.2 To Examine the Land use/cover Change between 1995 and 2016 and Model the Future Scenarios for 2025 and 2036 in the Study Area

4.2.1 Accuracy Assessment

Table 18 shows the accuracy assessment for the classified maps for 1995, 2005, and 2016. The accuracy assessments founded on error matrices presented an overall accuracy of 98.01%, 99.71%, and 99.98% for 1995, 2005, and 2016. The Kappa coefficients of those periods were 0.98, 0.99, and 0.99, respectively. This assessment, shows the high model capacity to classify the 1995, 2005 and 2016 prevailing land use over the study area.

Table 18: Accuracy assessment of the land use/cover classification at Ngorongoro Conservation Area and surrounding

Land use/cover	1995		2005		2016	
	PA	UA	PA	UA	PA	UA
Forest	98.76	98.18	98.10	98.10	99.94	99.17
Woodland	98.91	99.06	97.91	97.93	100	99.20
Bushland	99.39	99.42	98.08	98.07	100	99.17
Grassland	99.91	99.93	99.98	98.10	99.98	99.18
Water	100	100	99.00	98.10	99.00	100
Wetland	99.98	100	98.10	98.10	99.80	99.20
Cultivated land	96.81	99.75	100	98.10	99.41	100
Built-up area	100	100	96.20	96.20	100	99.20
Bare land	100	100	100.00	98.10	100	99.20
Overall	98.01		99.71		99.98	
Kappa	0.98		0.99		0.99	

Note: PA-Producer's Accuracy, UA—User's Accuracy.

4.2.2 Land use/cover Change Pattern

The study considered Land use/cover changes analysis for 21 years to monitor the land use/cover changes over the study area. The study generated Land use/cover maps for 1995, 2005, and 2016 using remote sensing data and ground-truthed information collected from the study area. A difference in the pattern of the altered land use/cover types was observed. The land areas under different Land use/cover types and their percentage are given in Table 19. The spatial Land use/cover distribution for 1995, 2005, and 2016 are presented in Fig. 19. Land

use/cover of the year 1995 indicated that the area 43.975% was covered by bushland, 34.914% by grassland, 9.038% by woodland, 4.275% by forest, 3.103% by cultivated land, 3.088% by water, 1.528% by wetland, 0.071% by bare land and 0.008% by built-up area. While land use/cover of the year 2005, the area was covered by 42.387% by bushland, 39.467% by grassland, 7.631% by cultivated land, 3.322% by forest, 3.261% by water, 2.474% by woodland, 0.818% by wetland, 0.631% by bare land and 0.01% by built-up area. The distribution of Land use/cover in the year 2016 shows that about 44.452% was covered by bushland, 37.599% by grassland, 9.657% by cultivated land, 2.851% by water, 2.751% by forest, 1.891% by bare land, 0.661% by woodland, 0.118% by wetland and 0.021% by built-up area.

Table: 19: Land use/cover classification results for 1995, 2005 and 2016

	Land use/cover					
Year	**1995**		**2005**		**2016**	
Unit	**Ha**	**%**	**Ha**	**%**	**Ha**	**%**
Forest	143204	4.275	111277	3.322	92152	2.751
Woodland	302766	9.038	82860	2.474	22151	0.661
Bushland	1473057	43.975	1419863	42.387	1489040	44.452
Grassland	1169535	34.914	1322070	39.467	1259488	37.599
Water	103441	3.088	109233	3.261	95489	2.851
Wetland	51185	1.528	27411	0.818	3962	0.118
Cultivated land	103960	3.103	255619	7.631	323484	9.657
Built-up area	265	0.008	322	0.010	698	0.021
Bare area	2385	0.071	21143	0.631	63332	1.891
Total	3349797	100	3349797	100	3349797	100

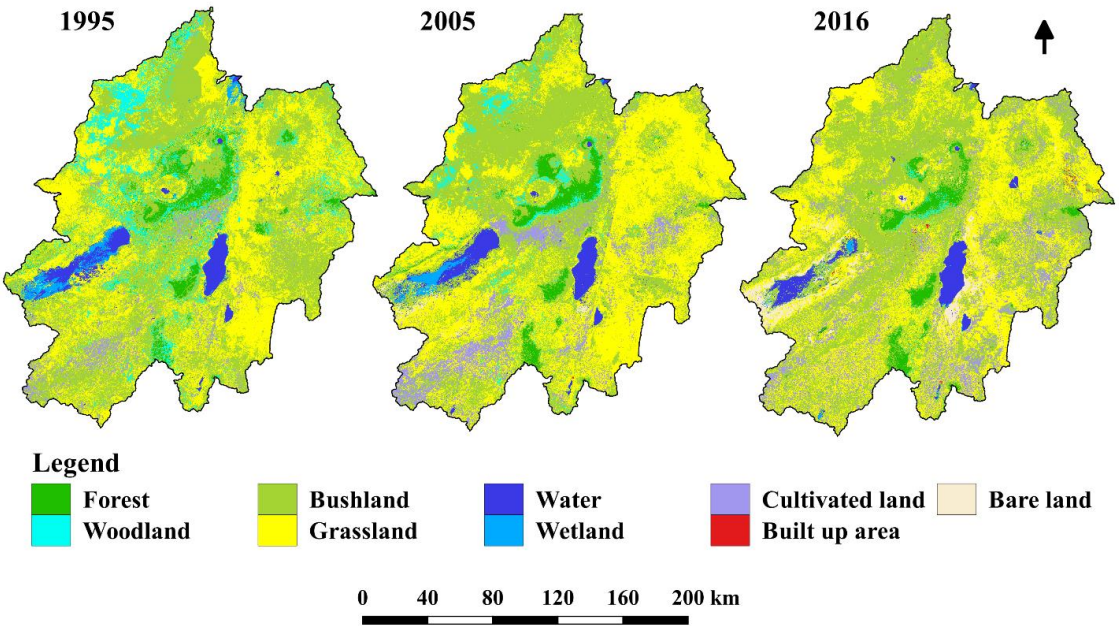

Figure 19: Land use/cover maps for 1995, 2005, and 2016 at Ngorongoro Conservation Area and surrounding

The changes in land use/cover for the study period (1995-2005, 2005-2016, and 1995-2016) are given in Table 20. During the study period 1995 - 2005, woodland decreased by 6.564%, bushland by 1.588%, forest by 0.953%, and wetland by 0.71%. The grassland experienced an increase of 4.553%, cultivated land by 4.528%, bare land by 0.56%, and water by 0.173%. While during 2005 to 2016, a decrease was observed in the grassland by 1.868%, woodland by 1.813%, wetland by 0.7%, forest by 0.571%, and water by 0.41%. The result showed an increase of bushland by 2.065%, cultivated land by 2.026%, bare land by 1.26%, and built-up land by 0.011% in the period 2005 - 2016. The results revealed that the highest net gain during the study period 2000 - 2016 was in cultivated land (6.554%), followed by grassland (2.685%), bare land (1.82%), bushland (0.477%), and built-up land (0.013%), while net loss was in woodland (8.377%), forest (1.524%), wetland (1.41%), and water (0.237%) (Table 20).

Table 20: Changes in land use/cover for the period between 1995 and 2016

variables	Land use/cover changes					
	1995-2005		2005-2016		1995-2016	
Unit	Ha	%	Ha	%	Ha	%
Forest	-31927	-0.953	-19125	-0.571	-51052	-1.524
Woodland	-219906	-6.564	-60709	-1.813	-280615	-8.377
Bushland	-53194	-1.588	69177	2.065	15983	0.477
Grassland	152535	4.553	-62582	-1.868	89953	2.685
Water	5792	0.173	-13744	-0.41	-7952	-0.237
Wetland	-23774	-0.71	-23449	-0.7	-47223	-1.41
Cultivated land	151659	4.528	67865	2.026	219524	6.554
Built-up area	57	0.002	376	0.011	433	0.013
Bare area	18758	0.56	42189	1.26	60947	1.82

The results for the study period (1995-2016) on different classes of Land use/cover indicate that maximum gains and losses occurred in cultivated land and woodland, respectively. In addition, bushland and grassland gain many shares from other Land use/cover, and the change matrix (Tables 21 to 23) supported the study's findings.

4.2.3 Land use/cover Change Pattern (Transition) Matrix

Table 21, Table 22, and Table 23 show the change matrix cross-tabulation for the areas and percentages changed from one Land use/cover class to another compared to each Land use/cover class's overall area for the period 1995-2005 2005-2016 and 1995 - 2016. During the study period 1995 - 2016 (Table 6), 61.09% of water remained unchanged, followed by bushland land (51%), grassland (50.46%), built-up land (48.14%), forest (36.67%), bare land (29.88%), cultivated land (22.29%), woodland (1.55%) and wetland (0.49%). Although bushland and grassland maintain 50% of unchanged Land use/cover, the largest share was gained from other Land use/cover. Furthermore, wetland faced the maximum change, with 99.51% of its area converted to bushland (34.47%), water (30.73%), grassland (20.08%), bare land (12.71%), cultivated land (1.25%), forest (0.23%) and woodland (0.03%).

The cross-tabulation matrix for the study period between 1995 and 2005 showed that 68.48% of water remained unchanged, followed by built-up land (58.75%), grassland (57.84%), forest (50.75%), bushland land (50.24%), cultivated land (39.03%), bare land (25.84%), wetland

(16.81%) and woodland (9.25%). This suggests that woodland experiences the maximum alteration, with 90.25% of its total area converted to bushland (57.86%), grassland (23.32%), cultivated land (4.9%), forest (4.16%), wetland (0.27%), water (0.19%), bare land (0.05%) and built-up land (0.01%). Furthermore, for the period between 2005 and 2016, 66.69% of built-up land persisted changes, followed by bushland land (58.42%), water (55.55%), bare land (51.86%), forest (51.98%), grassland (51.33%), cultivated land (24.85%), woodland by (5.04%) and wetland (0.85%). This means that woodland and wetland faced the maximum change, with 94.96% and 99.15% of their total area respectively converted to other Land use/cover.

Table 21: Transition matrix showing Land use/cover change at Ngorongoro Conservation Area between 1995 and 2016

Area (Ha)		2016								
		FR	**WL**	**BUL**	**GL**	**WT**	**WET**	**CL**	**BLT**	**BL**
1995	FR	52519	9944	70609	7279	297	213	1737	5	602
	WL	12016	4681	172065	93098	1347	252	18410	74	825
	BUL	22941	6357	751212	498744	7642	1557	157387	172	27047
	GL	4049	915	424070	590163	6964	968	121164	246	20994
	WT	311	19	19072	13903	63188	465	792	11	5679
	WET	120	15	17641	10278	15728	253	641	2	6506
	CL	163	219	33994	44906	229	249	23174	59	967
	BLT	15	1	85	28	1	0	8	128	0
	BL	18	1	291	1090	94	6	172	0	712
Percentage (%)		**FR**	**WL**	**BUL**	**GL**	**WT**	**WET**	**CL**	**BLT**	**BL**
1995	FR	36.67	6.94	49.31	5.08	0.21	0.15	1.21	0.00	0.42
	WL	3.97	1.55	56.83	30.75	0.44	0.08	6.08	0.02	0.27
	BUL	1.56	0.43	51.00	33.86	0.52	0.11	10.68	0.01	1.84
	GL	0.35	0.08	36.26	50.46	0.60	0.08	10.36	0.02	1.80
	WT	0.30	0.02	18.44	13.44	61.09	0.45	0.77	0.01	5.49
	WET	0.23	0.03	34.47	20.08	30.73	0.49	1.25	0.00	12.71
	CL	0.16	0.21	32.70	43.20	0.22	0.24	22.29	0.06	0.93
	BLT	5.64	0.47	31.90	10.49	0.24	0.00	3.12	48.14	0.00
	BL	0.76	0.03	12.22	45.71	3.94	0.24	7.20	0.02	29.88

FR-Forest, WL—Woodland, BUL—Bushland, GL—Grassland, WT—Water, WET-Wetland, CL—Cultivated land, BLT-Built-up land, BL- Bare land

Table 22: Transition matrix showing land use/cover change at Ngorongoro Conservation Area between 1995 and 2005

Area (Ha)		2005								
		FR	**WL**	**BUL**	**GL**	**WT**	**WET**	**CL**	**BLT**	**BL**
1995	FR	72669	8789	53060	5186	169	57	3271	0	1
	WL	12604	28002	175175	70594	573	805	14849	18	147
	BUL	24079	30931	740088	530138	10381	2040	122479	55	12866
	GL	1518	14504	386390	676457	9683	1670	73876	62	5375
	WT	339	59	12879	3891	70841	14188	343	0	902
	WET	45	61	21201	3010	17262	8606	148	2	851
	CL	17	500	30448	31659	310	37	40575	28	385
	BLT	0	0	76	11	0	0	21	156	0
	BL	5	14	545	1124	13	9	58	0	616
Percentage (%)		**FR**	**WL**	**BUL**	**GL**	**WT**	**WET**	**CL**	**BLT**	**BL**
1995	FR	50.75	6.14	37.05	3.62	0.12	0.04	2.28	0.00	0.00
	WL	4.16	9.25	57.86	23.32	0.19	0.27	4.90	0.01	0.05
	BUL	1.63	2.10	50.24	35.99	0.70	0.14	8.31	0.00	0.87
	GL	0.13	1.24	33.04	57.84	0.83	0.14	6.32	0.01	0.46
	WT	0.33	0.06	12.45	3.76	68.48	13.72	0.33	0.00	0.87
	WET	0.09	0.12	41.42	5.88	33.73	16.81	0.29	0.00	1.66
	CL	0.02	0.48	29.29	30.45	0.30	0.04	39.03	0.03	0.37
	BLT	0.03	0.17	28.63	4.31	0.00	0.10	8.01	58.75	0.00
	BL	0.23	0.57	22.87	47.14	0.56	0.37	2.42	0.01	25.84

FR-Forest, WL—Woodland, BUL—Bushland, GL—Grassland, WT—Water, WET-Wetland, CL—Cultivated land, BLT-Built-up land, BL- Bare land

Table 23: Transition matrix showing land use/cover change at Ngorongoro Conservation Area between 2005 and 2016

Area (Ha)		2016								
		FR	**WL**	**BUL**	**GL**	**WT**	**WET**	**CL**	**BLT**	**BL**
2005	FR	57845	11805	37699	2598	277	200	192	18	642
	WL	3672	4175	46663	25564	65	82	2439	10	191
	BUL	23842	4869	829494	423103	12668	1195	101785	237	22671
	GL	5933	1085	459236	678586	6599	1012	152399	186	17033
	WT	233	8	21799	16406	60683	977	873	11	8242
	WET	60	2	4739	6265	13768	233	171	0	2175
	CL	511	203	88632	100292	777	243	63526	22	1415
	BLT	33	0	56	15	1	0	3	215	0
	BL	25	3	723	6661	651	20	2097	0	10964
Percentage (%)		**FR**	**WL**	**BUL**	**GL**	**WT**	**WET**	**CL**	**BLT**	**BL**
2005	FR	51.98	10.61	33.88	2.33	0.25	0.18	0.17	0.02	0.58
	WL	4.43	5.04	56.32	30.85	0.08	0.10	2.94	0.01	0.23
	BUL	1.68	0.34	58.42	29.80	0.89	0.08	7.17	0.02	1.60
	GL	0.45	0.08	34.74	51.33	0.50	0.08	11.53	0.01	1.29
	WT	0.21	0.01	19.96	15.02	55.55	0.89	0.80	0.01	7.55
	WET	0.22	0.01	17.29	22.85	50.23	0.85	0.62	0.00	7.93
	CL	0.20	0.08	34.67	39.23	0.30	0.09	24.85	0.01	0.55
	BLT	10.11	0.11	17.49	4.53	0.28	0.00	0.78	66.69	0.00
	BL	0.12	0.01	3.42	31.50	3.08	0.10	9.92	0.00	51.86

FR-Forest, WL—Woodland, BUL—Bushland, GL—Grassland, WT—Water, WET-Wetland, CL—Cultivated land, BLT-Built-up land, BL- Bare land

4.2.4 Predicted Land use/ cover Patterns

The CA-Markov model was applied to forecast Land use/cover changes based on Land use/cover change trends between 1995 and 2016. The CA–Markov validation was succeeded, with 87.5% of ROC value. These results provided a basis for the following analysis of Land use/cover changes. The values for Kappa statistics such as Kno (85.95%), Klocation (86.57%), KlocationStrata (86.57%), and Kstandard (82.05%) were also above 80%, which shows the high model capacity to simulate the 2025 and 2035 land use. The study assumed the persistence of the current management (i.e., business as usual scenario) for the predicted Land use/cover maps for 2025 and 2035 using CA-Markov. Table 24 and 25 shows the extent of projected Land use/cover types from 2016 to 2025 and 2035. Also, Fig. 20 shows the predicted Land

use/cover maps for the years 2016, 2025 and 2035. Land use/cover of the projected the year 2025 indicated that the area 39.36% will be covered by bushland, 37.65% by grassland, 12.85% by cultivated land, 4.88% by bare land, 2.29% by forest, 1.99% by water, 0.37% by woodland, 0.32% by built-up land and 0.30% by the wetland. Moreover, the projected Land use/cover for the year 2035 shows that; grassland will cover 39.47% of the area, followed by 34.48% by bushland, 15.58% by cultivated land, 6.67% by bare land, 1.47% by forest, 1.23% by water, 0.45% by built-up area, 0.31% by woodland and 0.27% by the wetland. Net loss between 2025 and 2035 is expected in the forest, woodland, bushland, water, and wetland, while the net gain is anticipated in grassland, cultivated land, built-up area, and bare land. The bushland is expected to decrease by 4.88%, followed by forest by 0.82%, water by 0.77%, woodland by 0.07%, and wetland by 0.02%. Further, the cultivated land is expected to increase by 2.73%, followed by grassland by 1.91%, bare land by 1.79%, and built-up land by 0.14%.

Table 24: Areas of individual land use/cover change in the projected years 2025 and 2035

Variables	Land Use/Cover					
	2016 (Modelled)		2025		2035	
Unit	Ha	%	Ha	%	Ha	%
Forest	103949	3.10	76753	2.29	49152	1.47
Woodland	14092	0.42	12548	0.37	10218	0.31
Bushland	1494416	44.61	1317775	39.36	1154386	34.48
Grassland	1200979	35.85	1262030	37.65	1325857	39.55
Water	92361	2.76	66679	1.99	41049	1.23
Wetland	10577	0.32	9989	0.3	9207	0.27
Cultivated land	324823	9.70	430211	12.85	521632	15.58
Built-up area	6072	0.18	10563	0.32	15100	0.45
Bare area	102528	3.06	163249	4.88	223196	6.67
Total	3349797	100	3349797	100	3349797	100

Table 25: Changes in Land use/cover between 2016 and 2035

Year	Land Use/Cover Changes					
	2016 (Modelled) - 2025		2025-2035		2016-2035	
Unit	Ha	%	Ha	%	Ha	%
Forest	27196	0.81	-27601	-0.82	-43000	-1.28
Woodland	1544	0.05	-2330	-0.06	-11933	-0.35
Bushland	176641	5.25	-163389	-4.88	-334654	-9.97
Grassland	-61051	-1.80	63827	1.9	66369	1.95
Water	25682	0.77	-25630	-0.76	-54440	-1.62
Wetland	588	0.02	-782	-0.03	5245	0.15
Cultivated land	-105388	-3.15	91421	2.73	198148	5.92
Built-up land	-4491	-0.14	4537	0.13	14402	0.43
Bare area	-60721	-1.82	59947	1.79	159864	4.78

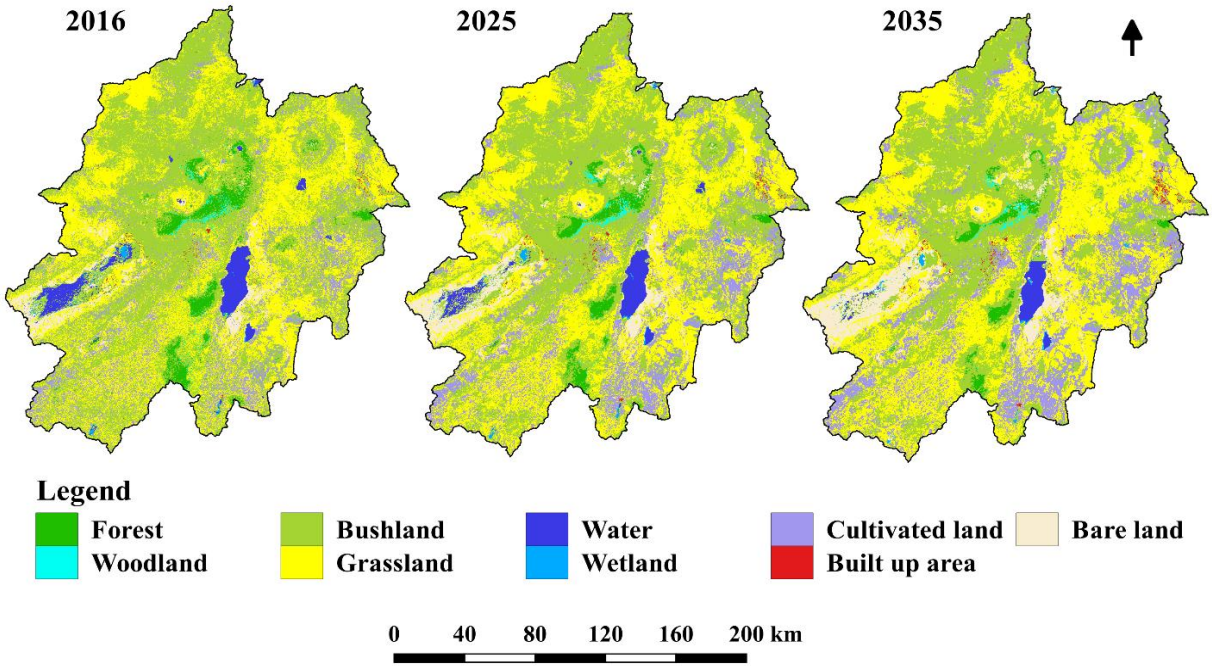

Figure 20: Map showing projected Land use/cover for the years 2016, 2025 and 2035

The results revealed that from 2016 to the future 2035, bushland, forest, water bodies, and woodland would decrease while cultivated land, grassland, bare land and built-up land would increase. These results are supported by the transitional matrix (Table 26) and transitional probability matrix and maps (Fig. 21) that express each pixel's probability of belonging to the designated class in the year 2035 from 2016. Thus, these maps are a cartographical presentation

of the transition probability matrix. During the period 2016 and projected 2035, 52% of built-up land and water will remain unchanged, followed by bushland (49%), bare land (46%), grassland (45%), forest (39%), cultivated land (26%), wetland (6%) and woodland (1%). This suggests that woodland will face the biggest change, with the probability of 63% being converted to bushland (34%), followed by grassland (25%), forest (6%), and cultivated land (5%). The projection results revealed that water and built-up land would maintain above 50% of unchanged Land use/cover, while the largest share will be gained from bushland and grassland. Furthermore, the expectation for one land use/cover class's enormous contribution to another is 53% of forest to bushland, 42% of cultivated land to grassland, and 38% of grassland to bushland. Also, 38% of bare land was converted to grassland, 37% of wetland to bushland, 36% of bushland to grassland, 25% of woodland to grassland, 25% of water to bushland and 23% of built-up land to grassland.

Table 26: Transitional probability matrix of individual land use/cover change for the period 2016 and projected 2035

Percentage		2035								
		FR	**WL**	**BUL**	**GL**	**WT**	**WET**	**CL**	**BLT**	**BL**
2016	FR	39	03	53	3	0	0	2	0	0
	WL	6	1	63	25	0	0	5	0	0
	BUL	2	0	49	36	0	0	9	0	4
	GL	0	0	38	45	0	0	13	0	4
	WT	0	0	25	10	52	6	0	0	7
	WET	0	0	37	15	28	6	0	0	14
	CL	0	0	30	42	0	0	26	0	2
	BLT	0	1	18	23	0	0	6	52	0
	BL	0	0	9	38	01	0	6	0	46

FR-Forest, WL—Woodland, BUL—Bushland, GL—Grassland, WT—Water, WET-Wetland, CL—Cultivated land, BLT-Built-up land, BL- Bare land

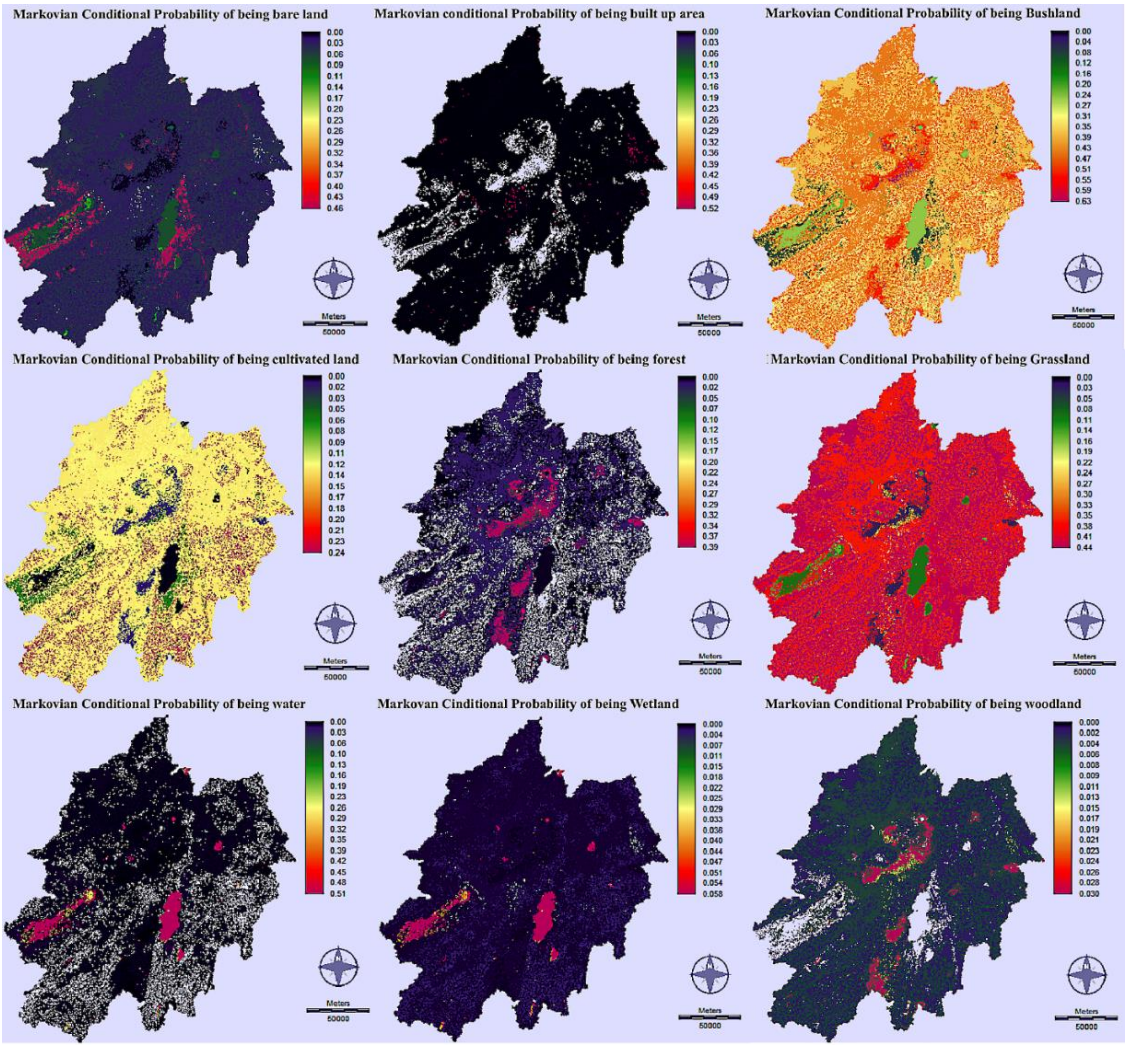

Figure 21: Markovian transitional Probability of individual land use/cover

Generally, these land use/cover trends in NCA may increase human-wildlife conflict, declines in habitat productivity, illegal resource extraction, and natural resource degradation including water (Defries *et al.*, 2007). The change reflects and identifies the interaction between biodiversity conservation and economic development. Managing ecosystem services cannot rely on short term restoration plans assumed without coordination across the entire watershed. When conducted in isolation, these plans are less likely to result in watershed-scale benefits than logical harmonized targets that are likely to restore the most ecosystem function. Managing ecosystem services cannot operate without monitoring or adaptive management. If the NCA communities want sustainable ecosystem services, they must manage land use and, for this, diverse sectors of the scientific community and the society must work together. Moreover, managing resources cannot succeed if the people living within the NCA watershed do not value the ecosystem services that may not meet their ideals of natural attraction but may nevertheless be entirely functional.

The suitable equilibrium between Land use/cover change to improve human welfare and secure areas to sustain other ecosystem services is eventually a societal decision in the argument between development and conservation (Defries *et al.*, 2007; Rescia *et al.*, 2010). A good starting point would be to effectively change the mindset toward ecosystem services and resource use by considering using it wisely regardless of priority rights. Such a change can only occur if there is more widespread recognition that natural resources, including land, are endangered. If the communities want the watershed to provide ecosystem services, they must move beyond narrowly focused management that reflects sectorial interlinkage. This shift in approach is intellectually tricky because it requires a more integrated and complex understanding than relying on a set of frameworks that describe ecosystem service only. As a result, the tradeoffs between human practices and longtime management of ecosystem amenities become difficult. These require adaptive management of ecosystems and natural resources (Singh *et al.*, 2018) , which lays a foundation to bring various stakeholders together to help accommodate diverse opinions and interests. These changes need to be monitored and managed at the catchment scales to manage tradeoffs between various ecosystem services and balance losses and gains of land cover. Simultaneously, multiple goals and strategies should aim to structure and promote synergies or reduce tradeoffs (Tesfaw *et al.*, 2018). To attain that, quantifying the potential impacts of land use/cover on the ecosystem is inevitable to ensure better management. Moreover, the quantification will help plan a better management system. Therefore, this study used a modelling approach to analyze the hydrological response of NCA and surrounding catchments to climate and land use/cover change.

4.3 To Model the Response of Hydrological Processes (Runoffs and Stream Flows) to Future (2021-2050) Climate Change Compared to Baseline (1982-2011), and Land use/cover Change of 2025 And 2035 Compared to Baseline 2016 in the Study Area

This study used the Soil Water Assessment Tool (SWAT) to analyze the hydrological response of the water resources to the change in climate and land use/cover changes. The outcome of this is crucial for effective management of the NCA and surroundings and a thorough understanding of the hydrological processes occurring in the water resources. This section discusses SWAT modelling results for management planning of water resources around the NCA.

4.3.1 Calibration and Validation of the SWAT Model

The calibration results demonstrated a high level of agreement between discharge observations and SWAT modeling results. The graphical comparison of observed and simulated flow for the calibration (1985–1987) and validation (1988–1989) periods are shown in Fig. 22 to 25. The simulation has captured the observed flow reasonably. Statistical performance indices are also shown in Table 27. The obtained R^2 (0.89 for calibration and 0.74 for validation) values show very good consistency between the observed and simulated data and indicate less error variance between the two data (Chaibou-Begou *et al.*, 2016; Gashaw *et al.*, 2018). The parameter values for NSE, RSR, PBIAS, and R2 were, respectively, estimated as 0.88, 0.34, 4.4, and 0.89 in calibration, and 0.83, 0.41, 2.6, and 0.74 in the validation. The simulation reproduced the observed flow rationally, indicating the good performance of the model in simulating the hydrological impacts of climate and land use/cover changes.

Table 27: Model performance statistics for the calibration and validation periods

Period		Average Monthly Flow(m^3/s)		Evaluated Statistics			
		Observed	Simulated	NSE	RSR	PBIAS	R^2
Jan 1985–Dec 1987	Calibration	8.03	8.40	0.88	0.34	4.4	0.89
Jan 1988–Dec 1989	Validation	8.76	8.48	0.83	0.41	2.6	0.74

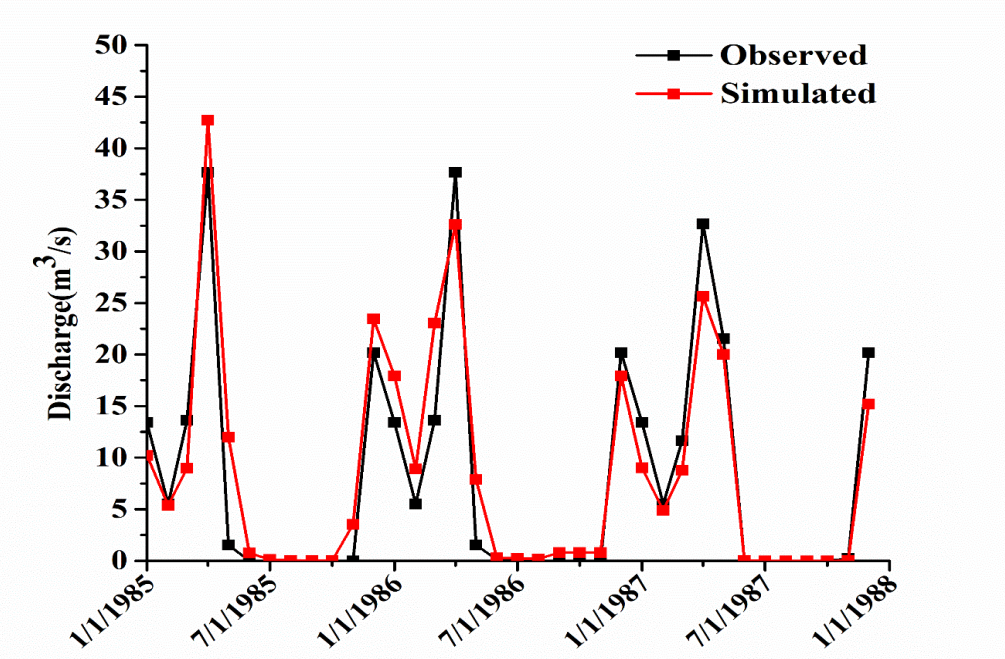

Figure 22: Observed and simulated monthly discharge data for the calibration period

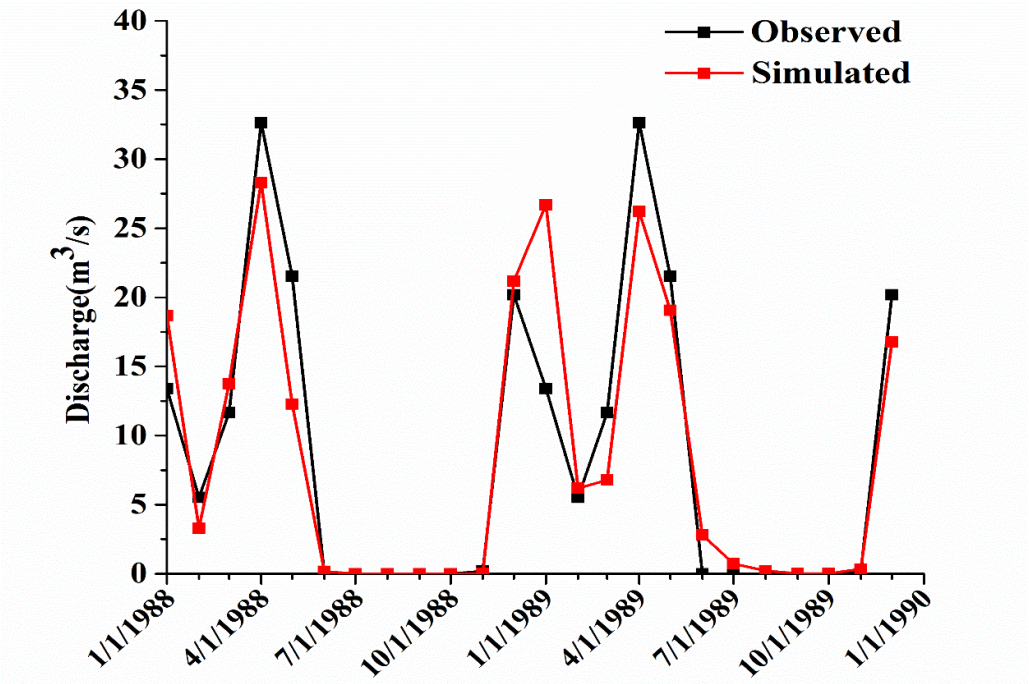

Figure 23: **Observed and simulated monthly discharge data for the validation period**

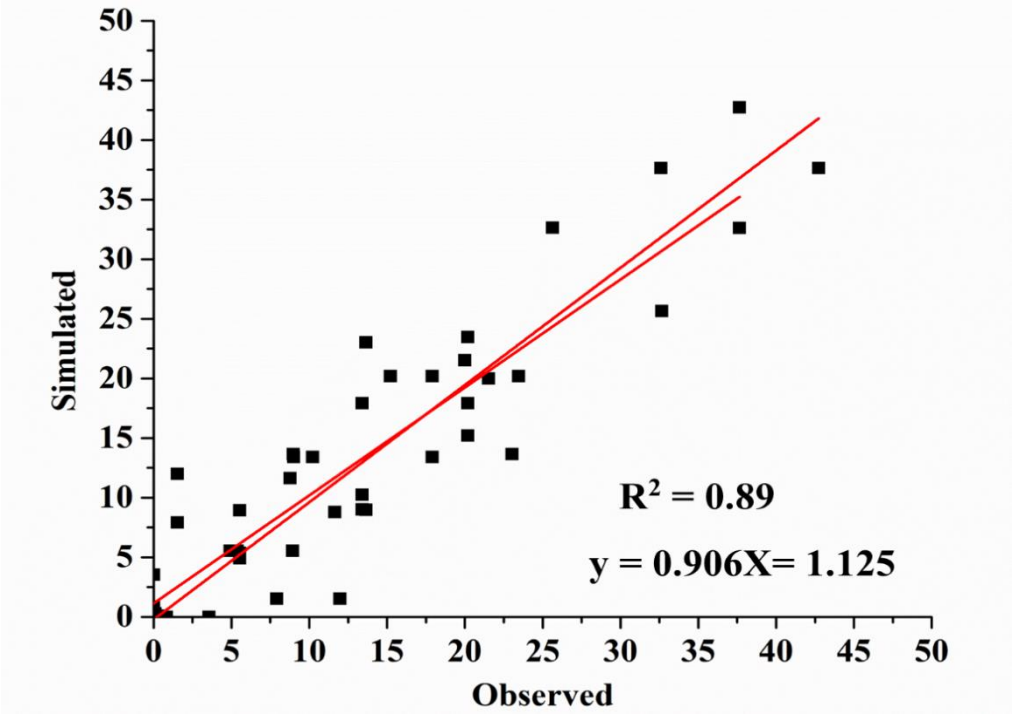

Figure 24: **Scatter plot of the observed and simulated monthly average flow in the calibration period**

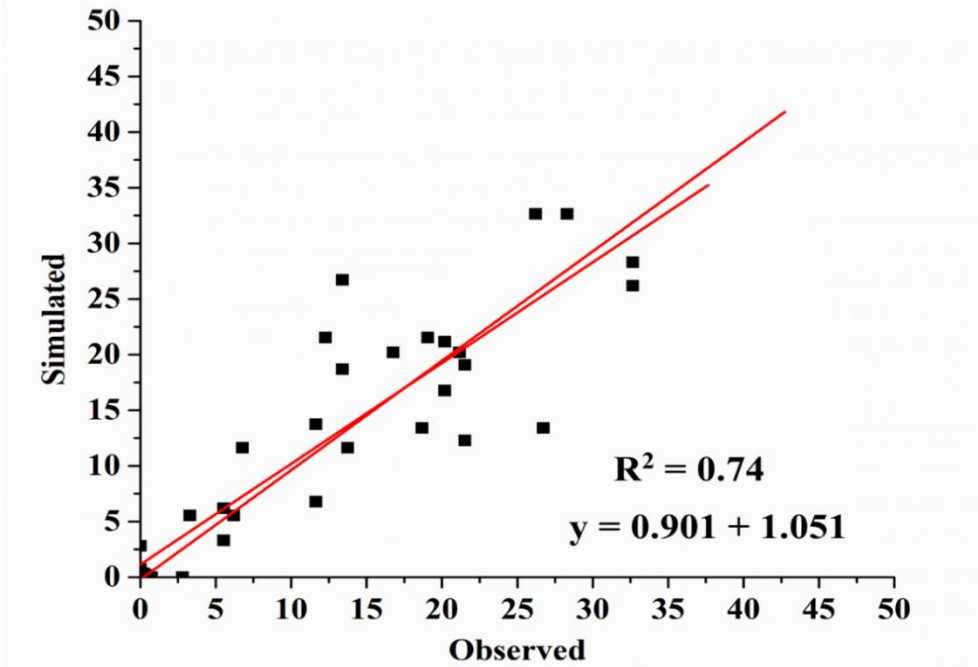

Figure 25: Scatter plot of the observed and simulated monthly average flow in the validation period

4.3.2 The SWAT Model Sensitive Parameters

Sensitivity analysis, which was carried out using 14 flow parameters presented in Table 9, identified the ten (10) most sensitive parameters controlling the output variable, as shown in Table 28.

Table 28: Sensitive flow parameters and their rank

SN	Parameter	Definition	Range	Fitted value
1	ALPHA_BF.gw	Baseflow alpha factor for bank storage	0.0-1.0	0.048
2	CN2.mgt	SCS runoff curve number	35-90	66.38
3	ESCO.bsn	Soil evaporation compensation factor	0.01-1	0.85
4	GW_DELAY, gw	Groundwater delay (days)	0- 500	31
5	GW_SPYLD(m^3)	Specific yield of the shallow aquifer (m^3/m^3)	0.0-0.4	0.003
6	HRU_SLP	Average slope steepness (m/m)	0.0-1.0	0.026630926
7	O VN	Maning "n" value for overland flow	0.04 -0.3	0.15
8	RCHRG_DP.gw	deep aquifer percolation fraction	0.0-1.0	0.05
9	SLSUBBSN	Average slope length(m)	10-150	91.46341463
10	SURLAG	surface runoff lag coefficient	0.0-24	2

4.3.3 Impacts of Land use and Climate Changes in Hydrological Components

Four simulation experiments were formulated based on the land use data and climate data. In the baseline scenario, the hydrological components were simulated with the land use data of 2016 and the climatic data from 1982 to 2011 (baseline climate). Then three scenarios were designed based on land use and climate change (Table 29 - 31). In the first scenario, the hydrological components were simulated using the baseline climate data from 1982 to 2011 with corresponding projected land use of 2025 and 2035 , respectively. In the second scenario, the hydrological components were simulated with the land use data in 2016 with corresponding 2021- 2050 future climate scenarios (RCP 4.5 and RCP 8.5). In the third scenario the hydrological components were simulated with the land use data in 2025 with corresponding 2021- 2050 future climate scenarios (RCP 4.5 and RCP 8.5); and land use data in 2035 with corresponding 2021- 2050 future climate scenarios (RCP 4.5 and RCP 8.5).

(i) Temporal Variations in Hydrological Components

The simulation result for hydrological components at a baseline was as follows: surface runoff, 64.52 mm/year; groundwater flow, 34.39 mm/year; evapotranspiration, 556.21 mm/year; lateral flow, 8.02 mm/year and water yield, 168.38 mm/year. For the first Scenario, the dominant land use types of the catchment were bushland, grassland, forest, bare land and cultivated land. Therefore, to evaluate the impacts of land-use change on hydrological components, the calibrated SWAT model was simulated in historical land use (2016) and two future land use scenarios in 2025 and 2035 under the assumption that the weather did not change. The results (Table 29), showed that with projected land use in 2025, the hydrological components were as follows: surface runoff, 66.00 mm/year; groundwater flow, 9.43 mm/year; evapotranspiration, 563.22 mm/year; lateral flow, 33.87 mm/year and water yield, 171.63 mm/year. Additionally, with projected land use in 2035, surface runoff, groundwater flow, evapotranspiration, lateral flow and water yield were 86.42 mm/year, 8.08 mm/year, 553.34 mm, 30.74 mm/year and 172.77 mm/year, respectively. The results show that runoff and lateral flow may increase in the future under the change in land use in 2025 and 2035, respectively, compared with land use in 2016. Moreover, groundwater and water yield will decrease under the change in land use in 2025 and 2035, while evapotranspiration will increase under the change in land use in 2025 and will decrease under the change in land use in 2035 when compared with land use in 2016. During the study period (2016-2035), an increasing trend was observed in surface runoff (21.90 mm/year) and lateral flow (22.72 mm/year), while a

decreasing trend was observed in groundwater flow (26.32 mm/year), evapotranspiration (2.87 mm/year) and water yield (43.14 mm/year).

Table 29: Hydrological component change due to land use/cover

Hydrological component	Baseline	2025	2035	2016 - 2025	2025 - 2035	2016 - 2035
Surface runoff (mm/year)	64.52	66.00	86.42	1.48	20.42	21.90
Groundwater flow (mm/year)	34.39	9.43	8.08	-24.97	-1.35	-26.32
Evapotranspiration (mm/year)	556.21	563.22	553.34	7.01	-9.88	-2.87
Lateral flow (mm/year)	8.02	33.87	30.74	25.85	-3.13	22.72
Water yield (mm/year)	168.38	109.30	125.24	-59.08	15.94	-43.14

Furthermore, in the second scenario to analyse the impact of climate change on hydrological components, the calibrated SWAT model was simulated using the RCP 4.5 and RCP 8.5 future precipitation and temperature data scenarios, respectively. The study compared the simulated hydrological components for future periods under scenarios RCP 4.5 and RCP 8.5 to the corresponding values in the baseline period (1982–2011) with the assumption that land use/cover of 2016, did not change. Table 30 shows the changes in hydrological components under the climate scenarios for the 2021–2050 period. The simulation result for hydrological components for RCP 4.5 was as follows: Surface runoff, 263.15 mm/year; groundwater flow, 15.10 mm; evapotranspiration, 593.30 mm/year; lateral flow, 290.27 mm/year and water yield, 568.53 mm/year. Furthermore, the results showed that with RCP 8.5, the hydrological components were as follow: surface runoff, 302.46 mm/year; groundwater flow, 15.93 mm/year; evapotranspiration, 598.61 mm/year; lateral flow, 310.25 mm/year and water yield, 628.64 mm/year. In general, RCP 8.5 simulation results are higher than RCP 4.5 in all hydrological components.

Table 30: Hydrological component change due to climate change

Hydrological component	Baseline	2021-2050/RCP 4.5	2021-2050/RCP 8.5
Surface runoff (mm/year)	64.52	263.15	302.46
Groundwater flow (mm/year)	34.39	15.1	15.93
Evapotranspiration (mm/year)	556.21	593.3	598.61
Lateral flow (mm/year)	8.02	290.27	310.25
Water yield (mm/year)	168.38	568.53	628.64

In the third scenario, the study further simulated the combined impacts of future land use/cover and climate change on hydrological components in the study area with the calibrated SWAT model. The study compared the simulated hydrological components for future periods of land

use 2025 with future climate scenarios 2021-2050 (RCP 4.5 and RCP 8.5) and land use 2035 with future climate scenarios 2021-2050 (RCP 4.5 and RCP 8.5) with the baseline scenario. Table 31 represent the results for the third scenario. Initially, the simulation result for hydrological components for 2021- 2050 future climate scenarios RCP 4.5 and PCP 8.5 with the land use data in 2025 was as follows: surface runoff, 268.33 mm/year; groundwater flow, 15.51 mm/year; evapotranspiration, 606.59 mm/year; lateral flow, 227.62 mm/year and water yield, 511.48 mm/year, and surface runoff, 322.55 mm/year; groundwater flow, 16.36 mm/year; evapotranspiration, 612.95 mm/year; lateral flow, 252.94 mm/year and water yield, 591.86 mm/year, respectevely. Further, the simulation result for hydrological components for 2021- 2050 future climate scenarios RCP 4.5 and PCP 8.5 with the land use data in 2035 was as follows: surface runoff, 309.79 mm/year; groundwater flow, 15.20 mm/year; evapotranspiration, 578.43 mm/year; lateral flow, 207.29 mm/year and water yield, 532.27 mm/year; and surface runoff, 365.96 mm/year; groundwater flow, 16.02 mm/year; evapotranspiration, 600.04 mm/year; lateral flow, 230.81 mm/year and water yield, 612.79 mm/year, respectevely. Generally, RCP 8.5 simulation results are higher compared to RCP 4.5 in all hydrological components for both land use data in 2025 and 2035. Further, the results showed that surface runoff, evapotranspiration, lateral flow, and water yield would significantly increase in all four scenarios compared to the baseline scenario, while groundwater would decrease.

Table 31: Hydrological component change due to land use and climate change

Hydrological component	Baseline	Land 2025 (RCP 4.5)	Land 2025 (RCP 8.5)	Land 2035 (RCP 4.5)	Land 2035 (RCP 8.5)
Surface runoff (mm/year)	64.52	268.33	322.55	309.79	365.96
Groundwater flow (mm/year)	34.39	15.51	16.36	15.2	16.02
Evapotranspiration (mm/year)	556.21	606.59	612.95	578.43	600.04
Lateral flow (mm/year)	8.02	227.62	252.94	207.29	230.81
Water yield (mm/year)	168.38	511.48	591.86	532.27	612.79

(ii) Spatial Variations in Water Yield Component

Water yield is an important hydrological component that influences human well-being because many agricultural, industrial, and domestic activities rely on it (Fan & Shibata, 2014; Muthuwatta *et al.*, 2018). Furthermore, the total amount of water produced influences or limits

how people use water resources (Maliehe & Mulungu, 2017). The spatiotemporal variation of water yield is significant, which frequently creates a challenge in allocating water resources between seasons and between upstream and downstream areas (Muthuwatta *et al.*, 2018; Zhang *et al.*, 2020). Therefore, this study performed a spatial analysis for water yield among other simulated components by SWAT model to provide critical spatial information for water resource management plans in and around the NCA.

The spatial distribution for the first scenario shows the total water yield in the study area as an impact of future land use/cover scenarios compared to a baseline scenario (Fig. 26 a). The pattern of total water yield is similar for future land use/cover change in 2025 and 2035 are as shown in Fig. 26 b and c, respectevely, which indicates the decreasing amount of water yield. However, a slight increasing amount to maximum of 303.21 mm/year would occur in the eastern and central subbasins in 2035 future scenario compared to a maximu of 292.39 at a baseline scenario. Looking at the land use/cover maps for future 2025 and 2035 (Fig. 20) the eastern areas would have expansion of cultivation land, therefore decrease in water yield in 2025 could impact the acgiculture and human activities over the area. However, during 2035 the water yield would increas and agriculture activities at this area would benefit the availability of water resources which will maximise the agriculture production.

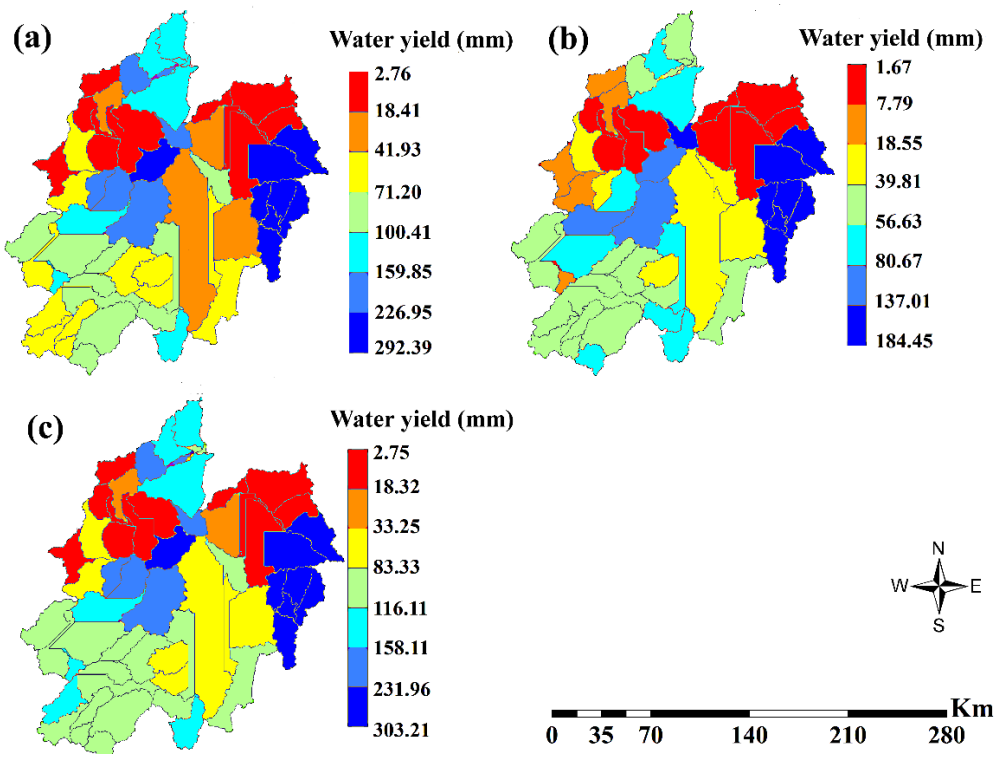

Figure 26: Spatial distribution of water yield (mm/year) at a baseline scenario (a) and future land use cover change scenarios of 2025 (b) and 2035 (c)

For the second scenario,the spatial distribution of the total water yield in the study area as an impact by 2021- 2050 future climate scenarios (RCP 4.5 and RCP 8.5) are shown in Fig. 27. The distribution shows an increasing pattern of total water yield in the 2021-2050 climate scenarios under RCP 4.5 and RCP 8.5, as shown in Fig. 27 b and c, respectively. A higher increase in water yield would occur in the northern, southern and some parts of the centre and west compared to the baseline scenario. However under RCP 8.5, the water yield would be much higher than under RCP 4.5. This increase in water yield in the future climate scenarios could be associated with the predicted increase in rainfall over the areas (mwabumba *et al.*, 2022). The highest water yield would occur in the western parts with amount of 1014.58 mm/year and 1218.18 mm/year for RCP 4.5 and RCP 8.5, respectively. The increase in water yield could support the conservation in the NCA and expected rise of socio-economic activities in the surrounding areas.

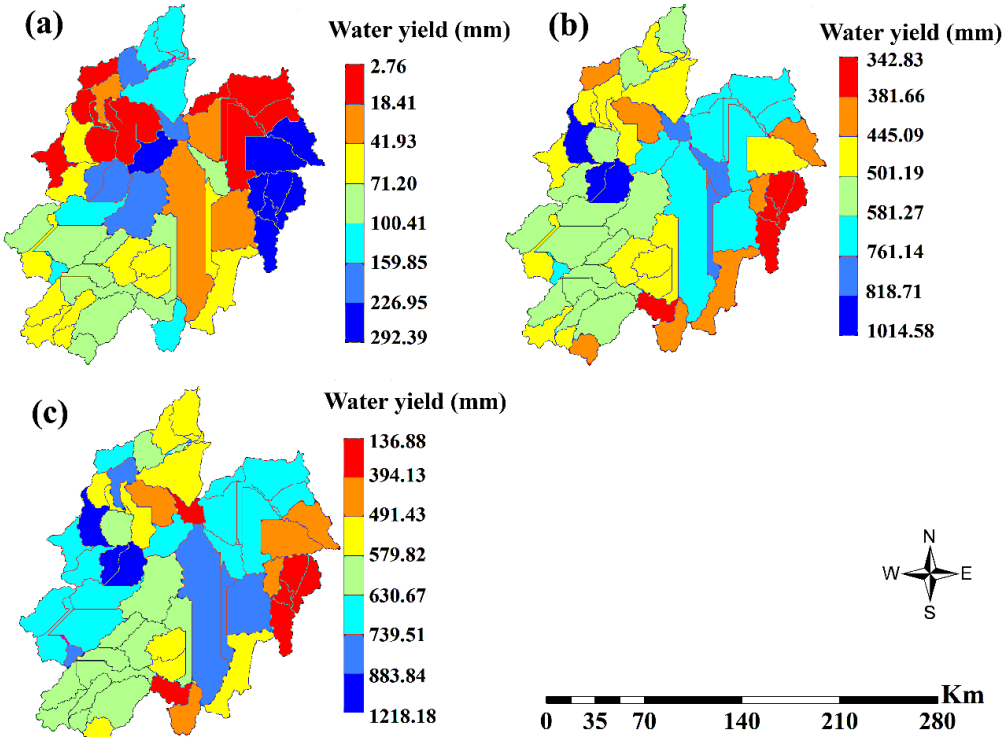

Figure 27: Spatial distribution of water yield (mm/year) at a baseline scenario (a) and future climate 2021-2050) scenarios under RCP4.5 (b) and RCP8.5 (c)

In the third scenario, the distribution shows an increasing pattern of total water yield in all settings: (a) Land use 2025 with climate 2021-2050 under RCP 4.5 (Fig. 28 b); (b) Land use 2025 with climate 2021-2050 under RCP 8.5 (Fig. 28 c); (c) 2035 land use with 2021-2050 climate under RCP 4.5 (Fig. 28 d) and (d) 2035 land use with 2021-2050 climate under RCP 8.5 (Fig. 28 e) compared to the baseline scenario (Fig. 28 a). A maximum increase in

water yield would occur at some parts in the west followed by central towards south and northestern parts in all scenarios. The increase in water yield in these areas coincides with the second scenario, in which land use remained unchanged with changes in climate (Fig. 27 c & d); also with the projected spatial precipitation distribution over the area as shown in Fig.16 a and b. In contrast to the spatial distribution in the baseline scenario and in the first scenario, which indicated the maximum water yield in the eastern and central parts.

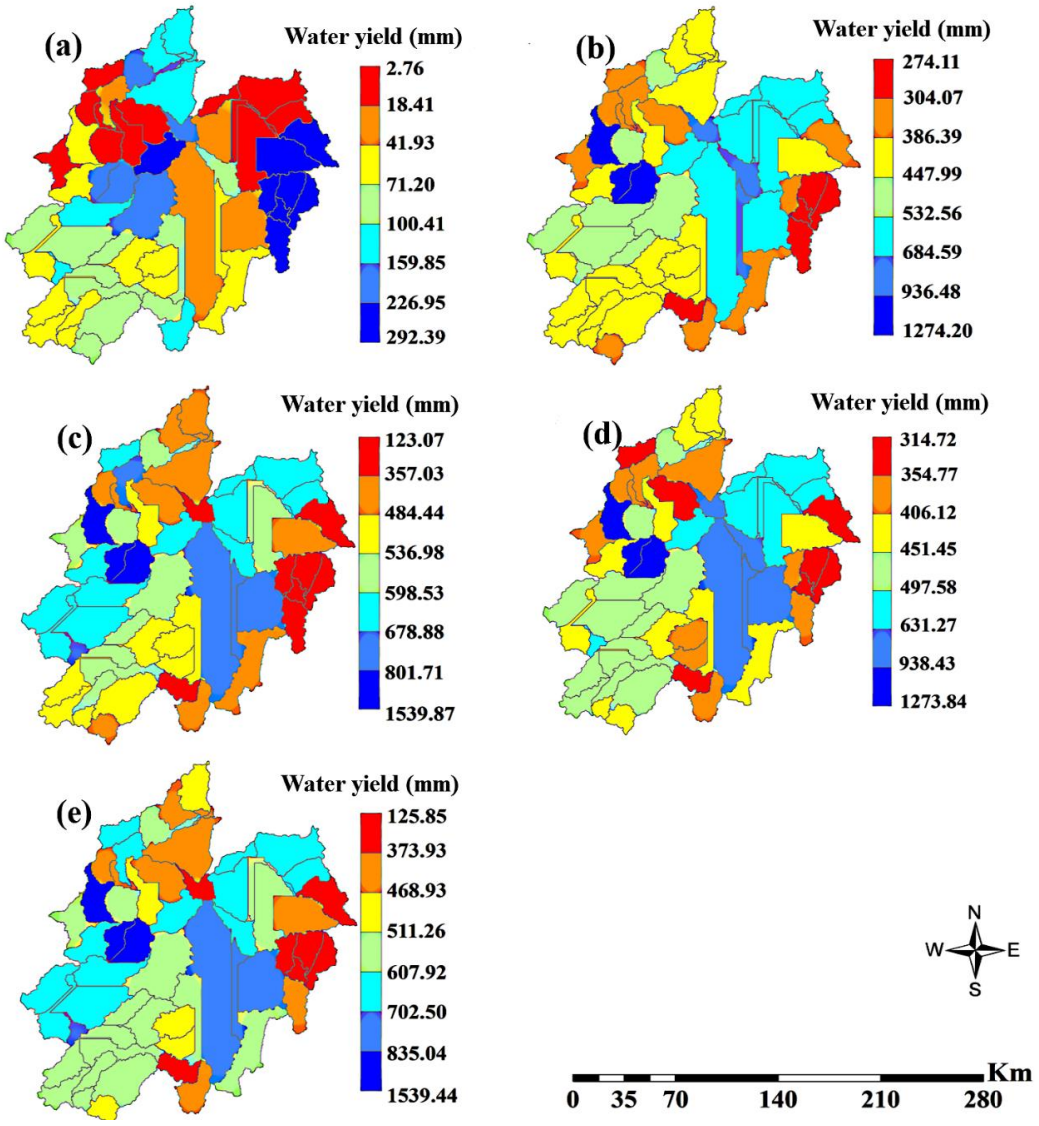

Figure 28: Spatial distribution of water yield (mm/year) at a baseline scenario (a), future climate 2021- 2050/RCP 4.5/land use/cover 2025 (b), future climate 2021- 2050/RCP 8.5/land use/cover 2025 (c), future climate 2021- 2050/RCP 4.5/land use/cover 2035 (d) and future climate 2021- 2050/RCP 8.5/land use/cover 2035 (e)

Generally, the findings of this study shows that the temporal and spatial changes of hydrological components were more affected by climate change than land-use change. This result indicates that the predicted increase in precipitation and temperature will cause more

significant impacts on the hydrological components than the expected land-use changes. It is evident that the impact of climate change on water resources and their services is increasing, particularly in the developing world (Obuobie *et al.*, 2012; Pachauri *et al.*, 2014). Furthermore, Burke *et al.* (2009) have emphasized that this impact will be substantial in Africa owing to poverty and political instability, amongst others in the region. The findings of this study projecting an increase in rainfall and temperature raise concern for the Ngorongoro Conservation Area and its surrounding ecosystems. The projected increase in rainfall has the advantage of a constant water supply to the biodiversity and ensuring food security for the expanding human population in the Ngorongoro Conservation Area and its surroundings (Galvin *et al.*, 2008). The conducted survey and focus group discussion by both local community and Park Managers in the NCA confirmed that about 80 - 90% of newly born livestock were lost in 2007/2008 due to diseases associated with intense drought. Therefore, projected increase in water availabity will be vital for the economy and livelihood of the communities around the NCA.

Mkiramweni *et al.* (2016) have recounted that the Ngorongoro Conservation Area (NCA) is one of the very important protected areas for ecotourism in Tanzania and fosters harmonious relationships between wildlife, people, and livestock. The results showed the potential influence of land use/cover and climate change to the hydrological components and water resources in and around the NCA. The resulting changes to the hydrological compoments and water resources availability will impact ecotourism resources such as wildlife, archaeological sites, beautiful landscapes and lifestyles/cultures of the local community (Galvin *et al.*, 2008) on which the NCA is based. Therefore, authorities and communities should plan for the adaptation measures which will involve all stakeholders around the NCA. In this way, we can find rational solutions to share with ecologic limits, and we have to be careful in setting new goals to bring attention to the reality, to the science and to protect water resources in NCA. Water is the primary medium through which land use/cover and climate change influence the ecosystem and well-being. A traditional, fragmented approach to water resource use is not going to yield sustainable benefits in the long run.

Water resources and how they are managed impact almost all aspects of the functioning of ecosystems. Thus, adapting to the new challenge of land use/cover and climate change requires an integrated water resource use and management approach. Adaptation to water resource management is mainly about better land use, while integrated solutions are needed at the

appropriate levels for adaptation and mitigation. Appropriate adaptation measures should be built upon the existing water resource use practices to foster resilience to land use/cover and climate change, thereby enhancing water security. Land use/cover and climate change impact in hydrological processes and may affect the water quality. Therefore, this study further analyses the hydrochemical composition of the water resources. Furthermore, it determines the hydrochemical movements to groundwater as influenced by the clmate and land use/cover changes.

4.4 Characterizations of the Hydrochemical Composition of Water Resources in the Study Area and Monitoring of their Movement to Groundwater around the Study Area

This section explains the hydrochemical compositions of water sources (i.e. Rivers, springs, lakes, wells) around the study area and their movement to the groundwater as influenced by the changes in climate and Landuse/ land cover changes around the study area. The study uses the HYDRUS 1D model to analyse the movement of cations (Na^+, Ca^{2+}, Mg^{2+}, and K^+) and anions (Cl^-, SO_4^{2-}, PO_4^{3-}, NO_3^-, HCO_3^-) to groundwater. Before modelling the movement of hydrochemical to groundwater, the study characterises the hydrochemical composition of surface water resources in the water sources surrounding the NCA. The water sources around the study area are assumed to have cations and anions contamination due to weathering of the rock materials. Therefore, water samples from different water sources were collected and analyzed in the laboratory to determine their hydrochemical contaminations. The laboratory results for the hydrochemical (cations and anions) were used as an input (initial conditions) in HYDRUS 1 D model to determine their movements to the groundwater.

4.4.1 Characteristics of the Hydrochemical Composition of Water Resources in the Study Area

The characterization of hydrochemical composition was performed through laboratory analysis for cations (Na^+, Ca^{2+}, Mg^{2+}, and K^+) and anions (Cl^-, SO_4^{2-}, PO_4^{3-}, NO_3^-, HCO_3^-) on water 30 water points from different water sources (rivers, lakes, springs, pools, wells and boreholes). The results for the concentration of cations and anions on the different water sources are presented in Table 32 and Table 33, respectively.

Table 32: Cation composition (mg/L) for water sources around the study area

SN	Name	Na^+	K^+	Mg^{2+}	Ca^{2+}
1	Takano spring	139	13.5	22.5	8.8
2	Engarisero river	212	50.3	9.3	16.3
3	Engong'was	154	15.4	14.8	9.5
4	Marite	48.3	23.9	70.5	13.8
5	Marite Spring	48.3	27.4	32.5	25.5
6	Ngopironi spring	48.6	16.5	5.8	41.8
7	Engaruka river	31	9.5	36	10.0
8	Lake Natron	305	27.9	5.8	5.5
9	Empakaai spring 1	50.4	19.5	17	41.3
10	Empakaai spring 2	53.5	21.1	16.3	12.5
11	Munge river	16.2	1.6	10.1	8.8
12	Mundus Hippo pool	65.6	17.5	38	23.3
13	Mti Mmoja	171	139	10	7.3
14	Lake Makat	199	123	10.8	14.5
15	Ngoitok tok spring	63.2	16.9	22.3	12.5
16	Gorgory swamp	226	112	27.5	20
17	Seneto	72	10.4	7.5	5.8
18	Olmoti Spring	38.2	12.2	14.5	40.3
19	Oljoro Nyukie	22.6	3.8	29.8	15.8
20	Mamahaw river	14.5	2.8	17.5	9.0
21	Selela-Kapambe	25.9	6.1	21.8	34.8
22	Karuwasa borehole	29.2	7.6	26.3	22.3
23	Karatu well(Mbowe)	69.8	30.2	6.3	1.6
24	kigongoni river	9.7	2	8.7	18.4
25	Mto wa mbu well	138.7	10	31.5	43.7
26	Majengo	277	18.9	26.1	18.0
27	Manyara hot spring	611	11.5	5.3	34.0
28	Manyara cold spring	24.4	4.3	18.2	20.7
29	mto wa mbu (River)	247.9	4.8	0	29.9
30	Lake Manyara	533.2	7.7	12.1	25.6

Table 33: Anion composition (mg/L) for water sources around the study area

SN	Name	NO_3^-	Cl^-	SO_4^{2-}	PO_4^{3-}	HCO_3^-
1	Takano spring	0.9	74.7	72.0	0.9	380.0
2	Engarisero river	1.2	123.1	240.0	3.0	400.0
3	Engong'was	0.7	118.9	76.0	0.4	400.0
4	Marite	0.9	10.5	29.0	0.3	300.0
5	Marite Spring	1.0	46.3	1.0	0.8	280.0
6	Ngopironi spring	4.9	20.9	29.6	0.1	220.0
7	Engaruka river	0.7	4.2	8.0	0.2	220.0
8	Lake Natron	1.2	685.1	45.0	0.0	0.0
9	Empakaai spring 1	33.0	7.4	98.0	0.5	220.0
10	Empakaai spring 2	0.5	9.5	15.0	0.5	300.0
11	Munge river	2.9	21.3	1.8	0.2	220.0
12	Mundus Hippo pool	0.3	14.7	12.0	1.6	95.0
13	Mti Mmoja	32.8	125.2	3.1	0.8	540.0
14	Lake Makat	4.7	152.6	141.0	0.6	480.0
15	Ngoitok tok spring	0.7	21.1	15.0	0.3	320.0
16	Gorgory swamp	7.2	126.3	88.0	4.0	1200.0
17	Seneto	0.6	16.8	9.0	0.3	200.0
18	Olmoti Spring	0.4	4.5	8.9	0.2	180.0
19	Oljoro Nyukie	2.6	5.3	23.0	0.3	140.0
20	Mamahaw river	0.7	11.6	9.0	0.2	80.0
21	Selela-Kapambe	0.4	9.5	1.0	0.0	180.0
22	Karuwasa borehole	0.6	11.6	0.0	0.5	260.0
23	Karatu well(Mbowe)	21.0	9.7	8.1	0.1	219.7
24	kigongoni river	0.5	3.0	7.6	0.0	315.3
25	Mto wa mbu well	7.6	32.4	54.3	0.0	128.0
26	Majengo	18.4	30.9	150.3	0.0	173.1
27	Manyara hot spring	n.a.	255.9	198.3	0.0	208.1
28	Manyara cold spring	11.1	9.5	9.0	0.0	162.7
29	mto wa mbu (River)	1.3	12.6	35.6	0.0	280.1
30	Lake Manyara	46.8	468.2	76.5	0.0	190.0

The composition of Na^+, K^+, $Mg^{2+,}$ and Ca^{2+} cations on the studied water sources ranges between 9.7 and 611 mg/L; 1.6 and 139 mg/L; 0 and 70.5 mg/L; 5.5 and 43.7 mg/L, respectively as shown in Table 32. For the Na^+, the allowable concentration for drinking water is 200 mg/L based on the WHO and TBS standards for drinking water. Therefore, the concentration is within permissible limits for most of the studied water sources except for the

Engarisero river and Lake natron at the Lake natron sub-catchment, with 212 mg/L and 305 mg/L. Also, the higher concentration is at Mtowambu river, Majengo well, Lake Manyara and Manyara hot spring in lake Manyara sub-catchment, with concentrations of 247.9 mg/L, 277 mg/L, 533.2 mg/L and 611 mg/L, respectively. Therefore water from the mentioned sources above was not suitable for consumption as it may lead to adverse health effects.

Similar conditions are observed for the K^+ concentration in which most of the studied water sources are composed of a concentration lower than the permissible limit of 50 mg/L set by the TBS standard. However, the K^+ concentration at Lake Makat, Gregory swamp and Mti mmoja spring were above the allowable limit with a concentration of 123 mg/L, 226 mg/L, and 139 mg/L, respectively. For the Mg^{2+}, all water sources have a concentration within the permissible limit set by WHO (50 mg/L) and TBS (100 mg/L). However, Marite spring at lake Natron sub-catchment has a concentration of 70.5 mg/L, exceeding the WHO limit but within the TBS limit. Therefore, the Mg^{2+} water resources in the study area are suitable for consumption. Furthermore, considering the Ca^{2+}, the concentrations at all studied water bodies were below the permissible concentration of 75 mg/L (WHO) and 150 mg/L (TBS). Therefore, the water quality in respect of Ca^{2+} for all studied water sources was suitable for consumption.

Besides the anions, NO_3^-, Cl^-, SO_4^{2-}, PO_4^{3-}, and HCO_3^- the composition ranges between 0.3 and 46.8 mg/L; 3 and 685.1 mg/L; 0 and 240 mg/L;0 and 4 mg/L; and 0 and 1200 mg/L, respectively as shown in Table 33. Looking at the individual anions, the NO_3^- is within the permissible limit of the TBS (45 mg/L) and WHO (30 mg/L) for the most studied water sources, except for Lake Manyara with 46.8 mg/L, which exceeds both TBS and WHO limits; while Embakai and Mti mmoja springs exceed WHO limits only with a concentration of 33 mg/L and 32.8 mg/L, respectively. For the Cl^- the concentration that exceeded the limits of 250 mg/L (WHO and TBS) were at Lake Natron (685.1 mg/L), Manyara hotspring (250.9 mg/L) and Lake Manyara (468.2 mg/L). The SO_4^{2-} concentrations are within the permissible limit by WHO and TBS of 250 mg/L and 400 mg/L, respectively, for all studied water sources. For the PO_4^{3-} all studied water sources have a concentration within the allowable limit except Engarisero spring in lake Natron and Gorgory swamp in NCA with 3.0 mg/L and 4.0 mg/L, respectfully that exceed the 2.2 mg/L allowable limits by WHO and TBS. Likewise, for the HCO_3^-, all studied water sources are within the permissible limit of 500 mg/L set by WHO and TBS for total hardness, except Mtimmoja spring and Gorgory swamp, with higher concentrations of 540 and 1200 mg/L, respectively.

4.4.2 Monitoring of the Hydrochemical Movement to Groundwater around the Study Area

This section explains the results from the HYDRUS 1D model to monitor the movement of cations and anions to groundwater as influenced by climate change and land use/cover change. The groundwater concentrations of cations (Na^+, Ca^{2+}, Mg^{2+}, and K^+) and anions (Cl^-, SO_4^{2-}, PO_4^{3-}, HCO_3^-) were simulated numerically based on the future climate conditions. Concentrations of these ions computed in groundwater at 30 locations are used to analyze the spatial distribution of the ions in the area.

(i) Analysis of Cations (Na^+, Ca^{2+}, Mg^{2+}, and K^+) and Anions (Cl^-, SO_4^{2-}, PO_4^{3-}, HCO_3^{1-}) Movement to the Groundwater as Influenced by Climate and Land use /cover Changes around the Study Area

Temporal Analysis for the Cations and Anions in the Groundwater

In general, temporal analysis shows an increase in the concentration of cations and anions in the groundwater. However, the rate of increase over the period is dependent on the changes in climate parameters and land use/cover types for the period between 2021-2050. Therefore, the groundwater concentration trends for cations (Na^+, Ca^{2+}, Mg^{2+}, and K^+) are presented in Fig. 29, while Fig. 30 is for anions (Cl^{1-}, SO_4^{2-}, $PO4_3^{1-}$, HCO_3^{1-}) and Fig. 32 is for NO_3^- from 2021 to 2050.

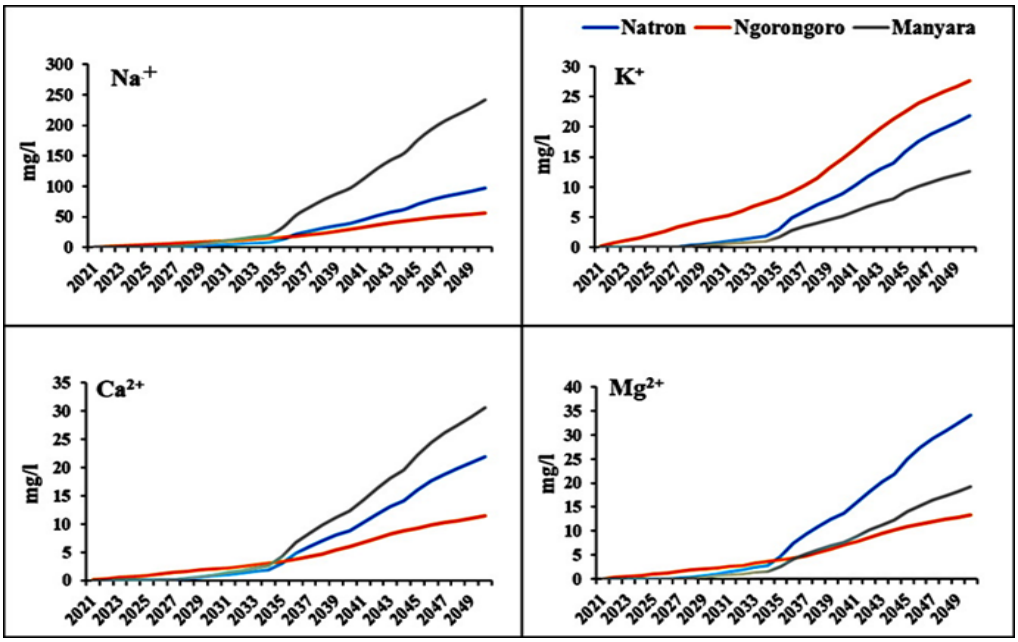

Figure 29 Trends for cations (Na^+, Ca^{2+}, Mg^{2+}, and K^+) concentrations are expected in the study area from 2021 to 2050

The increase in cation is more between 2036 and 2050 when most climate parameters are also increasing. However, the results show more increase in Na^+ compared to other cations, as shown in Fig. 29. Comparing the studied sub-catchments for the cations and anions (Fig. 29, 30 & 31), a higher increase of Na^+ and Ca^{2+} will be observed at Lake Manyara and lower at Ngorongoro. For the K^+, the higher increase would be at Ngorongoro, the lower at Lake Manyara, while the Mg^{2+} higher increase would be observed at lake Natron and lower at Ngorongoro. The high rise of Na^+ and Ca^{2+} around Lake Manyara could be associated with the increased agriculture activities and fertilizers. Similar trends are observed for anions, where the concentration of all anions increases with time. However, more rise in their concentration is expected between 2036 and 2050, with a higher concentration of HCO_3^- than other anions, as depicted in Fig. 30. Furthermore, the NO_3^{-1} indicate the increasing trends from 2029, with the highest increase in 2050.

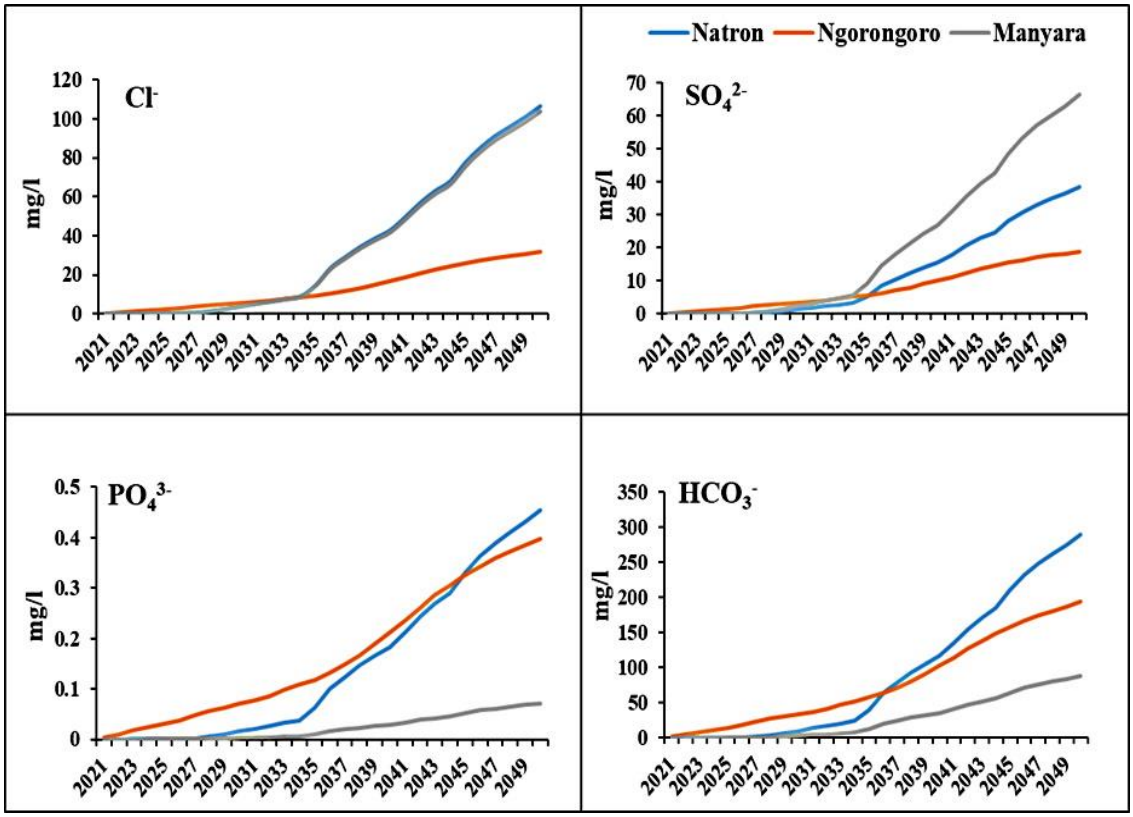

Figure 30: Trends for anions (Cl^-, SO_4^{2-}, $PO4_3^-$, HCO_3^-) concentrations that are expected in the study area from 2021 to 2050

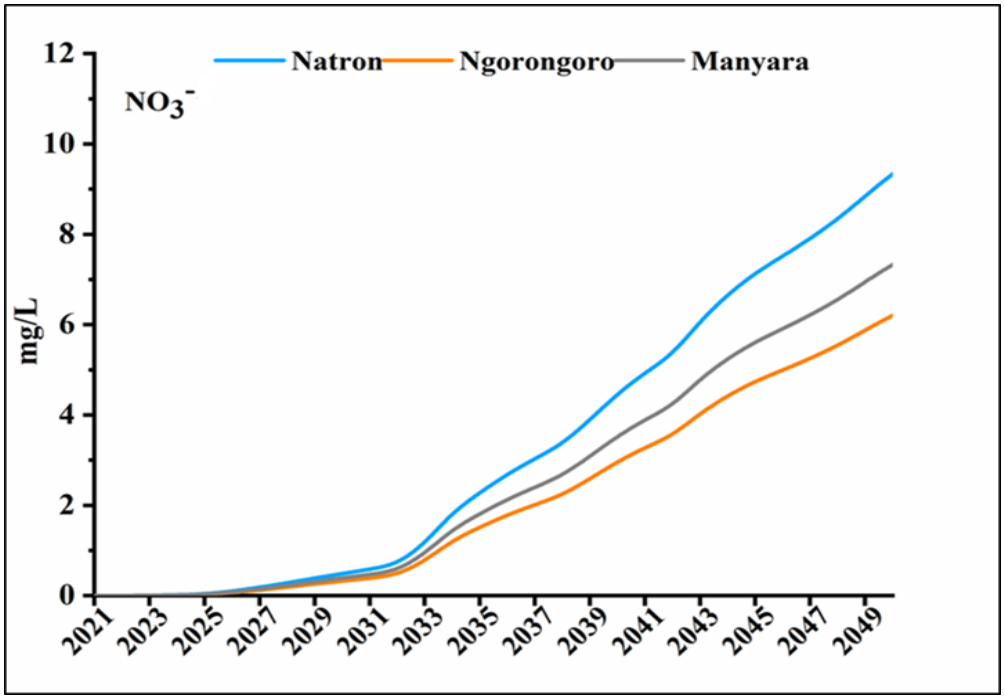

Figure 31: Trends for NO_3^{-1} anion concentrations that are expected in the study area from 2021 to 2050

For anions, the higher increase concentration of Cl^- was at Lake Natron and Lake Manyara, while for SO_4^{2-}, the high increase in concentration would be at Lake Manyara and the lowest at Ngorongoro. For the PO_4^{3-} and HCO_3^-, the higher rise would be in Ngorongoro and Lake Natron. However, for the NO_3^- (Fig. 31), the higher increase in concentration would be observed at Natron and the least at Ngorongoro. The variations in the increased concentration of cation and anions in these sub-catchments are related to the variations in mineral deposits and anthropogenic activities. At Lake Manyara and Natron sub-catchments, the increase in agriculture activities is likely to occur as these catchments are outside the conservation area. These could be a major source of pollution to the groundwater due to the application of fertilizers and other human activities. The trend analysis for cations and anions indicates the increase in concentration between 2036 and 2050 in all sub-catchments. On average, the concentrations are within the allowable limits by WHO and TBS; however, spatially, the distribution is not equal. As a result, some areas would have higher concentrations than the permitted limits.

Spatial Distribution for Cations and Anions in the Groundwater

Spatially, the cations and anions distribution in the study area were analyzed by comparing their distribution during the monitoring period (2018-2020) with the spatial distribution of the simulated concentration from 2021 to 2050. In addition, the future period was separately

analyzed in intervals from 2021-2035 and 2036-2050 and found that the distribution of ions varied over the study area. The spatial distribution of the annual concentration of cations (Na^+, K^+, Ca^{2+}, and Mg^{2+}) and anions (Cl^-, SO_4^{2-}, PO_4^{3-} and HCO_3^-) are presented in Fig. 32 and 33, respectively. However, the spatial distribution for NO_3^- is presented in Fig. 34.

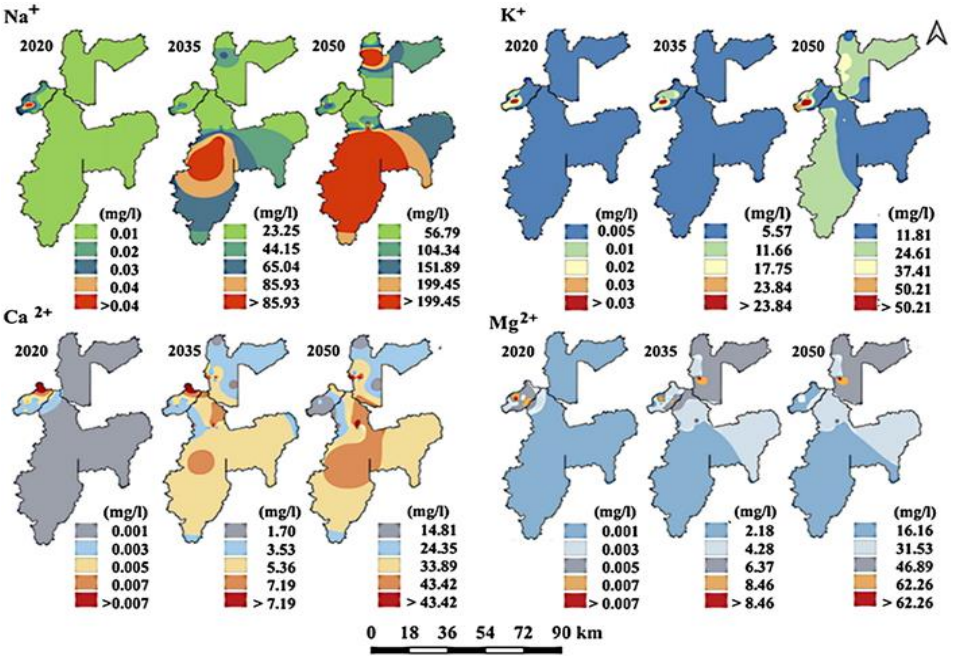

Figure 32: Spatial distribution maps of Na^+, K^+, Ca^{2+}, and Mg^{2+} Cations at the end of baseline (2018-2020) and future periods (2021-2035 and 2036- 2050)

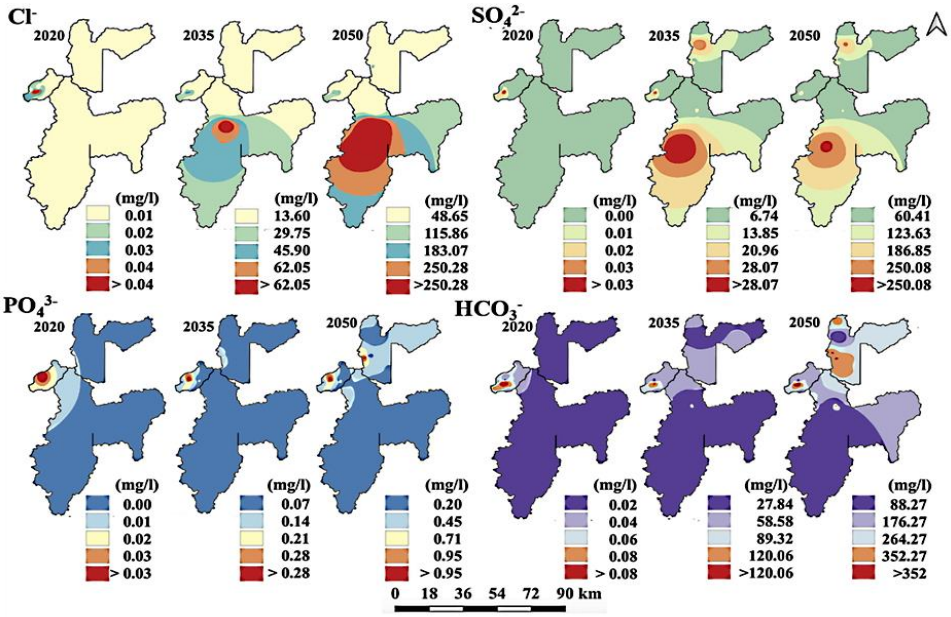

Figure 33: Spatial distribution maps of Cl^-, SO_4^{-2}, PO_4^{-3} and HCO_3^- Anions (mg/L) at the end of baseline (2018-2020) and future periods (2021-2035 and 2036-2050)

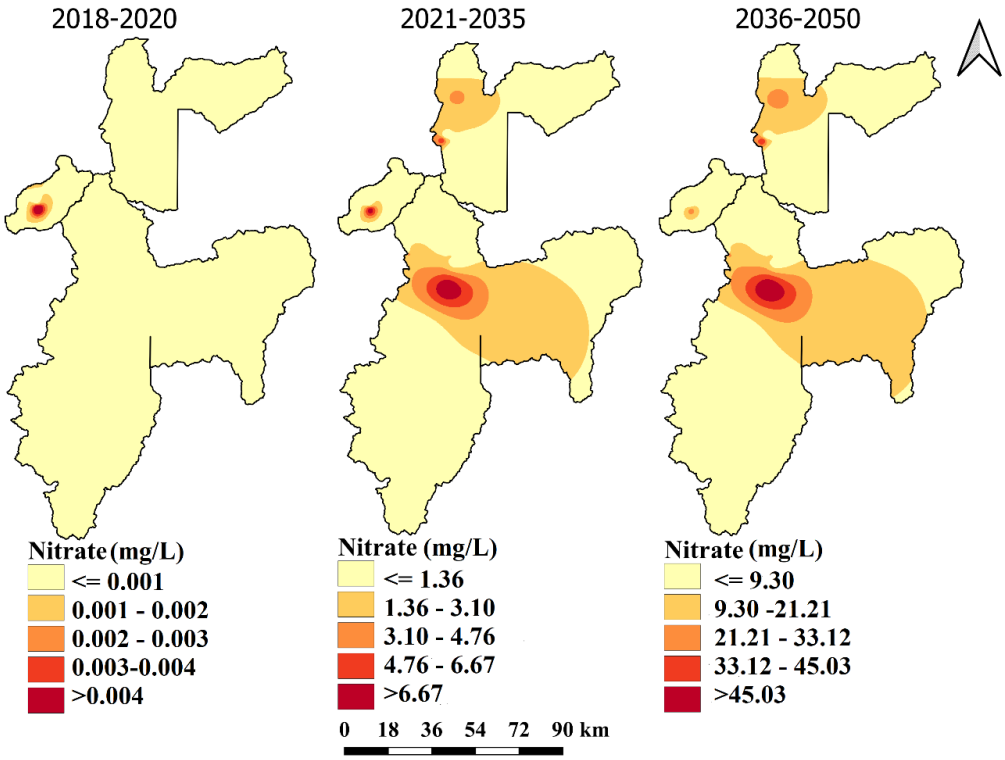

Figure 34: Spatial distribution of the concentration of the NO_3^{-1} anion in the groundwater

- **Spatial Distribution of The Concentration of the Cation (Na^+, K^+, Ca^{2+}, and Mg^{2+}) in the Groundwater**

For Na^+, the spatial distribution is lower than the allowable concentration of 200mg/l by the WHO and TBS at the baseline (2018-2020), as shown in Fig. 32. The concentration will increase but remains within the permissible limit between 2021 and 2035, with a high amount over the central and western of Lake Manyara. However, the concentration of Na^+ will be above the permissible limit over the central and southern parts of Lake Manyara and the western parts of Lake Natron from 2036 to 2050. Though, the entire study area has shown an increase in Na^+ concentration but within the permissible limit. Excess Na^+ in water resources that exceed 200 mg/L may lead to bad water tests and adverse health effects on the community. However, there is no information on the minimum allowable Na^+ daily intake in water (WHO, 2008). The findings from different studies reported that the high Na^+ intake might raise cardiovascular diseases and raise the mortality rate (Arega, 2020). Mineral deposits and saline intrusion can be the primary sources that significantly contribute to high Na^+ in groundwater. In addition, some agricultural activities that can be found around lake Manyara can also be the source of Na^+ in water resources.

Similar conditions were observed for the K^+ (Fig. 32) in which, at the baseline, the concentration was lower than the permissible limit of 50 mg/L set by the TBS standard for Tanzania's drinking water. However, the concentration will increase spatially to the entire study area, with a higher amount exceeding the permissible limit over the western part of the Ngorongoro crater highlands between 2036 and 2050. Thus, for the future period of 2021 - 2035, the entire study area will have increased K^+ but within the allowable limit, as Fig. 32 depicts. The K^+ concentration of more than 50 mg/L is not a major component in water supplies. However, Potassium's high concentration could threaten human health conditions, including Kidney diseases and other conditions such as hypertension, heart diseases, coronary artery diseases, and Adrian insufficiency (Arega, 2020; WHO, 2008). Infants could be more vulnerable because of immature kidney function and limited renal reserve in their bodies.

For the Ca^{2+}, initially, the concentrations are below the permissible concentration of 75 mg/L (WHO) and 150 mg/L (TBS). In 2021-2035, the concentration increases spatially but remains within the permissible limit. A further increase is observed in the future 2036- 2050 over most areas; however, the concentration is observed to be within the allowable limit. Although the concentrations are within the acceptable limit, the increase in Ca^{2+} concentration between 2036 and 2050 is alarming in the entire study area. The groundwater quality in the areas with an excess concentration of Ca^{2+} from acceptable amounts is considered poor and may cause health problems to humans and animals (wildlife and domestic). Likewise, for the Mg^{2+} (Fig. 32), low concentrations are observed during the baseline period, increasing over the entire study area in the future between 2021 and 2035. However, the distribution is within WHO's permissible limit (50 mg/L) and TBS (100 mg/L). Between 2036 and 2050, the distribution of Mg^{2+} concentrations in the groundwater will increase but within the WHO and TBS limits except for a few areas of Lake Natron where the concentrations will exceed the WHO limit.

- **Spatial Distribution of the Concentration of the Anions (Cl^-, SO_4^{2-}, PO_4^{3-}, NO_3^- And HCO_3^-) in the Groundwater**

The spatial distribution of Cl^- concentration was lower at a baseline period (2018-2020) compared to the allowable concentration of 250 mg/L by the WHO and TBS, as shown in Fig. 26. However, the concentration will increase during the future period 2021-2035 all over the study area but will remain well within the permissible limits. Therefore, Cl^{-1} concentration will spatially increase above the allowable limit over the central to the southern parts of Lake Manyara from 2036 to 2050. Chloride is a widely distributed anion in many rocks type. In

Natural water, Chloride may occur due to agricultural activities and chloride-rich rock materials (Selvakumar *et al.*, 2017). Its concentration in groundwater varies with temperature and rainfall amounts. Therefore, a high concentration of chloride is expected when the temperature is high and rainfall is less. Higher chloride consumption causes hypertension and the risk of stroke, renal stones, and asthma to the human being (Mccarty, 2004). Likewise, for the SO_4^{2-}, the baseline concentration was lower than the permissible limit of 250 mg/L (WHO) and 400 mg/L (TBS). However, the concentration will increase spatially to the entire study area between 2021 and 2035; but within the permissible limit. Similarly, for the future period of 2036 - 2050, the whole study area will have an increased SO_4^{2-} concentration but not cross the allowable limits (Fig. 33). This increase could be related to the development of anthropogenic activities through the use of sulphate fertilizers and future climate trends. In addition, the SO_4^{2-} is an important anion present in natural water that can impact human health by causing dehydration and gastrointestinal irritation when consumed in excess (Sarala & Ravi, 2012).

The spatial distribution of PO_4^{3-} (Fig. 26) showed a lower concentration at the baseline period (2018-2020) than TBS's allowable concentration of 2.2 mg/L. However, the concentrations will increase beyond the permissible limits around Ngorongoro crater highlands from 2021 to 2035. The concentration of PO_4^{3-} will further increase above the allowable limit around Ngorongoro crater highlands, northwestern lake, Manyara, and most areas of lake Natron except northern and southern parts during 2036 - 2050. A high intake of PO_4^{-3} in the body is detrimental. Hence, future monitoring of the PO_4^{-3} concentration in the groundwater is vital for the mentioned areas considering the possibility of exceeding the permissible limits. The primary source of PO_4^{-3} is point sources, including natural decomposition of rocks and minerals, erosions, rainfall runoffs, agricultural runoffs, direct inputs from animals/wildlife, and atmospheric deposition. Other non-point sources include wastewater treatment plants and industrial discharge. However, many parts of the area are conserved; therefore, the main source remains non-points.

The spatial distribution of the HCO_3^- (Fig. 33) shows at the baseline period from 2018 to 2020; the concentration was lower than the permissible limit of 600 mg/L set by the TBS for alkalinity in natural water sources. The concentration will increase spatially to the entire study area between 2021 and 2035. However, the concentration will still be within the permissible limit. Similarly, for the future period of 2036 - 2050, model results indicate there will be an increase in HCO_3^- concentration over the entire study area but within permissible limits. The study

area's primary carbonate source is the active carbonatite volcano found around the Oldoinyo Lengai, located in the Gregory rift valley. However, high concentrations were observed in the southwestern parts of Lake Natron and the southern Ngorongoro crater (Fig. 33). The HCO_3^-, when in large amounts, affects the taste and corrosiveness of water.

Likewise, for the Nitrate (NO_3^-) (Fig. 34), spatial distribution indicated a lower concentration at a baseline (2018-2020) with a concentration less than 0.01 mg/L. However, the distribution showed an increase in NO_3^- to 8.67 mg/L for the future 2021-2035 in the central part of the Lake Manyara sub-catchment. At this period, the concentration of NO_3^- would be within the allowable limit of 10 mg/L for the natural concentration in groundwater under aerobic conditions (Sadler *et al.*, 2016). Further, the results showed an increase of NO_3^- to the concentration above the allowable limits between 2036 and 2050 at the central and eastern parts of Lake Manyara sub-catchment, western parts of lake Natron and around Lake Makat in the Olduvai sub-catchment. Therefore, more concentrations would be in the Natron and Lake Manyara sub-catchments. This increase could be mainly to human activities, especially Agriculture expansions, which are expected to increase over those areas outside the conserved area. The NO_3^- is toxic when consumed as it can be converted to nitrite ion (NO_2^-) in the stomach and may result in severe illness and sometimes death in infants of less than six months. In addition, NO_2^- combines with haemoglobin, giving complete methaemoglobin that deprives the tissue of oxygen supply. The blueness of the skin is the main symptom of the acute illness associated with the consumption of NO_3^-.

(ii) Impacts of Climate and Land use/cover Changes on Cations and Anions Transport to the Groundwater

The pairwise relationships between the climate parameters and annual concentration (mg/L) for cations and anions transported to the groundwater are listed in Table 34 and 35. The correlation was performed at 0.01 and 0.05 levels of significance. Based on Table 34, all cations (Na^+, K^+, Mg^{2+}, and Ca^{2+}) showed a significant correlation to the Tmax, Tmin, Tmean, and ET with low to moderate Pearson correlation coefficient (*r*), ranging from 0.35 - 0.67. Likewise, for the anions (Cl^-, SO_4^{2-}, PO_4^{-3}, NO_3^- and HCO_3^-), as Table 35 shows, the results significantly correlated with Tmax, Tmin, Tmean, and ET with low to moderate person correlation (r) between 0.35 and 0.85. However, Tmin shows the highest correlation among all climate variables to both cations and anions.

Furthermore, the study determined a pairwise relationship between the land use/cover types and annual concentration (mg/L) for the cations and anions. The results are as presented in Table 36 and 37, respectively. The correlation was performed at a 0.05 level of significance. Based on the results in Table 36, all cations (Na^{+}, K^{+}, Mg^{2+}, and Ca^{2+}) significantly correlate to the changes in all land use/ cover types. Pearson correlation coefficient (r), ranging from 0.56 to 0.99. Likewise, for the anions (Cl^{-}, SO_4^{2-}, PO_4^{-3}, NO_3^{-} and HCO_3^{-}), as Table 37 shows, the results significantly correlated with all land use /cover types with Pearson correlation (*r*) between 0.56 and 0.96. However, forest, bushland, woodland, and wetland negatively correlated with all cations and anions. On the other hand, cultivated land, grassland, built-up area, and water positively correlated with all cations and anions. Therefore, besides other factors such as volcanic activities and accelerated human interventions that could affect water quality, climate change can be considered the main driver for hydrochemical movements to the groundwater around the study area.

Table 34: Correlation Matrix between annual variation in climatic parameters and cation concentration (mg/L) changes to the groundwater

	Rain	**Tmax**	**Tmin**	**Tmean**	**RH**	**WS**	**ET**	**Na^+**	**K^+**	**Mg^{2+}**	**Ca^{2+}**
Rain	1										
Tmax	-0.76**	1									
Tmin	-0.51**	0.88**	1								
Tmean	-0.68**	0.98**	0.96**	1							
RH	0.84**	-0.88**	-0.63**	-0.79**	1						
WS	-0.79**	0.70**	0.57**	0.66**	-0.70**	1					
ET	-0.84**	0.93**	0.73**	0.87**	-0.95**	0.83**	1				
Na^+	-0.23	0.48**	0.67**	0.56**	-0.21	0.32*	0.36*	1			
K^+	-0.24	0.49**	0.64**	0.57**	-0.22	0.34	0.35*	0.99**	1		
Mg^{2+}	-0.23	0.48**	0.63**	0.56**	-0.21	0.31	0.37*	0.99**	0.99**	1	
Ca^{2+}	-0.23	0.48**	0.63**	0.56**	-0.21	0.32	0.36*	0.99**	0.99**	0.99**	1

**Correlation is significant at the 0.01 level. *Correlation is significant at the 0.05 level.

Table 35: Correlation Matrix between annual variation in climatic parameters and anions concentration (mg/L) changes to the groundwater

Variable	Rain	Tmax	Tmin	Tmean	RH	WS	ET	Cl^-	SO_4^{2-}	NO_3^-	PO_4^{3-}	HCO_3^-
Rain	1											
Tmax	-0.76**	1										
Tmin	-0.51**	0.88**	1									
Tmean	-0.68**	0.98**	0.96**	1								
RH	0.84**	-0.88**	-0.63**	-0.79**	1							
WS	-0.79**	0.70**	0.57**	0.66**	-0.70**	1						
ET	-0.84**	0.93**	0.73**	0.87**	-0.95**	0.83**	1					
Cl^-	-0.23	0.48**	0.66**	0.54**	-0.21	0.32	0.36*	1				
SO_4^{2-}	-0.25	0.48**	0.62**	0.59**	-0.22	0.34	0.35*	0.99**	1			
NO_3^-	-0.09	-0.28	0.65**	0.03	0.46*	-0.85**	-0.58*	0.99**	0.99**	1		
PO_4^{3-}	-0.24	0.49**	0.64**	0.57**	-0.22	0.32	0.35*	0.99**	0.99**	0.99**	1	
HCO_3^-	-0.23	0.49**	0.64**	0.57**	-0.21	0.32	0.38*	0.99**	0.99**	0.99**	0.99**	1

**Correlation is significant at the 0.01 level. *Correlation is significant at the 0.05 level

Table 36: Correlation Matrix between changes in land use/cover types and Cations concentration (mg/L) changes to the groundwater

Variables	FR	WL	BUL	GL	WT	WET	CL	BLT	BL	Na^+	K^+	Mg^{2+}	Ca^{2+}
FR	**1**												
WL	0.85	**1**											
BUL	0.99	0.91	**1**										
GL	-0.98	-0.73	-0.95	**1**									
WT	0.99	0.92	1.00	-0.94	**1**								
WT	-0.49	-0.88	-0.60	0.32	-0.62	**1**							
CL	-0.99	-0.92	-1.00	0.94	-1.00	0.61	**1**						
BLT	-0.94	-0.98	-0.98	0.86	-0.98	0.75	0.98	**1**					
BL	-0.97	-0.96	-0.99	0.90	-0.99	0.70	0.99	1.00	**1**				
Na^+	-0.71	-0.98	-0.79	0.56	-0.81	0.96	0.81	0.91	0.87	**1**			
K^+	-0.77	-0.99	-0.84	0.63	-0.86	0.94	0.85	0.94	0.91	0.99	**1**		
Mg^{2+}	-0.73	-0.98	-0.81	0.58	-0.82	0.96	0.82	0.91	0.88	0.99	0.99	**1**	
Ca^{2+}	-0.72	-0.98	-0.80	0.57	-0.82	0.96	0.81	0.91	0.87	0.99	0.99	0.99	**1**

Correlation is significant at the 0.05 level. FR-Forest, WL—Woodland, BUL—Bushland, GL—Grassland, WT—Water, WET-Wetland, CL—Cultivated land, BLT-Built-up land, BL- Bare land

Table 37: Correlation Matrix between changes in land use/cover types and anions concentration (mg/L) changes to the groundwater

Variables	FR	WL	BUL	GL	WT	WET	CL	BLT	BL	Cl^-	SO_4^{-2}	NO_3^-	PO_4^{-3}	HCO_3^-
FR	**1**													
WL	0.85	**1**												
BUL	0.99	0.91	**1**											
GL	-0.98	-0.73	-0.95	**1**										
WT	0.99	0.92	1.00	-0.94	**1**									
WET	-0.49	-0.88	-0.60	0.32	-0.62	**1**								
CL	-0.99	-0.92	-1.00	0.94	-1.00	0.61	**1**							
BLT	-0.94	-0.98	-0.98	0.86	-0.98	0.75	0.98	**1**						
BL	-0.97	-0.96	-0.99	0.90	-0.99	0.70	0.99	1.00	**1**					
Cl^-	-0.71	-0.97	-0.79	0.56	-0.81	0.96	0.80	0.90	0.87	**1**				
SO_4^{2-}	-0.71	-0.98	-0.80	0.57	-0.81	0.96	0.81	0.91	0.87	1.00	**1**			
NO_3^-	-0.72	-0.98	-0.80	0.57	-0.82	0.96	0.81	0.91	0.87	1.00	1.00	**1**		
PO_4^{-3}	-0.76	-0.99	-0.84	0.63	-0.85	0.94	0.85	0.94	0.90	1.00	1.00	1.00	**1**	
HCO_3^-	-0.75	-0.99	-0.83	0.61	-0.84	0.94	0.84	0.93	0.89	1.00	1.00	1.00	1.00	**1**

Correlation is significant at the 0.05 level. FR-Forest, WL—Woodland, BUL—Bushland, GL—Grassland, WT—Water, WET-Wetland, CL—Cultivated land, BLT-Built-up land, BL- Bare land

(iii) Different Responses of Cations and Anions Movements to the Groundwater as Influenced by the Climate and Land use/cover Changes

The PLSR models were constructed separately for the cations and anions with independent parameters of climate and land use/cover change. For the cations and anions components models, the prediction error decreased with an increasing number of components, while an additional increase in the number of components generated a higher prediction error. Thus model is suggesting that the other components were not strongly correlated with the residuals of the predicted variable (Onderka *et al.*, 2012).

Four PLSR models were developed for different response variables, namely the PLSR1 component (cations & climate change), PLSR2 component (anions and climate change), and PLSR3 (cations and land-use/cover change) and PLSR4 component (anions and land-use/cover change). The cross-validation for response variables in PLSR1, PLSR2, PLSR3 and PLSR4 selected three significant components, each using an auto-fit approach. The PLSR model constructed for cation and anions components against climate change and land-use/cover change was strong ($R^2 > 0.50$), as shown in Table 38 and 39; hence both were considered to have predictive power.

Contribution of Climate Changes on Cations and Anions Components

The first component in PLSR1 explained 70.3% of the Na^{2+}, K^{+}, Mg^{2+}, and Ca^{2+} variability. The addition of the second component led to the models cumulatively explaining 74.6% of the total variance. The first component in PLSR2 explained 80.6% of the variability in the Cl^{-}, SO_4^{2-}, PO_4^{-3}, NO_3^{-} and HCO_3^{-}. The addition of the second component led to the models cumulatively explaining 84.7% of the total variance. Adding more components to the PLSR1 and PLSR2 models did not substantially improve the variance explained (Table 38).

Table 38: List of regression coefficients for the hydrochemical components of the PLSR models with respect to climate changes in the NCA and surroundings

Response Variable Y	R^2	R^2_{cross}	Component	% of explained variability in Y	Cumulative explained variability in Y (%)	R^2 cum
Cations	0.801	0.404	1	70.3	70.3	0.420
Component			2	4.3	74.6	0.492
(Na^+, K^+,			3	1.3	71.56	0.437
Mg^{2+}, Ca^{2+})			4	1.3	72.86	0.431
Anions	0.996	0.968	1	80.6	80.6	0.998
Components			2	4.1	84.7	0.994
(Cl^-, SO_4^{-2},			3	0.2	84.9	0.950
NO_3^-, PO_4^{-3}&			4	0.2	85.1	0.977
HCO_3^-)						

The first component for PLSR1 (Table 38) for cations was dominated by rainfall, Tmin, and relative humidity on the positive side and wind speed on the negative side. Tmax, Tmin and Tmean dominated the second component on the positive side, and rainfall and relative humidity on the negative side. The last component was dominated by rainfall, Tmin and relative humidity on the positive side and wind speed on the negative side. The results of the relative importance of predictors of the model showed that Tmin and wind speed (VIP < 1) are significance affecting cations while Tmax and Tmean were relatively less important in affecting cations compared to other climate factors. The first component for PLSR2 (Table 39) for anions was dominated by all climate factors, where the positive side included Tmax, Tmin, and Tmean, while the negative side included rainfall and relative humidity. The second component was dominated by wind speed on the positive side and Tmin and Tmean on the negative side. The last component was dominated by Tmax, Tmin, Tmean and wind speed on the positive side and rainfall and relative humidity on the negative side. The results of the relative importance of predictors of the model showed that rainfall, Tmax and relative humidity (VIP < 1) are significance affecting anions, while all climate factors were relatively important in affecting anions.

Table 39: Variable importance for the projection (VIP) values and PLSR weights of cations and anions in the NCA and surroundings with respect to climate parameters

PLSR parameters	Cations (Na^+, K^+, Mg^{2+}, Ca^{2+})				Anions (Cl^-, SO_4^{-2}, NO_3^-, PO_4^{-3} and HCO_3^-)			
	VIP	**W*1**	**W*2**	**W*3**	**VIP**	**W*1**	**W*2**	**W*3**
Rainfall	0.765	**0.312**	**-0.362**	**0.312**	1.017	**-0.415**	-0.271	**-0.415**
Tmax	0.337	-0.137	**0.432**	-0.137	1.012	**0.413**	-0.116	**0.413**
Tmin	1.764	**0.720**	**0.472**	**0.720**	0.967	**0.395**	**-0.583**	**0.395**
Tmean	0.393	0.161	**0.508**	0.161	0.995	**0.406**	**-0.349**	**0.406**
RH	0.808	**0.330**	**-0.354**	**0.330**	1.018	**-0.416**	-0.093	**-0.416**
Wind Speed	1.175	**-0.480**	0.275	**-0.480**	0.990	**0.404**	**0.665**	**0.404**

Contribution of Land use on Cations and Anions Components

The first component in PLSR3 explained 56.1% of the Na^{2+}, K^+, Mg^{2+}, and Ca^{2+} variability. The addition of the second component led to the models cumulatively explaining 60.4% of the total variance. The first component in PLSR4 explained 58.7% of the variability in the Cl^-, SO_4^{-2}, NO_3^-, PO_4^{-3} and HCO_3^-. The addition of the second component led to the models cumulatively explaining 65.3% of the total variance. Adding more components to the PLSR3 and PLSR4 models did not substantially improve the variance explained (Table 40).

Table 40: List of regression coefficients for the hydrochemical components of the PLSR models with respect to Land use/cover changes in the NCA and surroundings

Response Variable Y	R^2	R^2_{cross}	Component	% of explained variability in Y	Cumulative explained variability in Y (%)	R^2_{cum}
Cations	0.897	0.617	1	56.1	56.1	0.458
Component			2	4.3	60.4	0.385
(Na^+, K^+,			3	0.1	60.5	0.442
Mg^{2+}, Ca^{2+})			4	0.1	60.6.4	0.448
Anions	0.812	0.897	1	58.7	58.7	0.462
Components			2	6.6	65.3	0.455
(Cl^{-1}, SO_4^{-2},			3	1.2	66.5	0.450
NO_3^{-1}, PO_4^{-3}			4	0.1	66.6	0.388
& HCO_3^{-1})						

The first component for PLSR 3 (Table 40) was dominated by wetland, cultivated land, built-up land and bare land on the positive side, and woodland, bushland and water on the negative side. The second component was dominated by forest and wetland on the positive side and grassland on the negative side. The last component was dominated by wetland, cultivated land, Built-up area and bare land on the positive side and woodland, bushland and water on the negative side. The results of the relative importance of predictors of the model showed that woodland, wetland, Built-up area and bare land (VIP < 1) are significant affecting cations, while forest and grassland were relatively less important in affecting cations compared to other land use. The first component of PLSR 4 (Table 41) was dominated by wetland, cultivated land, Built-up area and bare land on the positive side, and woodland, bushland and water on the negative side. The second component was dominated by forest and wetland on the positive side and grassland on the negative side. The last component was dominated by wetland, cultivated land, Built-up area and bare land on the positive side and woodland, bushland and water on the negative side. The results of the relative importance of predictors of the model showed that woodland, wetland, built-up land and bare land (VIP < 1) are significance affecting anions, while forest and grassland were relatively less important in affecting anions compared to other land use.

Table 41: Variable importance for the projection (VIP) values and PLSR weights of cations and anions in the NCA and surroundings with respect to Land use types

PLSR parameters	Cations (Na^+, K^+, Mg^{2+}, Ca^{2+})				Anions (Cl^-, SO_4^{-2}, NO_3^-, PO_4^{-3} & HCO_3^-)			
	VIP	**W*1**	**W*2**	**W*3**	**VIP**	**W*1**	**W*2**	**W*3**
FR	0.869	-0.290	**0.309**	-0.290	0.869	-0.290	**0.309**	-0.290
WL	1.164	**-0.388**	-0.259	**-0.388**	1.164	**-0.388**	-0.259	**-0.388**
BL	0.963	**-0.321**	0.183	**-0.321**	0.963	**-0.321**	0.183	**-0.321**
GL	0.697	0.232	**-0.494**	0.232	0.698	0.233	**-0.494**	0.233
WT	0.981	**-0.327**	0.155	**-0.327**	0.982	**-0.327**	0.155	**-0.327**
WET	1.132	**0.377**	**0.711**	**0.377**	1.131	**0.377**	**0.711**	**0.377**
CL	0.975	**0.325**	-0.164	**0.325**	0.976	**0.325**	-0.164	**0.325**
BLT	1.088	**0.363**	0.038	**0.363**	1.088	**0.363**	0.038	**0.363**
BL	1.047	**0.349**	-0.045	**0.349**	1.047	**0.349**	-0.045	**0.349**

FR-Forest, WL—Woodland, BUL—Bushland, GL—Grassland, WT—Water, WET-Wetland, CL—Cultivated land, BLT-Built-up land, BL- Bare land

CHAPTER FIVE

CONCLUSION AND RECOMMENDATIONS

5.1 Conclusion

Annual and seasonal rainfall would increase in 2021-2050 compared to the baseline 1982-2011, with increases in rainfall for all seasons except the June to September (JJAS) season, which indicates a decreasing trend for RCP 4.5 and RCP 8.5. Likewise, for the maximum and minimum temperatures, the annual increase in temperature would occur in the future for both RCPs, with a higher rise predicted under RCP 8.5. Spatially, the highest increase in rainfall would generally occur from the central to the southern parts of the study area for all future periods under both RCP 4.5 and RCP 8.5. For the maximum and minimum temperature, the highest rise would occur over the central and southern parts of the study area for all future periods and RCPs. The projected increase in rainfall and temperature, both maximum and minimum, over the study area call for the development of adaptation measures and a strategic plan for the ecosystem management of the NCA and surrounding areas.

Between 1995 and 2016, the analyzed change in land use/cover showed the greatest decrease in woodland and the greatest increase in cultivated land. The predicted future (2016–2035) Changes in land use/cove reveal a reduction in forest, woodland, bushland, and water, but an increase in grassland, wetland, cultivated built-up area, and bare land. Change analysis using time-series maps revealed the overall Land use/cover change, including the comprehensive discovery of an area's diverse forms of variation. Natural forests with high environmental values are continuously declining as a result of the current trend in land management, resulting in the loss of the NCA's ecological importance. Therefore, for sustainable management, the authorities must conciliate between the existing Land use/cover change and ecosystem services monitoring.

The hydrological response to climate and land use/cover changes varied between scenarios. In the first scenario shows that future runoff and lateral flow would increase with land use change in 2025 and 2035, respectively, compared to land use in 2016. Furthermore, groundwater and water yields will decrease with land use change in 2025 and 2035, while evapotranspiration will increase in 2025 and decrease in 2035. For the second scenarios, surface runoff, evapotranspiration, lateral flow, and water yield would increase significantly, while groundwater would decrease with future (2021-2050) climate changes for both RCP 4.5 and

RCP 8.5. Similarly for the third combined land use/cover change scenario of 2025 and 2035 with future (2021-2050) climate change under RCP 4.5 and 8.5. In general, the results of this study indicate that climate change has a greater impact on temporal and spatial changes in hydrological components than land use/cover changes.

The groundwater quality of the NCA and surrounding catchments is currently suitable for drinking and domestic use. However, due to the predicted changes in climate and land use/cover in the study area, a deterioration in quality is to be expected in the future. In general, significant concentrations of Na^+ and K^+ in groundwater are expected between 2036 and 2050, exceeding the WHO and TBS limits of 200 and 50 mg/L, respectively. Similarly, Cl and PO_4^{-3} anions in groundwater exceed the WHO and TBS maximum allowable concentrations of 250 and 2.2 mg/L, respectively. The remaining cations and anions would also rise, but not exceeding the allowable maximum limits by the WHO and TBS standards for drinking water. Changes in groundwater quality for both cations and anions are statistically significant correlated with evapotranspiration and temperature (maximum, minimum, and mean), with Pearson's coefficient of determination, r, ranging between 0.35 and 0.85. Likewise to the land use/ cover types, it was found that changes in all land use/cover types significantly correlate with the movement of cations and anions to the groundwater, with Pearson's coefficient of determination, *r*, between 0.56 and 0.99.

Individually minimum temperature (Tmin) and wind speed are significantly affecting cations. Besides rainfall, Maximum temperature (Tmax) and relative humidity significantly affect anions. Looking at the impact of individual land use/cover types, the model showed that woodland, wetland, Built-up area and bare land significantly affecting cations. Besides, woodland, wetland, built-up land and bare land would significantly influence the anions movement to the groundwater. Therefore, apart from other factors such as volcanic activities and accelerated human interventions that could affect water quality, climate change and land use cover changes can be considered the main driver for hydrochemical movements to the groundwater around the study area.

5.2 Recommendations

(i) Installation of weather stations and river flow gauging stations in the conservation areas are highly recommended to monitor environmental changes that could occur in these sensitive area. Monitoring of environmental changes is necessary for planning better conservation management practices and better adaptation strategies.

(ii) Adapting to the new challenge of land use/cover and climate change requires an integrated approach to water resource use and management. The adaptation should focus on better land use, with integrated solutions at the appropriate levels for climate change adaptation and mitigation.

(iii) Appropriate adaptation measures should be implemented to strengthen resilience to land use/cover change and climate change, thereby improving water security.

(iv) The adaptation measures should consider a trade-off between Land use, climate change adaptation, water resource need, society need and livelihood.

(v) Further studies to quantify the ecological, economic and social significance of the climate and land use/cover changes impacts to water resources in the NCA and surroundings are highly encouraged.

REFERENCES

Abbasi, F., Feyen, J., & Van Genuchten, M. T. (2004). Two-dimensional simulation of water flow and solute transport below furrows: Model calibration and validation. *Journal of Hydrology, 290*(1-2), 63-79.

Abbaspour, K. C. (2013). "*Swat-cup 2012J" in SWAT Calibration Uncertainty Program: A User Manual*. https://scholar.google.com/

Abdulkareem, J. H., Pradhan, B., Sulaiman, W. N. A., & Jamil, N. R. (2018). Quantification of runoff as influenced by morphometric characteristics in a rural complex catchment. *Earth Systems Environmental Earth Sciences, 2*(1), 145-162.

Abou Zaki, N., Torabi-Haghighi, A., Rossi, P. M., Tourian, M. J., & Klove, B. (2018). Monitoring groundwater storage depletion using gravity recovery and climate experiment data in the semi-arid catchments. *Hydrology and Earth System Sciences Discussions*, 2018, 1-21.

Adeyeri, O. E., Laux, P., Lawin, A. E., & Oyekan, K. S. A. (2020). Multiple bias-correction of dynamically downscaled CMIP5 climate models temperature projection: A case study of the transboundary Komadugu: Yobe river basin, Lake Chad region, West Africa. *Applied Sciences*, 2(7), 1-18.

Aggarwal, P. (2007). Climate change: Implications for Indian agriculture. *Jalvigyan Sameeksha, 22*(1), 37-46.

Akhtar, M., Ahmad, N., & Booij, M. J. (2009). Use of regional climate model simulations as input for hydrological models for the Hindukush-Karakorum-Himalaya region. *Hydrology and Earth System Sciences,* 13(7), 1075-1089.

Al-Bakri, J. T., Salahat, M., Suleiman, A., Suifan, M., Hamdan, M. R., Khresat, S., & Kandakji, T. (2013). Impact of climate and land use changes on water and food security in jordan: Implications for transcending “the tragedy of the commons”. *Sustainability*, 5(2), 724-748.

Aliani, H., Malmir, M., Sourodi, M., & Kafaky, S. B. (2019). Change detection and prediction of urban land use changes by CA–Markov model (case study: Talesh County). *Environmental Earth Sciences, 78*(17), 1-12.

Andaryani, S., Nourani, V., Ball, J., Jahanbakhsh, A. S., Keshtkar, H., & Trolle, D. (2021). A comparison of frameworks for separating the impacts of human activities and climate change on river flow in existing records and different near-future scenarios. *Hydrological Processes,* 35(7), e14301.

Ansari, A., & Golabi, M. H. (2019). Prediction of spatial land use changes based on LCM in a GIS environment for Desert Wetlands: A case study of Meighan Wetland, Iran. *International Soil Water Conservation Research, 7*(1), 64-70.

Antar, M. A., Elassiouti, I., & Allam, M. N. (2006). Rainfall-runoff modelling using artificial neural networks technique: A Blue Nile catchment case study. *Hydrological Processes*: *An International Journal,* 20(5), 1201-1216.

Arega, T. (2020). Sodium and Potassium Analysis of Drinking Water Quality Assessment and Its Health Effects in Ethiopia: A Retrospective Study. *Journal Oral Health Dentistry*, 4(1), 261-266.

Arnold, J., Allen, P., Volk, M., Williams, J., & Bosch, D. (2010). Assessment of different representations of spatial variability on SWAT model performance. *Transactions of the American Society of Agricultural and Biological Engineers, 53*(5), 1433-1443.

Arnold, J. G., Allen, P. M., & Bernhardt, G. (1993). A comprehensive surface-groundwater flow model. *Journal of Hydrology*, 142(1-4), 47-69.

Arnold, J. G., & Fohrer, N. (2005). SWAT2000: Current capabilities and research opportunities in applied watershed modelling. *Hydrological Processes: An International Journal, 19*(3), 563-572.

Arnold, J. G., & Fohrer, N. (2005). SWAT2000: Current capabilities and research opportunities in applied watershed modelling. *Hydrological Processes: An International Journal*, 19(3), 563-572.

Arnold, J. G., Moriasi, D. N., Gassman, P. W., Abbaspour, K. C., White, M. J., Srinivasan, R., Santhi, C., Harmel, R. D., Van Griensven, A., Van Liew, M.W., & Kannan, N., (2012). SWAT: Model use, calibration, and validation. *Transactions of the American Society of Agricultural and Biological Engineers*, 55(4), 1491-1508.

Arnold, J. G., Srinivasan, R., Muttiah, R. S., & Williams, J. R. (1998). Large area hydrologic modeling and assessment part I: Model development. *Journal of the American Water Resources Association*, 34(1), 73-89.

Arnold, J. G., & Williams, J. R. (1987). Validation of SWRRB: Simulator for water resources in rural basins. *Journal of Water Resources Planning and Management*, 113(2), 243-256.

Arnold, J. G., Williams, J. R., & Maidment, D. R. (1995). Continuous-time water and sediment-routing model for large basins. *Journal of Hydraulic Engineering*, 121(2), 171-183.

Arsanjani, J. J., Helbich, M., Kainz, W., & Boloorani, A. D. (2013). Integration of logistic regression, Markov chain and cellular automata models to simulate urban expansion. *International Journal of Applied Earth Observation and Geoinformation*, 21, 265-275.

Arsanjani, J. J., Kainz, W., Mousivand, A. J., & Fusion, D. (2011). Tracking dynamic land-use change using spatially explicit Markov Chain based on cellular automata: The case of Tehran. *International Journal of Image, 2*(4), 329-345.

Assfaw, A. T. (2019). Calibration, validation and performance evaluation of SWAT model for sediment yield modelling in Megech reservoir catchment, Ethiopia. *Journal of Environmental Geography, 12*(3-4), 21-31.

Ayugi, B., Dike, V., Ngoma, H., Babaousmail, H., Mumo, R., & Ongoma, V. (2021). Future changes in precipitation extremes over East Africa based on CMIP6 models. *Water*, 13(17), 2358.

Baja, S., Nurmiaty, U., & Arif, S. (2014). GIS-based soil erosion modeling for assessing land suitability in the urban watershed of tallo river, South Sulawesi, Indonesia. *Modern Applied Science, 8*(4), 50.

Bárdossy, A., & Singh, S. (2008). Robust estimation of hydrological model parameters. *Journal of Hydrology earth system sciences, 12*(6), 1273-1283.

Basommi, L. P., Guan, Q. F., Cheng, D. D., & Singh, S. K. (2016). Dynamics of land use change in a mining area: A case study of Nadowli District, Ghana. *Journal of Mountain Science,* 13(4), 633-642.

Begou, C. J., Jomaa, S., Benabdallah, S., Bazie, P., Afouda, A., & Rode, M. (2016). Multi-site validation of the SWAT model on the Bani catchment: Model performance and predictive uncertainty. *Water Resources Research, 8*(5), 178.

Bessah, E., Boakye, E. A., Agodzo, S. K., Nyadzi, E., Larbi, I., & Awotwi, A. (2021). Increased seasonal rainfall in the twenty-first century over Ghana and its potential implications for agriculture productivity. *Environment, Development Sustainability, 23*(8), 12342-12365.

Boakye, E., Odai, S., Adjei, K., & Annor, F. (2008). Landsat images for assessment of the impact of land use and land cover changes on the Barekese catchment in Ghana. *European Journal of Scientific Research, 22*(2), 269-278.

Bornschein, A., & Pohl, R. (2018). Land use influence on flood routing and retention from the viewpoint of hydromechanics. *Journal of Flood Risk Management, 11*(1), 6-14.

Brooks, R. H., & Corey, A. T. (1963). *Hydraulic Properties of Porous Media and their Relationship to Drainage Design [Doctoral dissertation]*. Colorado State University. Libraries. https://scholar.google.com

Brown, L. C., & Barnwell, T. O. (1987). *The Enhanced Stream Water Quality Models QUAL2E and QUAL2E-UNCAS: Documentation and user Manual (P. 189). Athens: US Environmental Protection Agency*. Office of Research and Development. Environmental Research Laboratory. https://scholar.google.com

Burke, M. B., Lobell, D. B., & Guarino, L. (2009). Shifts in African crop climates by 2050, and the implications for crop improvement and genetic resources conservation. *Global Environmental Change, 19*(3), 317-325.

Chacha, N., Njau, K. N., Lugomela, G. V., & Muzuka, A. N. (2018). Hydrogeochemical characteristics and spatial distribution of groundwater quality in Arusha well fields, Northern Tanzania. *Journal of Applied Water Science, 8*(4), 1-23.

Chaibou-Begou, J., Jomaa, S., Benabdallah, S., Bazie, P., Afouda, A., & Rode, M. (2016). Multi-site validation of the SWAT model on the Bani catchment: Model performance and predictive uncertainty. *Water, 8*(5), 178.

Chang, H., & Bonnette, M. R. (2016). Climate change and water-related ecosystem services: Impacts of drought in California, USA. *Ecosystem Health Sustainability, 2*(12), e01254.

Chang, H., & Franczyk, J. (2008). Climate change, land-use change, and floods: Toward an integrated assessment. *Journal of Geography Compass, 2*(5), 1549-1579.

Charnley, S. (2005). From nature tourism to ecotourism? The case of the Ngorongoro Conservation Area, Tanzania. *Human Organization, 64*(1), 75-88.

Chaves, E. D M., Picoli, M. C. A, & Sanches, I. D. (2020). Recent applications of Landsat 8/OLI and Sentinel-2/MSI for land use and land cover mapping: A systematic review. *Remote Sensing*, 12(18), 3062.

Chen, H., Guo, J., Zhang, Z., & Xu, C. Y. (2013). Prediction of temperature and precipitation in Sudan and South Sudan by using LARS-WG in future. *Theoretical Applied Climatology, 113*(3), 363-375.

Chen, Z. P., Li, L. M., Yu, R. Q., Littlejohn, D., Nordon, A., Morris, J., Dann, A. S., Jeffkins, P. A., Richardson, M. D., & Stimpson, S. L. (2011). Systematic prediction error correction: A novel strategy for maintaining the predictive abilities of multivariate calibration models. *Analyst, 136*(1), 98-106.

Chen, Z., Huang, M., Zhu, D., & Altan, O. (2021). Integrating remote sensing and a markov-FLUS model to simulate future land use changes in Hokkaido, Japan. *Remote Sensing, 13*(13), 2621.

Chiew, F. H., & McMahon, T. A. (2002). Modelling the impacts of climate change on Australian streamflow. *Hydrological Processes, 16*(6), 1235-1245.

Chisanga, C. B., Phiri, E., & Chinene, V. R. (2020). Reliability of Rain-Fed Maize Yield Simulation Using LARS-WG Derived CMIP5 Climate Data at Mount Makulu, Zambia. *Journal of Agricultural Science, 12*(11), 275.

Chomitz, K. M., & Thomas, T. S. (2003). Determinants of land use in Amazonia: A fine-scale spatial analysis. *American Journal of Agricultural Economics, 85*(4), 1016-1028.

Chong, I. G., & Jun, C. H. (2005). Performance of some variable selection methods when multicollinearity is present. *Chemometrics Intelligent Laboratory Systems, 78*(1-2), 103-112.

Chow, V., Maidment, D., & Mays, L. (1988). *Applied Hydrology McGraw-Hill International Editions*. New York, USA. https://scholar.google.com/

Cooper, P. J., Dimes, J., Rao, K., Shapiro, B., Shiferaw, B., & Twomlow, S. (2008). Coping better with current climatic variability in the rain-fed farming systems of sub-Saharan Africa: An essential first step in adapting to future climate change? *Agriculture, Ecosystems Environment, 126*(1-2), 24-35.

Curtis, G. H., & Hay, R. L. (1972). Further geological studies and potassium-argon dating at Olduvai Gorge and Ngorongoro Crater. *Calibration of Hominoid Evolution, 289*, 301.

Daggupati, P., Pai, N., Ale, S., Douglas-Mankin, K. R., Zeckoski, R. W., Jeong, J., Parajuli, P. B., Saraswat, D., & Youssef, M. A. (2015). A recommended calibration and validation strategy for hydrologic and water quality models. *Transactions of the American Society of Agricultural and Biological Engineers, 58*(6), 1705-1719.

Daniel, E. B., Camp, J. V., LeBoeuf, E. J., Penrod, J. R., Dobbins, J. P., & Abkowitz, M. D. (2011). Watershed modeling and its applications: A state-of-the-art review. *The Open Hydrology Journal, 5*(1), 26-50.

Dawson, J. (2008). Geophysical evidence for the structure of the crust and upper mantle of the Tanzania Craton and the Gregory Rift Valley. *Geological Society, London, Memoirs, 33*(1), 13-20.

Dawson, J. B. (2008). *The Gregory Rift Valley and Neogene-recent Volcanoes of Northern Tanzania*. https://scholar.google.com/

De Jong, S. (1993). SIMPLS: An alternative approach to partial least squares regression. *Chemometrics Intelligent Laboratory Systems, 18*(3), 251-263.

DeFries, R., & Eshleman, K. N. (2004). Land-use change and hydrologic processes: A major focus for the future. *Hydrological Processes, 18*(11), 2183-2186.

DeFries, R., Hansen, A., Turner, B., Reid, R., & Liu, J. (2007). Land use change around protected areas: Management to balance human needs and ecological function. *Ecological Applications, 17*(4), 1031-1038.

DeFries, R., & Rosenzweig, C. (2010). Toward a whole-landscape approach for sustainable land use in the tropics. *Proceedings of the National Academy of Sciences, 107*(46), 19627-19632.

Deocampo, D. M. (2004). Hydrogeochemistry in the Ngorongoro Crater, Tanzania, and implications for land use in a World Heritage Site. *Journal of Applied Geochemistry, 19*(5), 755-767. doi:https://doi.org/10.1016/j.apgeochem.2003.10.006

Deocampo, D. M. (2004). Hydrogeochemistry in the Ngorongoro Crater, Tanzania, and implications for land use in a World Heritage Site. *Applied Geochemistry, 19*(5), 755-767.

Deus, D., Gloaguen, R., & Krause, P. (2013). Water balance modeling in a semi-arid environment with limited in situ data using remote sensing in Lake Manyara, East African Rift, Tanzania. *Journal of Remote Sensing, 5*(4), 1651-1680.

Deus, D., Gloaguen, R., & Krause, P. (2013). Water balance modeling in a semi-arid environment with limited in situ data using remote sensing in Lake Manyara, East African Rift, Tanzania. *Remote Sensing, 5*(4), 1651-1680.

Dixon, B., & Earls, J. (2012). Effects of urbanization on streamflow using SWAT with real and simulated meteorological data. *Applied Geography, 35*(1-2), 174-190.

Donat, M. G., Lowry, A. L., Alexander, L. V., O'Gorman, P. A., & Maher, N. (2016). More extreme precipitation in the world's dry and wet regions. *Nature Climate Change, 6*(5), 508-513.

Dosdogru, F., Kalin, L., Wang, R., & Yen, H. (2020). Potential impacts of land use/cover and climate changes on ecologically relevant flows. *Journal of Hydrology, 584*, 124654.

Eastman, J. (2012). Assessing the impact of alternative land-use zoning policies onfuture ecosystem services. *Environmental Impact Assessment Review, 40,* 2-35.

Ellis, E., & Pontius Jr, R. (2006). Land-use and land-cover change: Encyclopedia of earth. *Journal of Environmental Protection, 2*, 142-153.

Eshtawi, T., Evers, M., Tischbein, B., & Diekkrüger, B. (2016). Integrated hydrologic modeling as a key for sustainable urban water resources planning. *Water Research, 101*, 411-428.

Estes, R., Atwood, J., & Estes, A. (2006). Downward trends in Ngorongoro Crater ungulate populations 1986–2005: Conservation concerns and the need for ecological research. *Biological Conservation, 131*(1), 106-120.

Estes, R., Atwood, J., & Estes, A. (2006). Downward trends in Ngorongoro Crater ungulate populations 1986–2005: Conservation concerns and the need for ecological research. *Journal of Biological Conservation, 131*(1), 106-120.

Estes, R., & Small, R. (1981). The large herbivore populations of Ngorongoro Crater. *African Journal of Ecology, 19*(1-2), 175-185.

Faiz, M. A., Liu, D., Fu, Q., Li, M., Baig, F., Tahir, A. A., Khan, M. I., Li, T., & Cui, S. (2018). Performance evaluation of hydrological models using ensemble of General Circulation Models in the northeastern China. *Journal of Hydrology, 565,* 599-613.

Fan, M., & Shibata, H. (2014). Spatial and temporal analysis of hydrological provision ecosystem services for watershed conservation planning of water resources. *Journal of Water Resources Management, 28*(11), 3619-3636.

FAO, IIASA, ISRIC, & ISSCAS. (2012). *JRC, Harmonized World Soil Database.* FAO, Rome, Italy, IIASA, Laxenburg, Austria. https://scholar.google.com/

Foley, J. A., DeFries, R., Asner, G. P., Barford, C., Bonan, G., Carpenter, S. R., Chapin, F. S., Coe, M. T., Daily, G. C., Gibbs, H. K., & Helkowski, J. H. (2005). Global consequences of land use. *Science, 309*(5734), 570-574.

Fowler, H. J., Blenkinsop, S., & Tebaldi, C. (2007). Linking climate change modelling to impacts studies: Recent advances in downscaling techniques for hydrological modelling. *A Journal of the Royal Meteorological Society, 27*(12), 1547-1578.

Frank, I. E., Kalivas, J. H., & Kowalski, B. R. (1983). Partial least squares solutions for multicomponent analysis. *Analytical Chemistry, 55*(11), 1800-1804.

Fu, B., Zhang, L., Xu, Z., Zhao, Y., Wei, Y., Skinner, D., & Sediments. (2015). Ecosystem services in changing land use. *Journal of Soils, 15*(4), 833-843.

Funk, C., Peterson, P., Landsfeld, M., Pedreros, D., Verdin, J., Shukla, S., Husak, G., Rowland, J., Harrison, L., Hoell, A., & Michaelsen, J. (2015). The climate hazards infrared precipitation with stations: A new environmental record for monitoring extremes. *Scientific Data, 2*(1), 1-21.

Galvin, K. A., Thornton, P. K., Boone, R. B., & Knapp, L. M. (2008). *Ngorongoro Conservation Area, Tanzania: Fragmentation of a Unique Region of the Greater Serengeti Ecosystem*. https://scholar.google.com/

Gärdenäs, A., Hopmans, J., Hanson, B., & Šimůnek, J. (2005). Two-dimensional modeling of nitrate leaching for various fertigation scenarios under micro-irrigation. *Agricultural Water Management, 74*(3), 219-242.

Gärdenäs, A. I., Šimůnek, J., Jarvis, N., & Genuchten, M. T. (2006). Two-dimensional modelling of preferential water flow and pesticide transport from a tile-drained field. *Journal of Hydrology, 329*(3-4), 647-660.

Gashaw, T., Tulu, T., Argaw, M., & Worqlul, A. W. (2017). Evaluation and prediction of land use/land cover changes in the Andassa watershed, Blue Nile Basin, Ethiopia. *Environmental Systems Research, 6*(1), 1-15.

Gashaw, T., Tulu, T., Argaw, M., & Worqlul, A. W. (2018). Modeling the hydrological impacts of land use/land cover changes in the Andassa watershed, Blue Nile Basin, Ethiopia. *Science of the Total Environment, 619*, 1394-1408.

Gassman, P. W., Arnold, J. J., Srinivasan, R., & Reyes, M. (2010). *The Worldwide use of The SWAT Model: Technological Drivers, Networking Impacts, and Simulation Trends.*

Paper presented at the 21st Century Watershed Technology: Improving Water Quality and Environment Conference Proceedings, 21-24 February 2010, Universidad EARTH, Costa Rica. https://scholar.google.com

Gassman, P. W., Reyes, M. R., Green, C. H., & Arnold, J. G. (2007). The soil and water assessment tool: Historical development, applications, and future research directions. *Transactions of the American Society of Agricultural and Biological Engineers, 50*(4), 1211-1250.

Gassman, P. W., Sadeghi, A. M., & Srinivasan, R. (2014). Applications of the SWAT model special section: Overview and insights. *Journal of Environmental Quality, 43*(1), 1-8.

Gebrechorkos, S. H., Hülsmann, S., & Bernhofer, C. (2019). Statistically downscaled climate dataset for East Africa. *Journal of Scientific Data, 6*(1), 1-8.

Gebrechorkos, S. H., Hülsmann, S., & Bernhofer, C. (2019). Regional climate projections for impact assessment studies in East Africa. *Environmental Research Letters*, 14(4), 044031.

Gebremicael, T., Mohamed, Y., Betrie, G., Van der Zaag, P., & Teferi, E. (2013). Trend analysis of runoff and sediment fluxes in the Upper Blue Nile basin: A combined analysis of statistical tests, physically-based models and landuse maps. *Journal of Hydrology, 482*, 57-68.

Ghaffari, G., Keesstra, S., Ghodousi, J., & Ahmadi, H. (2010). SWAT-simulated hydrological impact of land-use change in the Zanjanrood basin, Northwest Iran. *Hydrological Processes: An International Journal, 24*(7), 892-903.

Giertz, S., Junge, B., & Diekkrüger, B. (2005). Assessing the effects of land use change on soil physical properties and hydrological processes in the sub-humid tropical environment of West Africa. *Physics Chemistry of the Earth, Parts A/B/C, 30*(8-10), 485-496.

Govindaraju, R. S. (2000). Artificial neural networks in hydrology II: Hydrologic applications. *Journal of hydrologic Engineering, 5*(2), 124-137.

Guilford, J. P., & Lacey, J. I. (1947). *Printed Classification Tests*. US Government Printing Office. https://scholar.google.com

Gulacha, M., & Mulungu, D. (2017). Generation of climate change scenarios for precipitation and temperature at local scales using SDSM in Wami-Ruvu River Basin Tanzania. *Physics and Chemistry of the Earth, Parts A/B/Ch, Parts A/B/C, 100*, 62-72.

Gyamfi, C., Ndambuki, J. M., & Salim, R. W. (2016). Application of SWAT model to the Olifants Basin: Calibration, validation and uncertainty analysis. *Journal of Water Resource, 8*(03), 397.

Hanson, B. R., Šimůnek, J., & Hopmans, J. W. (2006). Evaluation of urea–ammonium–nitrate fertigation with drip irrigation using numerical modeling. *Agricultural Water Management, 86*(1-2), 102-113.

Hargreaves, G. H. (1994). Defining and using reference evapotranspiration. *Journal of Irrigation Drainage Engineering, 120*(6), 1132-1139.

Hashmi, M. Z., Shamseldin, A. Y., & Melville, B. W. (2011). Comparison of SDSM and LARS-WG for simulation and downscaling of extreme precipitation events in a watershed. *Stochastic Environmental Research Risk Assessment*, 25(4), 475-484.

Hassan, Z., Shamsudin, S., & Harun, S. (2014). Application of SDSM and LARS-WG for simulating and downscaling of rainfall and temperature. *Theoretical Applied Climatology, 116*(1), 243-257.

Haunschild, R., Bornmann, L., & Marx, W. (2016). Climate change research in view of bibliometrics. *PloS One*, 11(7), e0160393.

Hay, R., & Kyser, T. (2001). Chemical sedimentology and paleoenvironmental history of Lake Olduvai, a Pliocene lake in northern Tanzania. *Geological Society of America Bulletin, 113*(12), 1505-1521.

Huang, J., Zhang, J., Zhang, Z., Sun, S., & Yao, J. Y. (2012). Simulation of extreme precipitation indices in the Yangtze River basin by using statistical downscaling method (SDSM). *Theoretical Applied Climatolog, 108*(3), 325-343.

Huang, S. W., & Jin, J. Y. (2008). Status of heavy metals in agricultural soils as affected by different patterns of land use. *Environmental Monitoring, 139*(1), 317-327.

Huntington, T. G. (2006). Evidence for intensification of the global water cycle: Review and synthesis. *Journal of Hydrology, 319*(1-4), 83-95.

Hyandye, C. B., Worqul, A., Martz, L. W., & Muzuka, A. N. (2018). The impact of future climate and land use/cover change on water resources in the Ndembera watershed and their mitigation and adaptation strategies. *Journal of Environmental Systems Research, 7*(1), 1-24.

Izaurralde, R., Williams, J. R., McGill, W. B., Rosenberg, N. J., & Jakas, M. Q. (2006). Simulating soil C dynamics with EPIC: Model description and testing against long-term data. *Journal of Ecological Modelling, 192*(3-4), 362-384.

Jacques, D., & Simunek, J. (2005). *User Manual of the Multicompenent Variably-Saturated Flow and Transport Model.* https://scholar.google.com

Jarvie, H. P., Withers, P. J., Hodgkinson, R., Bates, A., Neal, M., Wickham, H. D., Harman, S. A., & Armstrong, L. (2008). Influence of rural land use on streamwater nutrients and their ecological significance. *Journal of Hydrology, 350*(3-4), 166-186.

Jeong, J., Kannan, N., Arnold, J., Glick, R., Gosselink, L., & Srinivasan, R. (2010). Development and integration of sub-hourly rainfall–runoff modeling capability within a watershed model. *Water Resources Management, 24*(15), 4505-4527.

Jones, D. S., Garvin, C. P., & Gorman, S. P. (2004). Relationship between biomedical catheter surface properties and lubricity as determined using textural analysis and multiple regression analysis. *Biomaterials, 25*(7-8), 1421-1428.

Joshi, P., Kumar, A., Singh, P., & Jahangeer, J. (2020). Sediment outflow under simulated rainfall conditions with varying geotechnical properties. *Journal of Hazardous, Toxic, and Radioactive Waste, 24*(3), 13. doi:10.1061/(ASCE)HZ.2153-5515.0000513.

Kabigumila, J. (1993). Feeding habits of elephants in Ngorongoro Crater, Tanzania. *African Journal of Ecology, 31*(2), 156-164.

Kamusoko, C., Oono, K., Nakazawa, A., Wada, Y., Nakada, R., Hosokawa, T., Tomimura, S., Furuya, T., Iwata, A., Moriike, H., & Someya, T. (2011). Spatial simulation modelling

of future forest cover change scenarios in Luangprabang province, Lao PDR. *Forests, 2*(3), 707-729.

Khalid, K., Ali, M. F., Abd Rahman, N. F., Mispan, M. R., Haron, S. H., Othman, Z., & Bachok, M. F. (2016). Sensitivity analysis in watershed model using SUFI-2 algorithm. *Procedia Engineering, 162*, 441-447.

Kim, J., Waliser, D. E., Mattmann, C. A., Goodale, C. E., Hart, A. F., Zimdars, P. A., Crichton, D. J., Jones, C., Nikulin, G., Hewitson, B., & Jack, C. (2014). Evaluation of the CORDEX-Africa multi-RCM hindcast: Systematic model errors. *Climate Dynamics, 42*(5), 1189-1202.

Kindu, M., Schneider, T., Teketay, D., & Knoke, T. (2015). Drivers of land use/land cover changes in Munessa-Shashemene landscape of the south-central highlands of Ethiopia. *Environmental Monitoring, 187*(7), 1-17.

Kityuttachai, K., Tripathi, N. K., Tipdecho, T., & Shrestha, R. (2013). CA-Markov analysis of constrained coastal urban growth modeling: Hua Hin seaside city, Thailand. *Sustainability, 5*(4), 1480-1500.

Knisel, W. G. (1980). *CREAMS: A Field Scale Model for Chemicals, Runoff, and Erosion from Agricultural Management Systems*. USA: Department of Agriculture, Science and Education Administration. https://scholar.google.com

Koch, M., & Cherie, N. (2013). *SWAT-Modeling of the Impact of Future Climate Change on the Hydrology and the Water Resources in the Upper Blue Nile River Basin, Ethiopia. Paper Presented at the Proceedings of the 6th International Conference on Water Resources and Environment Research, ICWRER*. https://scholar.google.com

Koomen, E., Dekkers, J., & Broitman, D. (2018). *Analyzing and Simulating Urban Density Exploring the Difference Between Policy Ambitions and Actual Trends in the Netherlands.* https://scholar.google.com

Koutsouris, A., Destouni, G., Jarsjö, J., & Lyon, S. W. (2010). Hydro-climatic trends and water resource management implications based on multi-scale data for the Lake Victoria region, Kenya. *Environmental Research Letters, 5*(3), 034005.

Krysanova, V., & Srinivasan, R. (2015). Assessment of climate and land use change impacts with SWAT. *Regional Environmental Change, 15*(3), 431-434.

Kumar, V. (2017). Statistical distribution of rainfall in Uttarakhand, India. *Journal of Applied Water Science, 7*(8), 4765-4776.

Lamba, J., Thompson, A. M., Karthikeyan, K., Panuska, J. C., & Good, L. W. (2016). Effect of best management practice implementation on sediment and phosphorus load reductions at subwatershed and watershed scale using SWAT model. *International Journal of Sediment Research, 31*(4), 386-394.

Lambin, E. F., Geist, H. J., & Lepers, E. (2003). Dynamics of land-use and land-cover change in tropical regions. *Annual Review of Environment, 28*(1), 205-241.

Lamichhane, B. (2008). *Dynamics and Driving Forces of Land use/Forest cover Change and Indicators of Climate Change in a Mountain Sub-Watershed of Gorkha.* https://scholar.google.com/

Larbi, I., Forkuor, G., Hountondji, F., Agyare, W. A., & Mama, D. (2019). Predictive land use change under business-as-usual and afforestation scenarios in the vea catchment, West Africa. *International Journal of Advanced Remote Sensing & GIS, 8*, 3011-3029.

Larbi, I., Hountondji, F. C., Annor, T., Agyare, W. A., Mwangi-Gathenya, J., & Amuzu, J. (2018). Spatio-temporal trend analysis of rainfall and temperature extremes in the Vea Catchment, Ghana. *Climate, 6*(4), 87.

Larbi, I., Hountondji, F. C., Dotse, S. Q., Mama, D., Nyamekye, C., Adeyeri, O. E., Djan'na Koubodana, H., Odoom, P. R. E., & Asare, Y. M. (2021). Local climate change projections and impact on the surface hydrology in the Vea catchment, West Africa. *Journal of Hydrology Research, 52*(6), 1200-1215. doi:doi: 10.2166/nh.2021.096

Larbi, I., Nyamekye, C., Hountondji, F. C., Okafor, G. C., & Odoom, P. R. E. (2020). Climate change impact on climate extremes and adaptation strategies in the Vea catchment, Ghana. *African Handbook of Climate Change Adaptation*, 2020,1-17.

Lawuo, Z. A., Mbasa, B., Mnyawi, S., & Research, S. (2014). Persistence of Land Conflicts Between Maasai Community and Ngorongoro Conservation Area Authority in Ngorongoro Conservation Area. *International Journal of Innovation, 5*(2), 154-161.

Leonard, R., Knisel, W., & Still, D. (1987). GLEAMS: Groundwater loading effects of agricultural management systems. *Journal of Transactions of the ASAE, 30*(5), 1403-1418. doi:doi: 10.13031/2013.30578

Leweri, C. M., Msuha, M. J., &Treydte, A. C. (2021). Rainfall variability and socio-economic constraints on livestock production in the Ngorongoro Conservation Area, Tanzania. *Journal of Applied Sciences, 3*(1), 1-10.

Li, H., & Reynolds, J. F. (1997). Modeling effects of spatial pattern, drought, and grazing on rates of rangeland degration: A combined Markov and cellular automation approach. *Scale in Remote Sensing, 1997*, 211-230.

Li, X., & Babovic, V. (2019). Multi-site multivariate downscaling of global climate model outputs: an integrated framework combining quantile mapping, stochastic weather generator and Empirical Copula approaches. *Climate Dynamics, 52*(9), 5775-5799.

Ligate, F., Ijumulana, J., Ahmad, A., Kimambo, V., Irunde, R., Mtamba, J. O., Mtalo, F., & Bhattacharya, P. (2021). Groundwater resources in the East African Rift Valley: Understanding the geogenic contamination and water quality challenges in Tanzania. *Scientific African, 13*, e00831.

Liu, J., Kuang, W., Zhang, Z., Xu, X., Qin, Y., Ning, J., Zhou, W., Zhang, S., Li, R., Yan, C., & Wu, S. (2014). Spatiotemporal characteristics, patterns, and causes of land-use changes in China since the late 1980s. *Journal of Geographical Sciences, 24*(2), 195-210.

Liu, X., Liang, X., Li, X., Xu, X., Ou, J., Chen, Y., Li, S., Wang, S., & Pei, F. (2017). A future land use simulation model for simulating multiple land use scenarios by coupling human and natural effects. *Urban Planning Landscape, 168*, 94-116.

López-Moreno, J. I., Vicente-Serrano, S., Moran-Tejeda, E., Zabalza, J., Lorenzo-Lacruz, J., & García-Ruiz, J. (2011). Impact of climate evolution and land use changes on water yield in the Ebro basin. *Hydrology Earth System Sciences, 15*(1), 311-322.

Lu, Z., Li, W., Wang, Y., & Zhou, S. (2022). Bibliometric Analysis of Global Research on Ecological Networks in Nature Conservation from 1990 to 2020. *Sustainability, 14*(9), 4925.

Luhunga, P. M., Kijazi, A. L., Chang'a, L., Kondowe, A., Ng'Ongolo, H., & Mtongori, H. (2018). Climate change projections for Tanzania based on high-resolution regional climate models from the coordinated regional climate downscaling experiment (CORDEX)-Africa. *Frontiers in Environmental Science*, 122, 1-20.

Ma, J., Pu, H., Sun, D. W., Gao, W., Qu, J. H., & Ma, K. Y. (2015). Application of Vis–NIR hyperspectral imaging in classification between fresh and frozen-thawed pork Longissimus Dorsi muscles. *International Journal of Refrigeration, 50*, 10-18.

MacDonald, A. M., Bonsor, H. C., Dochartaigh, B. É. Ó., & Taylor, R. G. (2012). Quantitative maps of groundwater resources in Africa. *Journal of Environmental Research Letters, 7*(2), 024009.

Mahaffey, B. L., Wheaton, M. G., Fabricant, L. E., Berman, N. C., andAbramowitz, J. S. (2013). The contribution of experiential avoidance and social cognitions in the prediction of social anxiety. *Behavioural Cognitive Psychotherapy, 41*(1), 52-65.

Maliehe, M., & Mulungu, D. M. (2017). Assessment of water availability for competing uses using SWAT and WEAP in South Phuthiatsana catchment, Lesotho. *Journal Physics Chemistry of the Earth, Parts A/B/C, 100*, 305-316.

Mannan, M., Al-Ansari, T., Mackey, H. R., & Al-Ghamdi, S. G. (2018). Quantifying the energy, water and food nexus: A review of the latest developments based on life-cycle assessment. *Journal of Cleaner Production, 193*, 300-314.

Catherine, A. M., Revocatus, M., & Hussein, S. (2015). Will Ngorongoro Conservation Area remain a world heritage site amidst increasing human footprint?. *International Journal of Biodiversity and Conservation*, 7(9), 394-407.

Masao, C. A., Makoba, R., & Sosovele, H. (2015). Will Ngorongoro Conservation Area remain a world heritage site amidst increasing human footprint? *International Journal of Biodiversity Conservation, 7*(9), 394-407.

Mathur, S., & Yadav, B. K. (2009). Phytoextraction modeling of heavy metal (lead) contaminated site using maize (Zea mays). *Practice Periodical of Hazardous, Toxic, Radioactive Waste Management, 13*(4), 229-238.

Mbungu, W. B., & Kashaigili, J. J. (2017). Assessing the hydrology of a data-scarce tropical watershed using the soil and water assessment tool: Case of the Little Ruaha River Watershed in Iringa, Tanzania. *Open Journal of Modern Hydrology*, 7(2), 65-89.

McCarty, M. F. (2004). Should we restrict chloride rather than sodium? *Medical Hypotheses, 63*(1), 138-148.

Melita, A. W., & Mendlinger, S. (2013). The impact of tourism revenue on the local communities' livelihood: A case study of Ngorongoro Conservation Area, Tanzania. *Journal of Service Science and Management, 6*(1), 117-126.

Milewski, A., Sultan, M., Al-Dousari, A., & Yan, E. (2014). Geologic and hydrologic settings for development of freshwater lenses in arid lands. *Hydrological Processes, 28*(7), 3185-3194.

Millette, T. L., Tuladhar, A. R., Kasperson, R. E., &Turner II, B. (1995). The use and limits of remote sensing for analysing environmental and social change in the Himalayan Middle Mountains of Nepal. *Global Environmental Change, 5*(4), 367-380.

Mishra, V. N., & Rai, P. K. (2016). A remote sensing aided multi-layer perceptron-Markov chain analysis for land use and land cover change prediction in Patna district (Bihar), India. *Journal of Geosciences, 9*(4), 1-18.

Mishra, V. N., Rai, P. K., & Mohan, K. (2014). Prediction of land use changes based on land change modeler using remote sensing: A case study of Muzaffarpur (Bihar), India. *Journal of the Geographical Institute" Jovan Cvijic", 64*(1), 111-127.

Mkiramweni, N., DeLacy, T., Jiang, M., & Chiwanga, F. (2016). Climate change risks on protected areas ecotourism: Shocks and stressors perspectives in Ngorongoro Conservation Area, Tanzania. *Journal of Ecotourism, 15*(2), 139-157.

Mollel, G. F., & Swisher III, C. C. (2012). The Ngorongoro Volcanic Highland and its relationships to volcanic deposits at Olduvai Gorge and East African Rift volcanism. *Journal of Human Evolution, 63*(2), 274-283.

Molua, E. L. (2009). An empirical assessment of the impact of climate change on smallholder agriculture in Cameroon. *Global Planetary Change, 67*(3-4), 205-208.

Monteith, J. L. (1965). *Evaporation And Environment. Paper Presented at the Symposia of the Society for Experimental Biology*. https://scholar.google.com/

Moriasi, D. N., Arnold, J. G., Van Liew, M. W., Bingner, R. L., Harmel, R. D., & Veith, T. L. (2007). Model evaluation guidelines for systematic quantification of accuracy in watershed simulations. *Transactions of the American Society of Agricultural and Biological Engineers, 50*(3), 885-900.

Moriasi, D. N., Gitau, M. W., Pai, N., & Daggupati, P. (2015). Hydrologic and water quality models: Performance measures and evaluation criteria. *Transactions of the American Society of Agricultural and Biological Engineers, 58*(6), 1763-1785.

Mosammam, H. M., Nia, J. T., Khani, H., Teymouri, A., & Kazemi, M. (2017). Monitoring land use change and measuring urban sprawl based on its spatial forms: The case of Qom city. *The Egyptian Journal of Remote Sensing Space Science, 20*(1), 103-116.

Mtongori, H. I., Stordal, F., & Benestad, R. E. (2016). Evaluation of empirical statistical downscaling models' skill in predicting Tanzanian rainfall and their application in providing future downscaled scenarios. *Journal of Climate, 29*(9), 3231-3252.

Munthali, M., Mustak, S., Adeola, A., Botai, J., Singh, S., & Davis, N. (2020). Modelling land use and land cover dynamics of Dedza district of Malawi using hybrid Cellular Automata and Markov model. *Remote Sensing Applications: Society, 17*, 100276.

Muthuwatta, L., Sood, A., McCartney, M., Silva, N. S., & Opere, A. (2018). Understanding the impacts of climate change in the Tana River Basin, Kenya. *Journal of Proceedings of the International Association of Hydrological Sciences, 379*, 37-42.

Mwabumba, M., Yadav, B. K., Rwiza, M. J., Larbi, I., Dotse, S. Q., Limantol, A. M., Sarpong, S., & Kwawuvi, D. (2022). Rainfall and temperature changes under different climate

scenarios at the watersheds surrounding the Ngorongoro Conservation Area in Tanzania. *Environmental Challenges*, 7, 100446.

Mwabumba, M., Yadav, B. K., Rwiza, M. J., Larbi, I., & Twisa, S. (2022). Analysis of land use and land-cover pattern to monitor dynamics of Ngorongoro world heritage site (Tanzania) using hybrid cellular automata-Markov model. *Journal of Current Research in Environmental Sustainability, 4*, 100126.

Myint, S. W., & Wang, L. (2006). Multicriteria decision approach for land use land cover change using Markov chain analysis and a cellular automata approach. *Canadian Journal of Remote Sensing, 32*(6), 390-404.

Narsimlu, B., Gosain, A. K., Chahar, B. R., Singh, S. K., & Srivastava, P. K. (2015). SWAT model calibration and uncertainty analysis for streamflow prediction in the Kunwari River Basin, India, using sequential uncertainty fitting. *Environmental Processes, 2*(1), 79-95.

Näschen, K., Diekkrüger, B., Evers, M., Höllermann, B., Steinbach, S., & Thonfeld, F. (2019). The impact of land use/land cover change on water resources in a tropical catchment in Tanzania under different climate change scenarios. *Sustainability, 11*(24), 7083.

Nash, J. E., & Sutcliffe, J. V. (1970). River flow forecasting through conceptual models part I: A discussion of principles. *Journal of Hydrology, 10*(3), 282-290.

Nash, M. S., & Chaloud, D. J. (2011). Partial least square analyses of landscape and surface water biota associations in the Savannah River Basin. *International Scholarly Research Notices, 2011*, 1-11.

Neitsch, S. L. (2005). *Soil and Water Assessment Tool. User's Manual Version 2005.* https://scholar.google.com

Neitsch, S. L., Arnold, J. G., Kiniry, J. R., & Williams, J. R. (2011). *Soil and Water Assessment Tool Theoretical Documentation Version 2009*. Texas A&M University System College Station, Texas 77843-2118. https://scholar.google.com

Ngana, J., Mwalyosi, R., Madulu, N., & Yanda, P. Z. (2003). Development of an integrated water resources management plan for the Lake Manyara sub-basin, Northern Tanzania. *Physics Chemistry of the Earth, Parts A/B/C, 28*(20-27), 1033-1038.

Niboye, E. (2010). Vegetation cover changes in Ngorongoro conservation area from 1975 to 2000. *The Open Geography Journal, 3*, 15-27.

Nie, W., Yuan, Y., Kepner, W., Nash, M. S., Jackson, M., & Erickson, C. (2011). Assessing impacts of landuse and landcover changes on hydrology for the upper San Pedro watershed. *Journal of Hydrology, 407*(1-4), 105-114.

Nkiaka, E., Nawaz, N., & Lovett, J. (2017). Evaluating global reanalysis precipitation datasets with rain gauge measurements in the Sudano-Sahel region: Case study of the Logone catchment, Lake Chad Basin. *Meteorological Applications, 24*(1), 9-18.

Notter, B., Hurni, H., Wiesmann, U., & Ngana, J. O. (2013). Evaluating watershed service availability under future management and climate change scenarios in the Pangani Basin. *Journal of Physics Chemistry of the Earth, Parts A/B/C, 61*, 1-11.

Noy-Meir, I. (1974). Multivariate analysis of the semiarid vegetation in south-eastern Australia. II. Vegetation catenae and environmental gradients. *Australian Journal of Botany, 22*(1), 115-140.

Nyahongo, J., Holmern, T., Kaltenborn, B., & Røskaft, E. (2009). Spatial and temporal variation in meat and fish consumption among people in the western Serengeti, Tanzania: The importance of migratory herbivores. *Oryx, 43*(2), 258-266.

Nyembo, L. O., Larbi, I., Mwabumba, M., Selemani, J. R., Dotse, S. Q., Limantol, A. M., & Bessah, E. (2022). Impact of climate change on groundwater recharge in the lake Manyara catchment, Tanzania. *Scientific African, 15*, e01072.

Obuobie, E., Kankam-Yeboah, K., Amisigo, B., Opoku-Ankomah, Y., & Ofori, D. (2012). Assessment of vulnerability of river basins in Ghana to water stress conditions under climate change. *Journal of Water and Climate Change, 3*(4), 276-286.

Omar, N. Q., Ahamad, M. S. S., Hussin, W., & Samat, N. (2014). Modelling land-use and land-cover changes using Markov-CA, and multiple decision making in Kirkuk city. *International Journal of Scientific Research and Engineering Studies*, *2*(1), 29-42.

Onderka, M., Wrede, S., Rodný, M., Pfister, L., Hoffmann, L., & Krein, A. (2012). Hydrogeologic and landscape controls of dissolved inorganic nitrogen and dissolved silica fluxes in heterogeneous catchments. *Journal of Hydrology, 450*, 36-47.

Onyutha, C., Asiimwe, A., Ayugi, B., Ngoma, H., Ongoma, V., & Tabari, H. (2021). Observed and future precipitation and evapotranspiration in water management zones of Uganda: CMIP6 projections. *Journal of Atmosphere, 12*(7), 887.

Organization, W. H. (2008). *Guidelines for Drinking-Water Quality: Second Addendum. Vol. 1, Recommendations*: *World Health Organization.* https://scholar.google.com

Osman, Y., Al-Ansari, N., Abdellatif, M., Aljawad, S. B., & Knutsson, S. (2014). Expected future precipitation in central Iraq using LARS-WG stochastic weather generator. *Engineering, 6*(13), 948-959.

Osman, Y. Z., & Abdellatif, M. E. (2016). Improving accuracy of downscaling rainfall by combining predictions of different statistical downscale models. *Water Science, 30*(2), 61-75.

Pachauri, R., & Meyer, L. (2014). *Climate Change 2014: Synthesis Report. Contribution of Working Groups I, II and III to the Fifth Assessment Report of the Intergovernmental Panel on Climate Change*. Geneva, Switzerland: IPCC. https://scholar.google.com/

Parkhurst, D. L., & Appelo, C. (1999). User's guide to PHREEQC (Version 2): A computer program for speciation, batch-reaction, one-dimensional transport, and inverse geochemical calculations. *Water-Resources Investigations Report, 99*(4259), 312.

Parry, M., Parry, M. L., Canziani, O., Palutikof, J., Van der Linden, P., & Hanson, C. (2007). *Climate Change 2007-Impacts, Adaptation and Vulnerability: Working Group II Contribution to the Fourth Assessment Report of the IPCC* (Vol. 4): Cambridge University Press. https://scholar.google.com/

Pervez, M. S., & Henebry, G. M. (2015). Assessing the impacts of climate and land use and land cover change on the freshwater availability in the Brahmaputra River basin. *Journal of Hydrology: Regional Studies, 3*, 285-311.

Pontius, R. G., & Schneider, L. C. (2001). Land-cover change model validation by an ROC method for the Ipswich watershed, Massachusetts, USA. *Agriculture, Ecosystems Environment, 85*(1-3), 239-248.

Pullanagari, R., Yule, I., Tuohy, M., Hedley, M., Dynes, R., & King, W. (2012). In-field hyperspectral proximal sensing for estimating quality parameters of mixed pasture. *Precision Agriculture, 13*(3), 351-369.

Pullanikkatil, D., Palamuleni, L. G., & Ruhiiga, T. M. (2016). Land use/land cover change and implications for ecosystems services in the Likangala River Catchment, Malawi. *Physics Chemistry of the Earth, Parts A/B/C, 93*, 96-103.

Racsko, P., Szeidl, L., & Semenov, M. (1991). A serial approach to local stochastic weather models. *Journal of Ecological Modelling, 57*(1-2), 27-41.

Rescia, A. J., Willaarts, B. A., Schmitz, M. F., & Aguilera, P. A. (2010). Changes in land uses and management in two Nature Reserves in Spain: Evaluating the social–ecological resilience of cultural landscapes. *Landscape Urban Planning, 98*(1), 26-35.

Richardson, C. W. (1981). Stochastic simulation of daily precipitation, temperature, and solar radiation. *Water Resources Research, 17*(1), 182-190.

Richardson, C. W., & Wright, D. A. (1984). *WGEN: A Model For Generating Daily Weather Variables*. https://scholar.google.com

Rigdon, E. E. (2012). Rethinking partial least squares path modeling: In praise of simple methods. *Long Range Planning, 45*(5-6), 341-358.

Rindfuss, R. R., Walsh, S. J., Turner, B. L., Fox, J., & Mishra, V. (2004). Developing a science of land change: Challenges and methodological issues. *Proceedings of the National Academy of Sciences, 101*(39), 13976-13981.

Ring, U., Schwartz, H. L., Bromage, T. G., & Sanaane, C. (2005). Kinematic and sedimentological evolution of the Manyara Rift in northern Tanzania, East Africa. *Geological Magazine, 142*(4), 355-368.

Rönkkö, M., McIntosh, C. N., Antonakis, J., & Edwards, J. R. (2016). Partial least squares path modeling: Time for some serious second thoughts. *Journal of Operations Management, 47*, 9-27.

Roose, M., & Hietala, R. (2018). A methodological Markov-CA projection of the greening agricultural landscape: A case study from 2005 to 2017 in southwestern Finland. *Environmental Monitoring Assessment, 190*(7), 1-13.

Rosegrant, M. W., Ringler, C., & Zhu, T. (2009). Water for agriculture: Maintaining food security under growing scarcity. *Annual Review of Environment, 34*, 205-222.

Rosenfield, G. H., & Fitzpatrick-Lins, K. (1986). A coefficient of agreement as a measure of thematic classification accuracy. *Photogrammetric Engineering Remote Sensing, 52*(2), 223-227.

Sadler, R., Maetam, B., Edokpolo, B., Connell, D., Yu, J., Stewart, D., Park, M.J., Gray, D., & Laksono, B. (2016). Health risk assessment for exposure to nitrate in drinking water from village wells in Semarang, Indonesia. *Environmental Pollution, 216*, 738-745.

Saito, H., Šimůnek, J., & Mohanty, B. P. (2006). Numerical analysis of coupled water, vapor, and heat transport in the vadose zone. *Vadose Zone Journal, 5*(2), 784-800.

Sang, L., Zhang, C., Yang, J., Zhu, D., & Yun, W. (2011). Simulation of land use spatial pattern of towns and villages based on CA–Markov model. *Mathematical Computer Modelling, 54*(3-4), 938-943.

Saraf, V. R., & Regulwar, D. G. (2016). Assessment of climate change for precipitation and temperature using statistical downscaling methods in Upper Godavari River Basin, India. *Journal of Water Resource Protection, 8*(01), 1-15.

Sarala, C., & Ravi-Babu, P. (2012). Assessment of groundwater quality parameters in and around Jawaharnagar, Hyderabad. *International Journal of Scientific Research Publication, 2*(10), 1-6.

Scanlon, B. R., Mace, R. E., Barrett, M. E., & Smith, B. (2003). Can we simulate regional groundwater flow in a karst system using equivalent porous media models? Case study, Barton Springs Edwards aquifer, USA. *Journal of Hydrology, 276*(1-4), 137-158.

Schaap, M. G., Leij, F. J., & Van Genuchten, M. T. (2001). Rosetta: A computer program for estimating soil hydraulic parameters with hierarchical pedotransfer functions. *Journal of Hydrology, 251*(3-4), 163-176.

Schulte, L. A., & Mladenoff, D. J. (2001). The original US public land survey records: Their use and limitations in reconstructing presettlement vegetation. *Journal of Forestry, 99*(10), 5-10.

Schwartz, H., Renne, P. R., Morgan, L. E., Wildgoose, M. M., Lippert, P. C., Frost, S. R., Harvati, K., Schrenk, F., & Saanane, C. (2012). Geochronology of the Manyara Beds, Northern Tanzania: New tephrostratigraphy, magnetostratigraphy and 40Ar/39Ar ages. *Journal of Quaternary Geochronology, 7*, 48-66.

Scott, D., Hall, C. M., & Gössling, S. (2016). A review of the IPCC Fifth Assessment and implications for tourism sector climate resilience and decarbonization. *Journal of Sustainable Tourism, 24*(1), 8-30.

Selvakumar, S., Ramkumar, K., Chandrasekar, N., Magesh, N., & Kaliraj, S. (2017). Groundwater quality and its suitability for drinking and irrigational use in the Southern Tiruchirappalli district, Tamil Nadu, India. *Applied Water Science, 7*(1), 411-420.

Semenov, M. A., & Barrow, E. M. (2002). *A Stochastic Weather Generator for use in Climate Impact Studies*. https://scholar.google.com

Semenov, M. A., Brooks, R. J., Barrow, E. M., & Richardson, C. W. (1998). Comparison of the WGEN and LARS-WG stochastic weather generators for diverse climates. *Climate Research, 10*(2), 95-107.

Semenov, M. A., & Stratonovitch, P. (2010). Use of multi-model ensembles from global climate models for assessment of climate change impacts. *Climate Research*, 41(1), 1-14.

Serneels, S., Said, M. Y., & Lambin, E. F. (2001). Land cover changes around a major east African wildlife reserve: The Mara Ecosystem (Kenya). *International Journal of Remote Sensing, 22*(17), 3397-3420.

Shagega, F. P., Munishi, S. E., & Kongo, V. M. (2019). Prediction of future climate in Ngerengere river catchment, Tanzania. *Physics and Chemistry of the Earth, Parts A/B/C*, 112, 200-209.

Sharma, A., Hettiarachchi, S., & Wasko, C. (2021). Estimating design hydrologic extremes in a warming climate: Alternatives, uncertainties and the way forward. *Philosophical Transactions of the Royal Society A, 379*(2195), 20190623.

Shi, T., Zhu, M., Zhou, X., Huo, X., Long, Y., Zeng, X., & Chen, Y. (2019). 1H NMR combined with PLS for the rapid determination of squalene and sterols in vegetable oils. *Food Chemistry, 287*, 46-54.

Shukla, P., & Singh, R. M. (2021). Statistical Downscaling of Climatic Variables in Indo-Gangatic Alluvial Plain. *Climate Change Impacts on Water Resources, 2021, 333-340.*

Shukla, R., Khare, D., & Deo, R. (2015). *Statistical Downscaling of Climate Change Scenarios of Rainfall and Temperature over Indira Sagar Canal Command Area in Madhya Pradesh, India. Paper Presented at The 2015 IEEE 14th International Conference on Machine Learning and Applications (ICMLA)*. https://scholar.google.com/

Sieck, K., & Jacob, D. (2016). Influence of the boundary forcing on the internal variability of a regional climate model. *Journal of Climate Change, 5*(03), 373. doi: 10. 4236/ ajcc. 2016.53028

Šimůnek, J., & Van Genuchten, M. T. (2008). Modeling nonequilibrium flow and transport processes using HYDRUS. *Vadose Zone Journal, 7*(2), 782-797.

Šimůnek, J., Van Genuchten, M. T., Gribb, M. M., & Hopmans, J. W. (1998a). Parameter estimation of unsaturated soil hydraulic properties from transient flow processes. *Soil Tillage Research, 47*(1-2), 27-36.

Šimunek, J., Van Genuchten, M. T., & Šejna, M. (2012). HYDRUS: Model use, calibration, and validation. *Transactions of the American Society of Agricultural and Biological Engineers*, *55*(4), 1263-1274.

Šimůnek, J., Van Genuchten, M. T., & Sejna, M. (2008b). Development and applications of the HYDRUS and STANMOD software packages and related codes. *Vadose Zone Journal*, *7*(2), 587-600.

Šimůnek, J., Van Genuchten, M. T., & Šejna, M. (2007). *Modeling Subsurface Water Flow and Solute Transport with Hydrus and Related Numerical Software Packages. Paper Presented at the Numerical Modelling of Hydrodynamics for Water Resources, an International Workshop, Centro Politecnico Superior, University of Zaragoza Spain*. https://scholar.google.com

Šimůnek, J., Van Genuchten, M. T., & Šejna, M. (2008). Development and applications of the HYDRUS and STANMOD software packages and related codes. *Vadose Zone Journal*, *7*(2), 587-600.

Šimůnek, J., Van Genuchten, M. T., & Šejna, M. (2016). Recent developments and applications of the HYDRUS computer software packages. *Vadose Zone Journal*, *15*(7), 1-25.

Šimůnek, J., Van Genuchten, M. T., & Sejna, M. J. V. Z. J. (2008). Development and applications of the HYDRUS and STANMOD software packages and related codes. *Vadose Zone Journal*, *7*(2), 587-600.

Singh, R., D'Alessio, M., Meneses, Y., Bartelt-Hunt, S., & Ray, C. (2021). Nitrogen removal in vermifiltration: Mechanisms, influencing factors, and future research needs. *Journal of Environmental Management*, *281*, 111868.

Singh, S. K., Laari, P. B., Mustak, S., Srivastava, P. K., & Szabó, S. (2018). Modelling of land use land cover change using earth observation data-sets of Tons River Basin, Madhya Pradesh, India. *Geocarto International*, *33*(11), 1202-1222.

Slingenberg, A., Braat, L., Van Der Windt, H., Rademaekers, K., Eichler, L., & Turner, K. (2009). S*tudy on Understanding the Causes of Biodiversity Loss and the Policy Assessment Framework*. https://www.fondazionesvilupposostenibile.org

Smith, M., Allen, R., Monteith, J., Perrier, A., & Segeren, A. (1992). *Expert Consultation on Revision of FAO Methodologies for Crop Water Requirements. Paper Presented at the Expert Consultation on Revision of FAO Methodologies for Crop Water Requirements*. Rome (Italy). https://scholar.google.com

Solomon, N., Segnon, A. C., Birhane, E., & Health, P. (2019). Ecosystem service values changes in response to land-use/land-cover dynamics in dry afromontane forest in northern Ethiopia. *International Journal of Environmental Research, 16*(23), 4653.

Song, K., Li, L., Tedesco, L. P., Li, S., Duan, H., Liu, D., Hall, B. E., Du, J., Li, Z., Shi, K., & Zhao, Y. (2013). Remote estimation of chlorophyll-a in turbid inland waters: Three-band model versus GA-PLS model. *Remote Sensing of Environment, 136*, 342-357.

Suarez, D. L., & Šimůnek, J. (1997). UNSATCHEM: Unsaturated water and solute transport model with equilibrium and kinetic chemistry. *Soil Science Society of America Journal, 61*(6), 1633-1646.

Subedi, P., Subedi, K., & Thapa, B. (2013). Application of a hybrid cellular automaton–Markov (CA-Markov) model in land-use change prediction: A case study of Saddle Creek Drainage Basin, Florida. *Applied Ecology Environmental Sciences, 1*(6), 126-132.

Sundaram, B., Feitz, A., Caritat, P. D., Plazinska, A., Brodie, R., Coram, J., & Ransley, T. (2009). Groundwater sampling and analysis: A field guide. *Journal Geoscience Australia Record, 27*(95), 104.

Swierenga, H., De Groot, P., De Weijer, A., Derksen, M., & Buydens, L. (1998). Improvement of PLS model transferability by robust wavelength selection. *Chemometrics Intelligent Laboratory Systems, 41*(2), 237-248.

Tang, F., Xu, H., & Xu, Z. (2012). Model calibration and uncertainty analysis for runoff in the Chao River Basin using sequential uncertainty fitting. *Procedia Environmental Sciences, 13*, 1760-1770.

Tang, F., Xu, H., & Xu, Z. (2012). Model calibration and uncertainty analysis for runoff in the Chao River Basin using sequential uncertainty fitting. *Procedia Environmental Sciences, 13*, 1760-1770.

Teferi, E., Bewket, W., & Uhlenbrook, S. (2013). Understanding recent land use and land cover dynamics in the source region of the Upper Blue Nile, Ethiopia: Spatially explicit statistical modeling of systematic transitions. *Agriculture, Ecosystems, 165*, 98-117.

Teferi, E., Uhlenbrook, S., Bewket, W., Wenninger, J., & Simane, B. (2010). The use of remote sensing to quantify wetland loss in the Choke Mountain range, Upper Blue Nile basin, Ethiopia. *Hydrology Earth System Sciences, 14*(12), 2415-2428.

Tesfaw, A. T., Pfaff, A., Kroner, R. E. G., Qin, S., Medeiros, R., & Mascia, M. B. (2018). Land-use and land-cover change shape the sustainability and impacts of protected areas. *Proceedings of the National Academy of Sciences, 115*(9), 2084-2089.

Tesfaye, Y. G., Meerschaert, M. M., & Anderson, P. L. (2006). Identification of periodic autoregressive moving average models and their application to the modeling of river flows. *Water Resources Research, 42*(1), 1-11.

Tibangayuka, N., Mulungu, D. M., & Izdori, F. (2022). Assessing the potential impacts of climate change on streamflow in the data-scarce Upper Ruvu River watershed, Tanzania. *Journal of Water and Climate Change*, 13(9), 3496-3513.

Torbick, N. M., Qi, J., Roloff, G. J., & Stevenson, R. J. (2006). Investigating impacts of land-use land cover change on wetlands in the Muskegon River Watershed, Michigan, USA. *Wetlands, 26*(4), 1103-1113.

Trap, J., Bureau, F., Perez, G., & Aubert, M. (2013). PLS-regressions highlight litter quality as the major predictor of humus form shift along forest maturation. *Soil Biology Biochemistry, 57*, 969-971.

Turner, B. L., Lambin, E. F., & Reenberg, A. (2007). The emergence of land change science for global environmental change and sustainability. *Proceedings of the National Academy of Sciences, 104*(52), 20666-20671.

Turner, B. L., Lambin, E. F., & Reenberg, A. (2007). The emergence of land change science for global environmental change and sustainability. *Proceedings of the National Academy of Sciences, 104*(52), 20666-20671.

Twisa, S., & Buchroithner, M. F. (2019). Land-use and land-cover change detection in Wami River Basin, Tanzania. *Land*, *8*(9), 1-15.

Twisa, S., Kazumba, S., Kurian, M., & Buchroithner, M. F. (2020). Evaluating and predicting the effects of land use changes on hydrology in Wami River Basin, Tanzania. *Hydrology*, *7*(1), 1-18.

Twisa, S., Mwabumba, M., Kurian, M., & Buchroithner, M. F. (2020). Impact of land-use/land-cover change on drinking water ecosystem services in Wami River Basin, Tanzania. *Resources*, *9*(4), 1-18.

Ty, T. V., Sunada, K., Ichikawa, Y., & Oishi, S. (2012). Scenario-based impact assessment of land use/cover and climate changes on water resources and demand: A case study in the Srepok River Basin, Vietnam—Cambodia. *Water Resources Management*, *26*(5), 1387-1407.

Valbuena, D., Verburg, P. H., & Bregt, A. K. (2008). A method to define a typology for agent-based analysis in regional land-use research. *Agriculture, Ecosystems & Environment*, *128*(1-2), 27-36.

Van Genuchten, M. T. (1980). A closed-form equation for predicting the hydraulic conductivity of unsaturated soils. *Soil Science Society of America Journal*, *44*(5), 892-898.

Vaughan, P. J., Šimůnek, J., Suarez, D. L., Corwin, D. L., & Rhoades, J. D. (1996). *Unsatchemgeo: Modeling Water Flow and Multicomponent Solute Transport in a Gis Context. Applications of Gis to the Modeling of Non-Point Source Pollutants in the Vadose Zone*, *48*, *235-246*. https://scholar.google.com.

Vilaysane, B., Takara, K., Luo, P., Akkharath, I., & Duan, W. (2015). Hydrological stream flow modelling for calibration and uncertainty analysis using SWAT model in the Xedone river basin, Lao PDR. *Procedia Environmental Sciences*, *28*, 380-390.

Vörösmarty, C. J., McIntyre, P. B., Gessner, M. O., Dudgeon, D., Prusevich, A., Green, P., Glidden, S., Bunn, S. E., Sullivan, C. A., Liermann, C. R., & Davies, P. M. (2010). Global threats to human water security and river biodiversity. *Nature*, *467*(7315), 555-561.

Wada, Y., Van Beek, L. P., Van Kempen, C. M., Reckman, J. W., Vasak, S., & Bierkens, M. F. (2010). Global depletion of groundwater resources. *Geophysical Research Letters*. *37*(20), 1-5.

Walter, R., Manega, P., Hay, R., Drake, R., & Curtis, G. (1991). Laser-fusion 40 Ar/39 Ar dating of Bed I, Olduvai Gorge, Tanzania. *Nature, 354*(6349), 145-149.

Wambura, F. (2014). Stream Flow Response to Skilled and Non-linear Bias Corrected GCM Precipitation Change in the Wami River Sub-basin, Tanzania. *British Journal of Environment and Climate Change, 4*(4), 389-408. doi:10.9734/bjecc/2014/13457

Wambura, F., Tumbo, S., Ngongolo, H., Mlonganile, P., & Sangalugembe, C. (2014). *Tanzania CMIP5 Climate Change Projections*. https://scholar.google.com/

Wang, S. Q., Zheng, X., & Zang, X. (2012). Accuracy assessments of land use change simulation based on Markov-cellular automata model. *Procedia Environmental Sciences, 13*, 1238-1245.

Wang, W., Guo, H., Chuai, X., Dai, C., Lai, L., & Zhang, M. (2014). The impact of land use change on the temporospatial variations of ecosystems services value in China and an optimized land use solution. *Environmental Science & Policy*, 44, 62-72.

Wang, Z., Feng, J., Li, L., Ni, W., & Li, Z. (2011). A multivariate model based on dominant factor for laser-induced breakdown spectroscopy measurements. *Journal of Analytical Atomic Spectrometry, 26*(11), 2289-2299.

Westberg, D. J., Stackhouse Jr, P. W., Hoell, J. M., & Chandler, W. S. (2013). An analysis of NASA's MERRA meteorological data to supplement observational data for calculation of climatic design conditions. *ASHRAE Transactions*, 119, 210-221.

Wilby, R. L., & Dawson, C. W. (2013). The statistical downscaling model: Insights from one decade of application. *International Journal of Climatology*, 33(7), 1707-1719.

Wilby, R. L., Dawson, C. W., & Barrow, E. M. (2002). SDSM: A decision support tool for the assessment of regional climate change impacts. *Environmental Modelling Software, 17*(2), 145-157.

Williams, J. R. (1990). The erosion-productivity impact calculator (EPIC) model: A case history. Philosophical Transactions of the Royal Society of London. Series B: *Biological Sciences*, 329(1255), 421-428.

Wold, S. (1995). PLS for multivariate linear modeling. *Chemometric Methods in Molecular Design*, 1995, 195-218.

Wold, S., Sjöström, M., & Eriksson, L. (2001). PLS-regression: A basic tool of chemometrics. *Chemometrics Intelligent Laboratory Systems, 58*(2), 109-130.

Woldesenbet, T. A., Elagib, N. A., Ribbe, L., & Heinrich, J. (2017). Hydrological responses to land use/cover changes in the source region of the Upper Blue Nile Basin, Ethiopia. *Science of the Total Environment, 575*, 724-741.

World Health Organization, W. (2008). *Guidelines for Drinking-Water Quality: Second Addendum Vol. 1*. Geneva, Switzerland: World Health Organization. https://scholar.google.com

World Health Organization, W. (2011). *Guidelines for Drinking-Water Quality, Fourth Edition.* https://scholar.google.com

Yadav, B. K., & Hassanizadeh, S. M. (2011). An overview of biodegradation of LNAPLs in coastal (semi)-arid environment. *Water, Air, & Soil Pollution, 220*(1), 225-239.

Yan, B., Fang, N., Zhang, P., & Shi, Z. (2013). Impacts of land use change on watershed streamflow and sediment yield: An assessment using hydrologic modelling and partial least squares regression. *Journal of Hydrology, 484*, 26-37.

Yira, Y., Diekkrüger, B., Steup, G., & Bossa, A. Y. (2016). Impact of climate change on water resources in a tropical West African catchment using an ensemble of climate simulations. *Hydrology and Earth System Sciences, 21*, 1-37.

Yira, Y., Diekkrüger, B., Steup, G., & Bossa, A. y. (2016). Modeling land use change impacts on water resources in a tropical West African catchment (Dano, Burkina Faso). *Journal of Hydrolog, 537,* 187-199.

Yirsaw, E., Wu, W., Shi, X., Temesgen, H., & Bekele, B. (2017). Land use/land cover change modeling and the prediction of subsequent changes in ecosystem service values in a coastal area of China, the Su-Xi-Chang Region. *Sustainability, 9*(7), 1204.

Żaba, J., & Gaidzik, K. (2011a). The Ngorongoro Crater as the biggest geotouristic attraction of the Gregory Rift (Northern Tanzania, Africa)–geological heritage. *Geotourism/Geoturystyka,* (24-25), 27-27.

Zeng, Q., Chen, H., Xu, C. Y., Jie, M. X., Chen, J., Guo, S. L., & Liu, J. (2018). The effect of rain gauge density and distribution on runoff simulation using a lumped hydrological modelling approach. *Journal of Hydrology, 563,* 106-122.

Zhang, D., Wang, X., Qu, L., Li, S., Lin, Y., Yao, R., Zhou, X., & Li, J. (2020). Land use/cover predictions incorporating ecological security for the Yangtze River Delta region, China. *Ecological Indicators, 119,* 106841.

Zhao, F., Zhang, L., Xu, Z., & Scott, D. F. (2010). Evaluation of methods for estimating the effects of vegetation change and climate variability on streamflow. *Water Resources Research, 46*(3), 1-14.

Zhou, J., Liu, Y., Guo, H., & He, D. (2014). Combining the SWAT model with sequential uncertainty fitting algorithm for streamflow prediction and uncertainty analysis for the Lake Dianchi Basin, China. *Hydrological Processes, 28*(3), 521-533.

Zhu, H., Li, Y., Huang, Y., Li, Y., Hou, C., & Shi, X. (2018). Evaluation and hydrological application of satellite-based precipitation datasets in driving hydrological models over the Huifa river basin in Northeast China. *Atmospheric Research, 207,* 28-41.

Zhu, M., Shi, T., Chen, Y., Luo, S., Leng, T., Wang, Y., Guo, C., & Xie, M. (2019). Prediction of fatty acid composition in camellia oil by 1H NMR combined with PLS regression. *Food Chemistry, 279*, 339-346.

Zorita, E., & Von-Storch, H. (1999). The analog method as a simple statistical downscaling technique: Comparison with more complicated methods. *Journal of Climate, 12*(8), 2474-2489.

RESEARCH OUTPUTS

(i) Publications

Mwabumba, M., Yadav, B. K., Rwiza, M. J., Larbi, I., Dotse, S. Q., Limantol, A. M., Sarpong, S., & Kwawuvi, D. (2022). Rainfall and temperature changes under different climate scenarios at the watersheds surrounding the Ngorongoro Conservation Area in Tanzania. *Environmental Challenges*, 2022, 100446.

Mwabumba, M., Yadav, B. K., Rwiza, M. J., Larbi, I., & Twisa, S. (2022). Analysis of land use and land-cover pattern to monitor dynamics of Ngorongoro world heritage site (Tanzania) using hybrid cellular automata-Markov model. *Current Research in Environmental Sustainability*, 4, 100126.

Mwabumba, M., Jahangeer, J., Beegum, S., Yadav, B. K., & Rwiza, M. J. (2022). Assessment of Groundwater Quality under Changing Climate in Ngorongoro Conservation Area, Tanzania. *Journal of Irrigation and Drainage Engineering*, 148(10), 04022032

(ii) Poster Presentation